REVIEW ARTICLE

Functional inks and printing of two-dimensional materials

Guohua Hu [a], Joohoon Kang [b], Leonard W. T. Ng [a], Xiaoxi Zhu [a], Richard C. T. Howe [a], Christopher G. Jones [a,c], Mark C. Hersam [b], and Tawfique Hasan [a,*]

Graphene and related two-dimensional materials provide an ideal platform for next generation disruptive technologies and applications. Exploiting these solution-processed two-dimensional materials in printing can accelerate this development by allowing additive patterning on both rigid and conformable substrates for flexible device design and large-scale, high-speed, cost-effective manufacturing. In this review, we summarise the current progress on ink formulation of two-dimensional materials and the printable applications enabled by them. We also present our perspectives on their research and technological future prospects.

1 Introduction

The unique and often complementary properties of graphene and related two-dimensional (2d) materials offer an abundance of opportunities for next generation applications and technologies[1,2]. These 2d materials can be exfoliated from their parent layered materials in low-cost, mass production methods *via* solution processing[3]. The exfoliated materials can be sorted in order of size and thickness to produce uniform dispersions with the potential for exploitation across a wide range of applications[4]. While a number of deposition techniques exist for the solution-processed 2d materials, printing holds specific promise for high-volume, low-cost manufacturing[5].

The range of printing processes, which include inkjet, screen, and roll-to-roll (R2R) gravure and flexographic printing, are widely used technologies to deliver additive patterning of ink pigments onto rigid, flexible and conformable surfaces. These processes enable the large-scale, ultra-low-cost production of packaging materials, everyday documents, magazines and newspapers. The adaptation of functional materials to perform as active pigments within ink formulations has gained an increasing interest over recent years. This approach takes advantage of well-established print production processes for functional device fabrication[5]. The advent of solution-processed 2d materials has intensified this interest, offering the promise of economic and scalable manufacturing for an entirely new generation of technologies and applications[6].

Printed 2d material applications were first reported in 2012,

when graphene from liquid phase exfoliation (LPE; a solution processing approach) was inkjet-printed to fabricate field-effect transistors (FETs)[7]. This field of research has since witnessed rapid progress in ink formulation and device fabrication. As well as graphene, various other 2d materials have since been investigated as active pigments, such as transition metal dichalcogenides (TMDs), black phosphorus (BP) and hexagonal boron nitride (*h*-BN)[8–13]. While the first generation of 2d material inks (*i.e.* the LPE dispersions) were not optimised for the relevant printing processes, new 2d material functional ink formulations are now beginning to emerge. The viability of a range of organic solvents, solvent mixtures and aqueous dispersions for ink formulation has now been demonstrated[12,13]. Polymers and surfactants widely used in conventional ink formulations as binders and additives have also been introduced[11,14]. The adaptation and tailoring of formulations have allowed the fluidic properties, drying dynamics and interaction with substrates of the functional inks to be optimised not only for inkjet printing but also for screen, gravure and flexographic printing[15–21]. Beyond electronics, a variety of printable 2d material applications have been demonstrated. Key applications include conductive inks, optoelectronics (*e.g.* photodetectors), photonics (*e.g.* non-linear optical devices), sensors, and energy storage (*e.g.* supercapacitors and batteries)[8–25]. Controlled additive patterning of the 2d materials has also enabled the fabrication of fully-printed heterostructures (*i.e.* stacks of multiple 2d materials) that exploit the complementary properties of 2d materials for unprecedented device performance[9–11].

While there have been many advances in functional ink formulations and printable applications for 2d materials since the first demonstration of inkjet-printed graphene transistors in 2012, there remains a lack of comprehensive reviews (or indeed published literature in general) that provide guidelines on how graphics ink formulations and printing technologies could lend themselves to functional ink formulations and printing of 2d ma-

[a] *Cambridge Graphene Centre, University of Cambridge, Cambridge CB3 0FA, UK. Tel: +44 (0)1223 7 48362. e-mail: th270@cam.ac.uk.*

[b] *Department of Materials Science and Engineering, Northwestern University, Evanston, IL 60208, USA.*

[c] *Novalia, Regent House, Impington, Cambridge CB24 9NP, UK.*

This journal is © The Royal Society of Chemistry [year]

Chem. Soc. Rev., [year], [vol.], 1–35 | 1

terials, a summary on the most recent progress in printable applications of 2d materials, and in particular the research and economic landscapes of 2d material inks and printing. With this in mind, to give a comprehensive review, we construct this article as follows: in the following two sections of this review we present a brief introduction to 2d materials and the recent developments in their solution processing and flake sorting strategies; in the fourth section, we discuss general composition, physical properties and processing principles of inks, and the demonstrated functional ink formulations of 2d materials for the most prevalently used printing processes; the fifth section covers the most recent progress in printable 2d material application development, drawing inspiration from published literature and industrial practices; finally, we present our views on the current trends, technology convergence, economic landscape and potential impact of 2d material inks and printing.

2 The 2d material family

Layered materials are structured as stacked atomically thin, planar layers with intralayer covalent bonds and interlayer van der Waals (vdW) forces [3,26]. The significant distinction of these compounds is that they can be exfoliated or thinned *via* shear in the in-plane direction while the planar sheets remain intact, as the chemical bonds and the vdW forces differ substantially in mechanical strength [3,26]. In extreme conditions, the layered compounds can be exfoliated into few-layers (<10) or even monolayers, termed as 2d materials [3,26].

Graphite is the most widely studied layered material that naturally occurs in metamorphic geology. It has a honeycomb hexagonal lattice structure. The use of graphite dates back to the *Neolithic* age when it was applied in ceramic decoration [27]. It later found widespread use in refractories due to its physical stability [28], and as a lubricant as it was found to be particularly easy to delaminate into thin sheets [3]. This gradually led to the establishment of fundamental understanding of the structure of graphite as a layered laminar material [3]. The elemental and regular arrangement of the carbon atoms allowed early modelling [29–31] of the likely material properties of monolayer graphite, *i.e.* graphene. The major concern was that such monolayers were thermodynamically unstable and could not physically exist independently against thermal fluctuations due to the generation of displacements of atoms or other crystal defects [32]. Stable graphene was first conclusively demonstrated in 2004 by repeatedly cleaving graphite with adhesive tape (the so-called mechanical exfoliation technique) [3], launching the 2d material research field.

Beyond graphite, there is a variety of layered materials with distinctly different properties. Among these, the most widely studied materials include naturally occurring TMDs [33], chemically synthesised *h*-BN [34] and BP [35]. TMDs are a group of ∼40 compounds that consist of a transition metal and a group VI element in a trigonal prismatic or octahedral lattice. This class of layered materials can be either metallic (*e.g.* NbSe$_2$) or semiconducting (*e.g.* MoS$_2$, WS$_2$ and MoSe$_2$), depending on the coordination and oxidation states of the transition metal atoms and the chemical structures [33]. Research into the exfoliation of TMDs has shared

a long history with graphene. The optical absorption features of exfoliated MoS$_2$ were initially investigated by R. Frindt and A. Yoffe in 1963 [36], and monolayer MoS$_2$ was reported as early as in 1986 [37]. But interest in MoS$_2$ or TMDs in general was resumed only in 2011 when Radisavljevic *et al.* demonstrated monolayer MoS$_2$ based transistors [38] with an I_{ON}/I_{OFF} (*i.e.* the ratio of currents in the ON- and OFF-state of the transistors) exceeding 10^8. BP is a puckered hexagonal phosphorus allotrope transformed from other allotropes (*e.g.* white or red phosphorus) [35]. Although BP was first successfully synthesised in 1914 [39], it took another 100 years before it was used as a 2d material in the demonstration of transistors with a mobility of 1,000 cm^{2}V^{-1}s^{-1} and an I_{ON}/I_{OFF} of 10^5 [35]. The application of BP, however, has been substantially limited due to its instability under ambient conditions [12,40–43]. *h*-BN is hexagonal crystalline form of boron nitride with the boron and nitride atoms alternatively covalently bonded in-plane [44,45]. With a layered structure similar to graphite, *h*-BN has been widely used as a lubricant, well known as the 'white graphite' [44,45]. However, unlike graphite, *h*-BN is an electrically insulating and thermally conductive material [45–47]. *h*-BN exhibits better lubricating properties than graphite, especially when under extreme conditions (*e.g.* vacuum, high temperature, oxidising atmosphere) [44,45]. *h*-BN also experienced a renewed interest in the field of 2d material electronics, in particular, as a screening substrate for other 2d materials or as an atomically thin insulator [48].

This broadening field has also created a renewed interest in a variety of other types of layered materials. Some examples are layered ternary carbides and nitrides (known as MAX phases), III-VI compounds, quintuple layered materials and mica. MAX phases (*e.g.* Ti$_3$AlC$_2$) are artificially produced 'layered materials', where the interlayer bonds between the metal atoms and the layers are too strong to allow direct exfoliation [49–52]. However, by selectively etching away these interlayer metal atoms from the MAX phases, the bulk materials can be readily exfoliated into atomically thin sheets, widely termed as MXenes [49–52]. The electronic properties of MXenes are of special interest, with theoretical studies suggesting that MXenes are either metallic or small bandgap semiconductors which can be engineered through chemical functionalisation [49–52]. Quintuple layered materials (consisting of 5 atom layers along the *z*-direction) such as bismuth selenide (Bi$_2$Se$_3$) and antimony telluride (Sb$_2$Te$_3$) can also be exfoliated from their bulk [53]. These 2d materials are attractive for various potential applications, in particular, for optoelectronics and thermoelectric power generation [54–56]. Finally, group III-VI layered compounds such as indium selenide (*e.g.* InSe and In$_2$Se$_3$), gallium selenide and copper indium selenide have also recently emerged as another promising family of 2d materials for (opto)electronic applications [57–60].

The above examples highlight the diversity of layered materials and the very broad spectrum of physical properties they represent. An even more important consideration is that their exfoliation into 2d materials can lead to radical performance improvements or exotic properties that do not exist in their bulk layered material forms [3,33]. These properties may enable next generation disruptive applications and technologies, in particular, in the field of (opto)electronics and photonics [1]. For graphene,

2 | *Chem. Soc. Rev.*, [year], [**vol**.], 1–35

This journal is © The Royal Society of Chemistry [year]

the combination of atomic thickness, high transparency[61] and good electrical conductivity[62] shows promise for the fabrication of flexible transparent conductors, while its exceptionally high carrier mobility[63] in addition to the zero-bandgap[64] can be exploited in high-frequency applications. Due to quantum confinement as a result of the decrease in thickness, exfoliated semiconducting TMDs (*e.g.* MoS_2, WS_2 and $MoSe_2$) and BP exhibit layer-dependent bandgaps[33,35]. For example, MoS_2 shifts significantly from an indirect bulk bandgap of ~1.2 eV towards a direct monolayer bandgap of ~1.8 eV, while BP transforms from direct 0.3 eV to direct 2.0 eV[35]. Such bandgap ranges are promising for the fabrication of logic electronics (requiring a bandgap of >0.4 eV and an I_{ON}/I_{OFF} of $>10^{4}$ [65]) [10,35,38]. The indirect to direct bandgap transition leads to significantly enhanced photoluminescence (over 10^4 times enhancement observed in MoS_2 [66]), making exfoliated semiconducting TMDs as well as direct bandgap BP and III-VI semiconductors appealing materials for optoelectronics such as photodetectors and light emitters[58,66–69]. 2d materials (*e.g.* graphene, MoS_2 and BP) may also exhibit nonlinear optical absorption and ultrafast carrier dynamics, making them a promising material platform for saturable absorbers (SAs), which act as fast nonlinear optical switches to convert a low peak power continuous-wave signal to a train of high peak power ultrashort pulses[12,70,71]. On the other hand, *h*-BN is a wide bandgap (~6 eV) material. This, in combination with the atomically smooth surface and the absence of dangling bonds, makes *h*-BN an ideal dielectric substrate for other 2d materials in heterostructure device designs[48,72,73].

Potential applications for 2d materials goes far beyond (opto)electronics and photonics. For instance, the use of graphene as a filler material by exploiting its high mechanical strength leads to high strength composites[74]. Exfoliated *h*-BN, on the other hand, presents outstanding dielectric and thermal properties, enabling its use as a filler material for the development of polymer composites, in particular where improved thermal but not electrical conductivity is desired[75]. The exposed large surface area of 2d materials (*e.g.* a theoretical value of 2,630 m^2 g^{-1} for graphene[76]) allows strong interaction with the ambient elements such as moisture, gas, chemicals and bioelements for sensing applications[1]. This large specific surface area is also particularly-suited to the development of electrode systems for energy storage applications[51,77,78]. It has been proposed that graphene electrodes may lead to a decrease in film thickness as well as an increase in electrode-to-electrolyte contact, which in combination with exceptional durability and electrical conductivity would offer better performance than current technologies[77]. MXenes also exhibit attractive electrochemical properties for high performance electrodes in batteries and supercapacitors[51].

3 Scalable production of 2d materials

In order to address scalable applications for 2d materials, a number of material production methods have been developed over the last decade. An important part of the research has been devoted to the development of cost-effective mass production methods. In general, the production methods can be classified either as top-down or bottom-up approaches: (1) top-down: bulk layered ma-
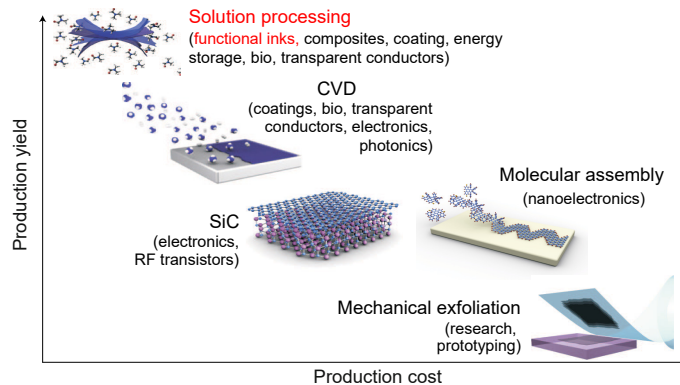

Fig. 1 Key production methods of graphene, differing in production rate and cost. The most suitable applications associated with the production methods are also indicated. Adapted with permission[81]. Copyright 2012, Nature Publishing Group.

terials are directly exfoliated to yield mono- and few-layer flakes. The most common methods are mechanical exfoliation and solution processing[3,79]; (2) bottom-up: individual flakes are grown or synthesised on substrates. The most commonly used method is chemical vapour deposition (CVD)[80]. As shown in Fig. 1, these production methods of graphene can profoundly differ in production yield and cost, and hence the target applications. We note that similar conclusion can be drawn for some other 2d materials, in particular, TMDs. Although mechanical exfoliation is very capable of producing high-quality materials, its application is limited by its extremely low and uncontrollable yield. CVD presents challenges in cost-effectiveness and scalability due to the demanding production conditions (*e.g.* high temperature, certain gases and precursors) and the expensive sacrificial growth substrates[80].
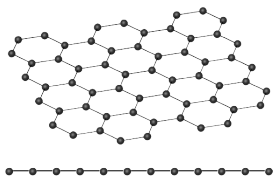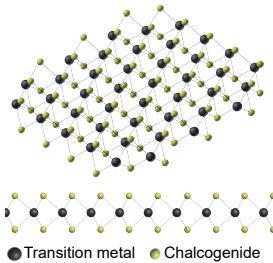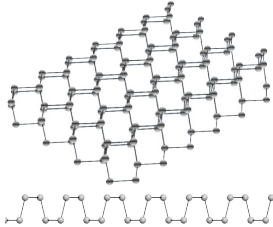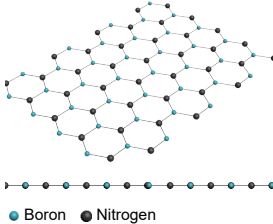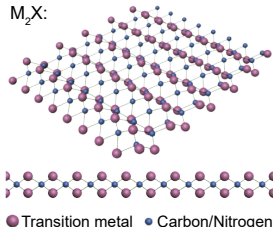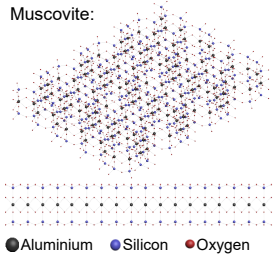
In contrast, top-down solution processing allows exfoliation of mono- and few-layer 2d material flakes from the bulk in a liquid medium in large quantities for a low setup and production cost (cost-effective equipment, raw materials and material processing)[3,82]. The exfoliated 2d materials are atomically thin and can be easily processed and adapted as active pigments for functional ink formulation, enabling the development of printable applications[6]. This provides an exciting prospect for the manufacturing of low-cost, large-scale functional devices[5,125].

Solution processing generally relies on exfoliation *via* ion intercalation, ion exchange, or pure shear forces (*i.e.* LPE)[3]. For the case of graphene, an alternative, widely exploited approach is through the reduction of graphene oxide, producing the so-called reduced graphene oxide (rGO)[87]. Unlike graphite, TMDs and other common layered materials, the exfoliation approach for the MAX phases using hydrofluoric acid or other etchants[52] sits slightly outside of the scope of typical solution processing, and is not discussed in this review.

3.1 Exfoliation based on ion intercalation/exchange

Ion intercalation is one of the earliest solution processing approaches of 2d materials. It dates back to 1841 when Schaffautl

This journal is © The Royal Society of Chemistry [year]

Chem. Soc. Rev., [year], [**vol.**], 1–35 | 3

Table 1 Common 2d materials, their structures, solution processing methods, and key applications.

2d materials	Typical structures	Solution processing methods	Key applications
Graphene		Liquid phase exfoliation (*via* sonication[82], ball milling[83], high-shear mixing[84] and microfluidisation[18]); Ion intercalation[85,86]. Reduction of graphene oxide[87].	Electronics[7,10,24]; Transparent conductors[6]; Functional inks[14,16,21,23,88,89]; Saturable absorbers[70,90]; Batteries[78]; Supercapacitors[91]; Thermoelectrics[92]; Sensors[93]; Composites[74].
TMDs MX$_2$, *e.g.*: MoS$_2$, WS$_2$, MoSe$_2$.	Transition metal ● Chalcogenide ●	Liquid phase exfoliation (*via* sonication[94], ball milling[95] and high-shear mixing[96]); Ion intercalation[97,98].	Electronics[10,11]; Photodetectors[8,9,11]; Functional inks[8–11,99]; Saturable absorbers[71,100–102]; Batteries[103]; Supercapacitors[104]; Sensors[105]; Composites[106].
BP		Liquid phase exfoliation (*via* sonication[12,40,43,107]).	Functional inks[12]; Electronics[40,43,108]; Photodetectors[12]; Saturable absorbers[109]; Sensors[105]; Supercapacitors[110]; Batteries[111].
***h*-BN**	Boron ● Nitrogen ●	Liquid phase exfoliation (*via* sonication[94], ball milling[112] and high-shear mixing[96]).	Dielectric composites[75]; Thermal composites[47]; Dielectric inks[10,11,24,113].
MXenes *e.g.*: M$_2$X, M$_3$X$_2$, M$_4$X$_3$.	M$_2$X: Transition metal ● Carbon/Nitrogen ●	Exfoliation with hydrofluoric or other etchants[49].	Batteries and supercapacitors[51,114,115]; Sensors[116]; Electronics[117]; Composites[118].
Mica *e.g.*: biotite, muscovite, phlogopite.	Muscovite: Aluminium ● Silicon ● Oxygen ●	Liquid phase exfoliation (*via* sonication[119]); Ion intercalation[120].	Inks[121]; Composites[122,123]; Barriers[121,124]; Capacitors[121]; Catalysis[121].

et al. reported graphite intercalation compounds[126]. Ion intercalation as a method of producing monolayer MoS$_2$ was reported as early as in 1986[37]. Subsequently, it was successfully exploited in obtaining monolayer graphene[85,86] and other 2d materials[127]. The ion intercalation process takes advantage of the layered structure of 2d materials: small molecules like ionic species (*e.g.* alkali metals Li$^+$, Na$^+$ and K$^+$) can intercalate between the atomic layers; the intercalated small molecules effectively increase the interlayer distance, such that the interlayer vdW forces are weakened which facilitates the separation of the layers[3]. The separated 2d material flakes can be then exfoliated into mono- and few-layers *via* agitation such as mild sonication or even stirring.

4 | *Chem. Soc. Rev.*, [year], [**vol**.], 1–35

This journal is © The Royal Society of Chemistry [year]

Ion intercalation allows production of relatively large flakes with a high yield of monolayer flakes[85,86,98,127]. However, this approach may introduce defects, impurities and structural changes to the 2d material lattices, which can lead to an alteration of the material properties. For instance, Eda *et al.* showed that Li$^+$ intercalation of MoS$_2$ could lead to a lattice change from trigonal prismatic phase (semiconducting) to metastable octahedral phase (metallic)[98]. To make use of the optoelectronic properties of MoS$_2$, the metallic phase then required a high temperature annealing to transform back to the semiconducting phase[98].

Solution processing *via* ion exchange is another widely applied strategy. It is limited to the layered materials (*e.g.* layered oxides) that contain an interlayer of cations[3]. For transition metal oxides, the layered planes tend to be negatively charged, but the alkali metal cations (*e.g.* K$^+$, Rb$^+$, Cs$^+$) occupy the interlayer space to ensure charge neutrality. The cations can be ion exchanged with organic ions, leading to swelling and separation of the transition metal oxide layers[128]. Mono- and few-layers can then be exfoliated from the bulk *via* agitation. Similar to ion intercalation, ion exchange can lead to alteration of the properties of the exfoliated 2d materials.

3.2 Liquid phase exfoliation

LPE is a solution processing technique that has been widely used in unbundling and dispersing carbon nanotubes (CNTs)[129–132]. It was first reported in graphene production by Hernandez *et al.* in 2008[82] where the authors recorded exfoliation of mono- and few-layer graphene flakes in organic solvents (*e.g.* N-Methyl-2-pyrrolidone (NMP)) by ultrasound sonication. This approach starts with immersing graphite into a liquid medium. Under the effect of ultrasound waves, localised bubbles (commonly termed as 'cavitation') are generated in the liquid. The bubbles then collapse and generate high shear forces, which overcome the interlayer vdW forces to yield exfoliated graphene flakes. This approach has since been successfully extended to a wide range of 2d materials, including TMDs, BP, *h*-BN and mica[12,94,119], as shown in Fig. 2(A, B).

In addition to ultrasound assisted exfoliation, other commonly adopted methods for shear force generation include high-shear mixing[84], high-pressure mixing[18] and ball milling[133]. As with sonication, the bulk material is exfoliated by introducing sufficient shear forces to overcome the interlayer vdW forces. Each of these methods differs in the generation of the shear forces. For the case of high-shear/pressure mixing, the forces are generated by flowing the mixture through a meshed screen with high-speed rotating mixing blade (*e.g.* blenders or blade mixers)[84], by forcing the mixture through narrow channels under high pressure (*e.g.* homogenisers)[18], or by flowing the mixture through meshed screens (*e.g.* impeller mixing)[84]. Ball-milling performs in a slightly different way in using a cylindrical 'jar' containing a charge of small balls/beads (typically steel or zirconia). Under rotation, the balls/beads generate shear forces perpendicular to the walls of the jar for exfoliation[133].

As LPE exploits shear forces to achieve exfoliation, the intermolecular interaction between the 2d materials and the liq-
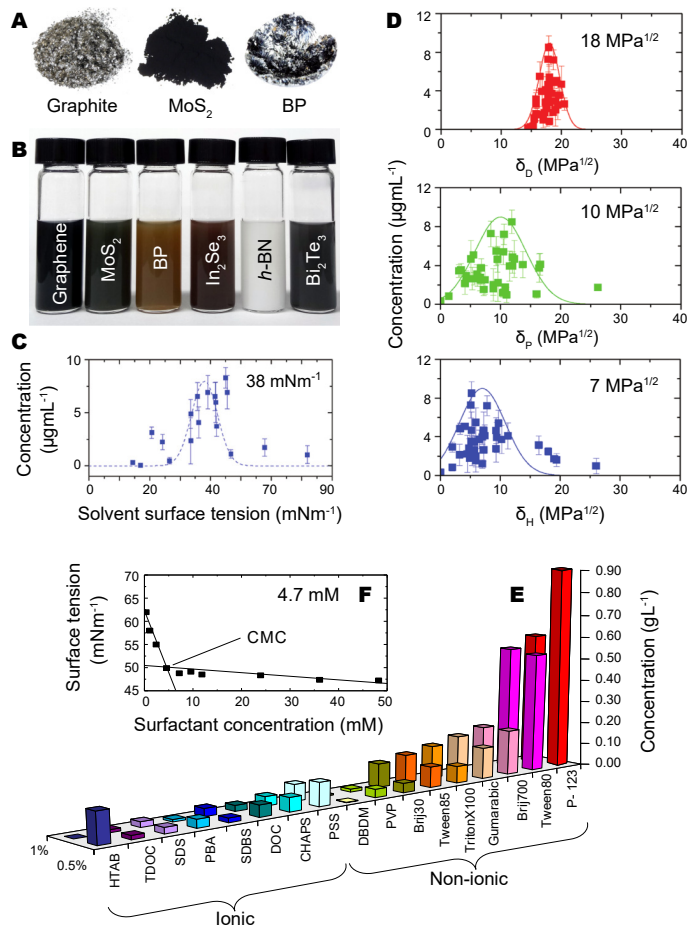

Fig. 2 Liquid phase exfoliation: Photographs of (A) selected bulk materials before exfoliation, and (B) 2d material dispersions. The concentration of graphene dispersions with respect to (C) solvent surface tension and (D) HSPs with fitted curves. Reproduced with permission[134]. Copyright 2012, American Chemical Society. (E) Concentration of graphene in stable aqueous dispersions using common surfactants. Reproduced with permission[135]. Copyright 2011, Elsevier Ltd. (F) Surface tension of SDC solution with respect to the surfactant concentration at ambient, showing the surface tension is stabilised above CMC. Reproduced with permission[71]. Copyright 2016, WILEY-VCH Verlag GmbH & Co. KGaA, Weinheim. The micrograph of bulk BP material is reproduced from Smart-Elements with permission.

uid medium significantly defines the exfoliation process and the subsequent dispersion of the exfoliated 2d materials in the liquid[82,94,136]. For the majority of the (opto)electronic applications, the preferable liquid medium is a pure solvent as this does not introduce impurities into the exfoliated 2d materials, and hence their subsequent deposition for device fabrication. The characteristics that define whether a pure solvent can perform a good intermolecular interaction are usually whether the solvent has a matched surface tension (to reduce the energy 'cost' associated with exfoliation) and Hansen solubility parameters (HSPs; to favour stabilisation) to those empirically derived for 2d materials[94,137]. As shown in Fig. 2(C), the concentration of graphene dispersions is maximised at a solvent surface tension of ~38 mNm^{-1}[134] (converted from the solvent surface energy[90]). Therefore the empirically obtained optimal solvent sur-

This journal is © The Royal Society of Chemistry [year]

Chem. Soc. Rev., [year], [**vol.**], 1–35 | 5

face tension for LPE of graphene is 38 mNm^{-1}. A more refined approach uses optimal matching of respective dispersive, polar and hydrogen-bonding HSPs of the solvents with empirically derived HSPs of the 2d materials, as depicted for graphene in Fig. 2(D) [134]. In this context, the solvents with optimal surface tension and HSPs are typically high boiling point organic solvents, for instance NMP (~204°C) and dimethylformamide (DMF; ~153°C) [138].

Such high boiling point solvents present significant challenges in dispersion processing and deposition for device fabrication [139]. For instance, the use of NMP as the primary solvent in 2d material inks results in particularly long drying/curing time and is impractical for the majority of printing technologies. It is therefore preferable to use LPE with low boiling point solvents, such as water and alcohols. However, both water and alcohols fail to meet the above solvent selection criteria with mismatched surface tension and HSPs [138,139]. For these solvents, a strategy of using their mixtures with optimised surface tension and HSPs distance has emerged [140,141]. For example, a mixture of water and alcohol has been successfully demonstrated as a viable liquid medium [140]. However, this only supports comparatively low concentrations of 2d materials [140,141]. Alternatively, as shown in Fig. 2(E), a range of ionic and non-ionic surfactants can be employed for electrostatic and/or steric stabilisation [136]. Surfactants act by adsorbing onto the surface of 2d materials, promoting their stabilisation in the solvents. This strategy typically supports higher concentrations of stabilised (*i.e.* not sedimented) flakes in the liquid environment.

It has been demonstrated that some of the most effective ionic surfactants for the dispersion of 2d materials are facial amphiphiles (*i.e.* molecules with a quasi-flat molecular structure with hydrophobic and hydrophilic faces), for instance bile salts such as sodium cholate (SC) and sodium deoxycholate (SDC) [71,90,142]. When such ionic surfactants and 2d materials interact in water, the surfactant molecules are adsorbed onto the 2d surface of the flakes, generating temporary effective charge. This can balance the intralayer vdW forces, and hence aid the exfoliation process [143]. The induced charge around the exfoliated 2d material flakes generates a Coulomb repulsion which further prevents reaggregation [90,144]. The required concentration of an ionic surfactant for stabilisation can be estimated by surfactant critical micelle concentration (CMC), which is typically determined by the critical surface tension of its solution against concentration, as shown in Fig. 2(F) [71]. Below CMC, further addition of the surfactant causes a large change in the surface tension as the surfactant molecules assemble at the solution-air interface. Above CMC, the interface is saturated where the surfactant molecules spontaneously arrange into micelles, such that further addition of surfactant causes minimal changes.

Typical non-ionic surfactants include Triton-X, Tween and Brij series, and polymers such as sodium carboxymethylcellulose (Na-CMC), polyvinylpyrrolidone (PVP) and ethyl cellulose [129,135,145]. The polymers can attach onto or encapsulate the 2d material flakes, and hence provide a physical separation between the flakes to allow enhanced exfoliation and stabilisation [146,147]. Liang *et al.* demonstrated the addition of ethyl cellulose in ethanol for exfoliation and stabilisation of graphene flakes using this strategy [147]. The authors suggested that the cellulose created a colloidal dispersion and prevented the graphene flakes from aggregation [147]. Polymers are of particular interest for subsequent ink formulation as they can function not only as binders but also can be used to tune the physical properties of the inks for relevant printing technologies (Section 4.1.1).

Unlike ion intercalation or exchange, as a purely physical exfoliation approach, LPE does not induce alteration of the properties of the 2d materials [3]. For example, Hernandez *et al.* demonstrated that the as-produced graphene flakes were pristine with minimal defects and chemical functionalisations [82]. LPE therefore offers greater potential for the exploitation of the intrinsic material properties of 2d materials for printable applications when compared to ion intercalation or exchange.

3.3 Reduced graphene oxide

Another widely employed production method of graphene, more specifically rGO, is through reducing graphene oxide (GO) [87,148]. In general, GO can be produced through oxidation of graphite by exposure to acid in the presence of an oxidising agent, following the Hummers, Brodie or Staudenmaier methods [80,148]. This oxidation process introduces functional groups such as hydroxyl and epoxide on the basal plane of graphite layers, and hence disrupts the interlayer forces and increases the interlayer spacing, allowing exfoliation into individual GO flakes [87,149,150].

GO can be reduced to graphene, *i.e.* rGO, through thermal or chemical treatments [87,149,150]. Chemical reduction typically makes use of hydrazine as the reductant, although a wide variety of other reducing agents or processes may also be used [80]. One common approach is to use thermal reduction which requires heating GO samples to 200-1,000°C. These reduction processes can only partially restore the properties of graphene, and hence rGO remains a highly disordered, defective material with oxygen functional groups in contrast to the pristine graphene produced by other solution-processing methods [87,149,150]. We note that, Voiry *et al.* demonstrated that by using microwave treatment, GO could be reduced to pristine graphene with the oxygen functional groups almost entirely removed [151].

Compared to typical solution processing methods, however, the chemical oxidation and reduction processes of graphene can be complex and can significantly raise the production cost. Although promising for inks, this may prove to be an obstacle in developing simple and inexpensive printable applications.

3.4 Sorting of the exfoliated 2d material flakes

After solution processing, the exfoliated 2d materials are heterogeneous in lateral size and thickness [4,152]. The physical properties of 2d materials, such as the electronic bandgap, are strongly layer dependent, especially at their atomically thin limit; therefore sorting of these flakes is essential to overcome the structural polydispersity. Centrifugation is a flake sorting technique to achieve structural homogeneity [4,152,153].

Upon centrifugation, a dispersed flake is mainly subjected to two forces: the centrifugal force, and the friction force opposite

to the centrifugal force. Sedimentation is driven by the imbalance between these two forces. As schematically illustrated in Fig. 3, centrifugation allows controlled separation of the flakes, and can be split into three major categories: (1) sedimentation-based separation or centrifugation (SBS) of 2d material flakes based on their mass; (2) sedimentation-based density gradient ultracentrifugation (sDGU), which also sediments 2d materials based on their mass, however, with controlled density gradients for precise lateral size separation; (3) isopycnic DGU (iDGU) for precise thickness separation of 2d material flakes based on their buoyant density.

SBS is the simplest, most straightforward and most widely exploited sorting technique [80]. It is practised in a uniform liquid medium with constant physical properties (*e.g.* density and viscosity), for instance pure solvents such as NMP. Upon centrifugation, polydispersed 2d material flakes sediment with different rates: larger and/or thicker flakes sediment more readily than smaller and/or thinner ones as a result of their larger mass to surface area ratio; flakes in general are more readily sedimented at higher larger centrifugation speeds. As presented in Fig. 3(B), an increased centrifugation speed led to an increased sedimentation of BP flakes in NMP, N-Cyclohexyl-2-pyrrolidone (CHP) and isopropanol (IPA), and hence lower concentration (represented by the respective visual contrast). Besides the dispersion stability against sedimentation, the difference in the BP concentration among these three solvents also indicated a smaller flake size distribution in NMP [12]. Indeed, the lower optical scattering exponent (n) from the BP flakes in NMP (1.9) compared to those in CHP (1.5) or IPA (0.5), as shown in Fig. 3(C), suggested smaller BP flake sizes [12]. The SBS approach is usually used for simple sorting of the exfoliated flakes from the unexfoliated larger and/or thicker flakes.

The sedimentation rate can be controlled by using density gradients which provide gradient density and viscosity, avoiding subsequent cross contamination in the size of the 2d material flakes [4,154]. Here the density gradient medium is required to be miscible with the 2d material dispersion. This is the so-called sDGU. In principle, a 2d material dispersion is initially placed on top of such a density gradient, such that the 2d material flakes can sediment with different sedimentation rates upon centrifugation. For instance, Backes *et al.* employed deuterium oxide (D_2O) and water mixture as a density gradient for a water-based MoS_2 dispersion to achieve separation of MoS_2 flakes with different lateral size [154]. Furthermore, sDGU with a linear density gradient can provide a narrower distribution in the flake lateral size. In Fig. 3(E), for example, lateral size separation of deoxygenated aqueous dispersion of BP flakes was achieved by performing sDGU in a linear iodixanol density gradient, allowing isolation of BP flakes with lateral size of >200 nm [40].

While both SBS and sDGU are based on mass sedimentation, iDGU is solely based on buoyant density [4]. In this process, 2d material flakes with surfactants (*i.e.* flake-surfactant complexes) sediment through the gradient until they arrive at their isopycnic points in the density gradient medium. Since buoyant density is strongly dependent on thickness and barely on lateral size of the flakes, this approach is promising to achieve layer-by-layer flake
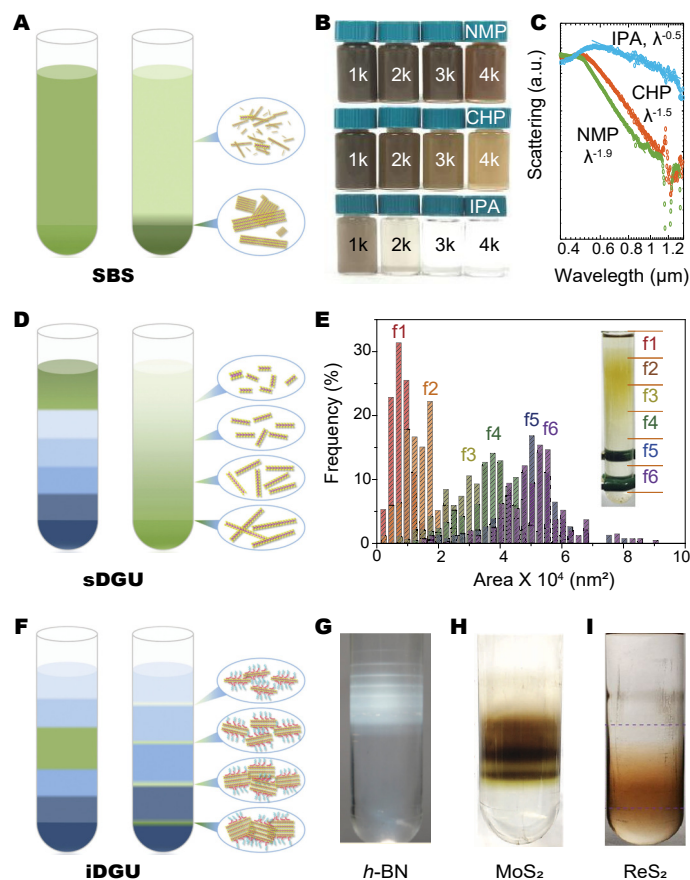

Fig. 3 Sorting of 2d material flakes: Schematics showing (A) SBS, (D) sDGU and (F) iDGU. Reproduced with permission [155]. Copyright 2016, WILEY-VCH Verlag GmbH & Co. KGaA, Weinheim. (B) BP size selection *via* SBS, and (C) the corresponding normalised scattering. The exponent of λ represents optical scattering exponent (n). Reproduced with permission [12]. Copyright 2017, Nature Publishing Group. (E) sDGU for precise size selection of BP. Reproduced with permission [40]. Copyright 2016, National Academy of Sciences. (G) Layer-by-layer iDGU selection of *h*-BN. Reproduced with permission [156]. Copyright 2015, American Chemical Society. (H) iDGU of high density MoS_2 by using polymeric surfactants. Reproduced with permission [157]. Copyright 2014, Nature Publishing Group. (I) iDGU of high density ReS_2 by using density gradient medium mixture of iodixanol and CsCl. Reproduced with permission [158]. Copyright 2016, American Chemical Society.

separation. iDGU was first exploited in the sorting of graphene flakes by Green *et al.* [142] In this process, low molecular weight, planar structure SC was used to encapsulate the graphene flakes and form graphene-SC complexes, which separated into multiple bands based on the graphene layer thickness upon centrifugation [142]. Later on, iDGU was extended to *h*-BN sorting due to a similar buoyant density (Fig. 3(G)) [156]. However, 2d materials such as TMDs that have a significantly higher buoyant density than the commonly used density gradient medium, iodixanol, may require modification of the surfactant chemistry to use iDGU, for instance by using bulkier co-polymeric surfactants with long hydrophilic chains to reduce the overall buoyant densities [157]. As shown in Fig. 3(H), Kang *et al.* demonstrated iDGU sorting of MoS_2 using Pluronic F68, where the MoS_2-Pluronic F68 complex

This journal is ©The Royal Society of Chemistry [year]

Chem. Soc. Rev., [year], [**vol.**], 1–35 | 7

presented effective hydration layer for a reduced overall buoyant density[157]. Alternatively, higher density gradient media can be used. For example, cesium chloride (CsCl) with a high density of up to $\sim$1.91 gcm^{-3} compared to that of iodixanol (1.32 gcm^{-3}) is a viable choice. However, CsCl based density gradients are relatively unstable, due to significantly lower viscosity and higher diffusivity, preventing its practicality for 2d material sorting. In this context, a desirably stable gradient with enough viscosity and high buoyant density may be achieved concurrently by using iodixanol and CsCl mixtures, as demonstrated in Fig. 3(I) where sorting of heavy ReS$_2$ was allowed in iodixanol and CsCl mixture[158].

4 Functional 2d material inks

The as-produced dispersions of exfoliated and/or sorted 2d material flakes can be readily formulated into functional inks for printing. Common printing processes include digital inkjet printing, and 'non-digital' screen, gravure and flexographic printing processes. These processes differ significantly in achievable resolution and production speed (Fig. 4). Therefore, the printing process selection depends largely on the target printed feature size, fabrication throughput and the printed substrates[125]. For instance, inkjet printing is a non-contact, high-resolution, maskless patterning technology. This makes inkjet printing particularly interesting for lab-scale 2d material based device demonstrations, especially during the prototyping stage where minimal volume (1-2 mL) of low loading inks (*e.g.* even the as-produced LPE dispersions with <0.1 wt.% 2d material concentration) are sufficient[7–13,24]. In contrast, the flexographic process has a much higher printed throughput which translates into inexpensive, scalable and efficient device manufacturing[125]. This in return requires large volume (typically >1 L) of high loading inks (typically >10 wt.% 2d material concentration) for prototyping[5,125]. Thus, it is important to select a specific printing process and ink to suit the target application. In this section, we discuss the basics of graphics and functional 2d material inks, providing a context for printable 2d material application development (Section 5).

4.1 Basic principles of ink systems

The use of inks originates from ancient China when soot was mixed with gum resins to make painting paste. It would be around 3,000 years later before hand-carved wooden images, the origin of printing, were developed to use inks for letter reproduction. The earliest printing press with replaceable/moveable wooden or metal letterpress was developed in 1436, laying the foundation for the modern printing technologies.[159]

4.1.1 Ink composition

The advances in printing over the last several hundred years also inspired ink development, with pigments evolving from soots, coloured earth and plants to organic/inorganic chemicals, along with various additives developed to tailor ink properties to suit the targeted printing processes[159]. Typically, modern graphic and functional ink systems are composed of pigments, binders, additives and solvents[160–162].
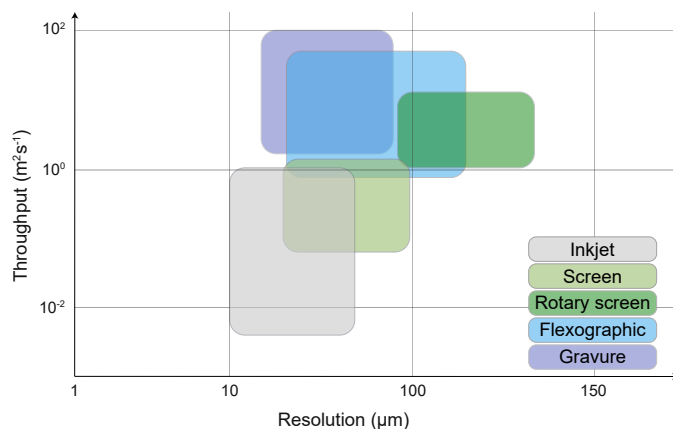

Fig. 4 Comparison of print throughput and best achievable resolution ranges of conventional print technologies for 2d materials.

Pigments The basic function of pigments is to give colour to the ink, just like the exploitation of soot, earth and plants in the early inks. More recent inks use chemical colouring pigments, for instance lithol (red), phthalocyanine (green) and indanthrene (blue). Pigments with special colouring functions may also be used. For example, extenders (*e.g.* CaCO$_3$) are pigments that reduce the colour intensity of other pigments, while opacifiers (*e.g.* TiO$_2$) make the print opaque to obscure any pigment underneath. There are also pigments that can provide gloss, abrasion resistance, and even protection against ambient conditions (*e.g.* light, heat, solvents and chemicals).

In the last twenty years, the use of printing for electronics has arisen, where functional materials are incorporated into the ink systems as active pigments[5,125]. These inks are then used as a vehicle to deposit and pattern these materials onto a substrate for functional device fabrication[5,125]. Common active pigments include various conducting, semiconducting and dielectric materials[5,125], for instance metallic nanoparticles[163], organics[164] and carbon materials (*e.g.* carbon black, CNTs)[165]. More recently, there is a great interest in investigating the solution-processed 2d materials as functional pigments as a way to exploit their unique material properties[6,155].

Binders The binders are typically polymers, such as acrylics, alkyds, cellulose and rubber resins. They form an integral part of the prints, binding the pigment particles to each other and to the substrate. Binders may simply dry and solidify by solvent evaporation, or may require some form of curing (*e.g.* annealing or exposure to radiation, such as ultraviolet light) in order to crosslink. Binder selection can contribute specific physical properties to the printed films, such as gloss level, adhesion or resistance to certain ambient conditions. For instance, water insoluble polymers (*e.g.* cellulose) can provide resistance to moisture.

Additives A <5 wt.% of additives may be used to modify or tailor specific properties of ink systems. For instance, additives such as surfactants may be used to improve the wetting properties of either the pigments or the substrates, whereas defoamers may be used to reduce the surface tension of water-based inks to avoid bubble formation during the print process. Additives may also be

selected to modify certain functionalities. For instance, alkalis can be incorporated into water-based inks to develop a mildly basic pH to dissolve polymeric binders (*e.g.* cellulose). The polymeric binders can then form an integral part of the dried printed films to aid moisture resistance.

Solvents   Solvents are the diluent to the other ink components (*i.e.* pigments, binders and additives). The primary function of solvents is to keep the ink in a fluid form such that the ink can be applied to the printing press (*e.g.* printing plate and cylinder) until it is transferred to the substrate.

Water or any of a broad range of organic solvents can be used, depending on the printing processes, the substrates, the drying conditions and the final purpose of the prints. For example, since high-speed processes such as gravure and flexographic printing require rapid ink drying, the solvents typically need to be volatile. Solvents commonly used for gravure and flexographic printing therefore include ethyl acetate, n-propyl acetate and IPA. Screen printing, however, requires slightly less volatile solvents with moderately low evaporative rates, such as aromatic distillates and butoxyethanol, to avoid clogging of the screen mesh associated with fast ink drying.

4.1.2   Ink viscosity

The precise composition of the ink components defines the physical properties of the inks (*e.g.* viscosity, surface tension, density and drying rate) that affect the printing process. Ink viscosity is a key consideration in suiting a particular printing process. Viscous inks are required for screen printing whilst highly fluent, low viscosity fluids are desired by inkjet printing. Table 2 presents the ink compositions and the static viscosities for common print technologies for 2d materials.

Viscosity is a rheological description of a fluid with respect to the shear stress, the shear rate and the shear time [166–168]: it is typically a measure of the resistance at a given time and is defined as the ratio of the shear stress to the shear rate; the measured viscosity is dependent on its prior exposure to the external stress. A higher viscosity means that the fluid is more difficult to flow and is more resistant to stress. Figure 5(A) shows common rheological behaviours of fluids. A typical fluid can be categorised into *Newtonian* fluids or *non-Newtonian* fluids. A *Newtonian* fluid is an ideal fluid with a linear shear stress/shear rate relationship, *i.e.* a constant viscosity. In practice, however, a fluid usually shows some level of deviation from this *Newtonian* behaviour as *pseudoplastic* fluids, *dilatant* fluids, or *Bingham* fluids [166–168].

A *pseudoplastic* fluid shows reduced shear stress under increased shear rate, observed as a drop in viscosity, meaning that the fluid requires less force to maintain flow at higher shear rates. The *pseudoplastic* behaviour is important for ink formulation, as in this case the ink pigments are more readily dispersed under stress. *Pseudoplastic* further suggests that the ink is easy to flow through the printing press by transferring from component to component and from roll to roll (high shear rate), but is prevented from overspreading once printed on to the substrates (low shear rate) [160,161]. As shown in Fig. 5(B), the graphene ink systems developed by a research group at the Northwestern University are all *pseudoplastic* fluids, with controlled viscosity and

Table 2 Typical compositions and viscosities of inks for common printing technologies. The data is collected from Ref. 160–162, 169–176.

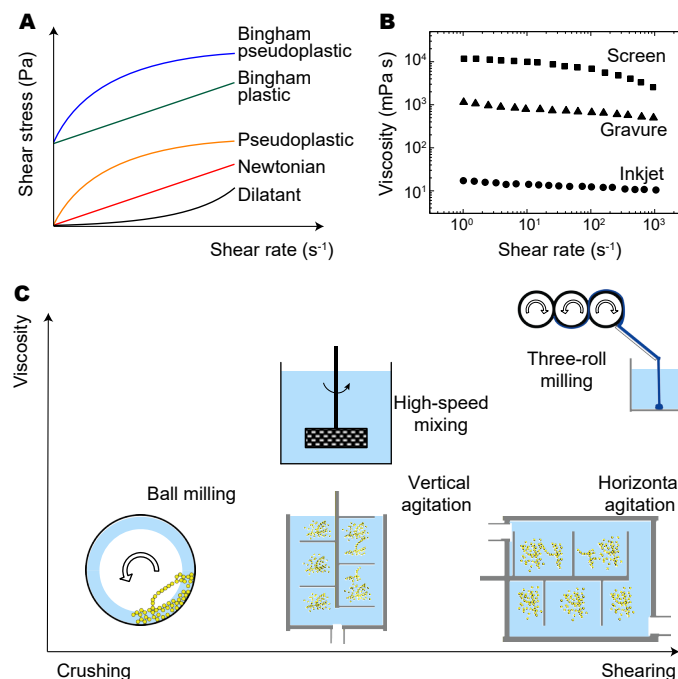|	Ink composition (wt.%)				Viscosity
	Pigment	Binder	Solvent	Additive	(mPas)
Inkjet	5-10	5-20	65-95	1-5	4-30
Screen	12-20	45-65	20-30	1-5	1 k-10 k
Gravure	12-17	20-35	60-65	1-2	100-1 k
Flexo	12-17	40-45	25-45	1-5	1 k-2 k

Fig. 5 Ink viscosity and processing: (A) Schematic showing shear stress of different fluids with respect to shear rate. (B) Comparison between viscosities of graphene inks for inkjet, gravure and screen printing with a graphene loading of ∼1 wt.%, ∼3 wt.% and ∼8 wt.%, respectively. Data collected from Ref. 16, 21, 23. (C) Common pigment processing techniques for ink formulation.

printability across different printing processes [16,21,23]. Note the viscosity was designed by the selection of solvents, binders and loading of graphene flakes.

As opposed to *pseudoplastic* fluid, a *dilatant* fluid shows increased viscosity under shear. A *dilatant* fluid is usually highly concentrated suspensions in a colloidal form. On the other hand, *Bingham* fluids exhibit yield stress, such that the fluids need to overcome this finite stress to flow. A *Bingham* fluid may behave as *Bingham plastic* of which the viscosity is constant upon stress, or *Bingham pseudoplastic* of which the viscosity decreases under stress.

4.1.3   Ink processing

For the ink systems, the mixture of binders, solvents and additives is commonly termed as varnish [160,162]. The ink is usually formulated in three steps: the first step is to develop a varnish; the second step is to disperse the pigments; the third step is let-down which is the final adjustment process of the physical properties of

This journal is © The Royal Society of Chemistry [year]

Chem. Soc. Rev., [year], [**vol.**], 1–35 | 9

the ink by tuning its compositions.

The varnish is simply a liquid vehicle to carry the pigment portion of the ink onto the substrate. To produce the varnish, the binders and additives are dissolved directly into the solvents. The physical properties of the produced varnish define the wetting of the pigment particles, and significantly govern the properties of the formulated inks[160,162]. Varnish development therefore requires a selection of binders and additives as well as the solvents to render physical properties that suit both the pigment themselves and the target printing process. Depending on the solvents, the varnish can be classified into two key types, *i.e.* water-based or organic solvent-based. A water-based varnish uses water as the primary solvent to dissolve the binders and additives. It is easy to apply as the varnish is easily solidified after the evaporation of water. There is a high demand to develop water-based ink formulations, as water is environmentally friendly. As opposed to this, organic solvent-based varnishes use organic solvents to dissolve the binders and additives. Solidifying the varnish usually takes place after the solvents are fully evaporated. In some situations, the varnish may require long drying times and even a curing process (*e.g.* annealing or exposure to ultraviolet radiation) to solidify.

Once the varnish is developed, the pigments are dispersed for ink formulation. The 'raw' pigments are usually available in the form of lumps and aggregates. A pigment dispersion process is required to break down such lumps and aggregates into primary acicular, cubic or spherical particles. A range of dispersion technologies can be selected depending on the viscosity and the desired particle size for the pigments, as shown in Fig. 5(C). Ball milling and agitation are suitable for low viscosity systems (*e.g.* inkjet inks), where ball milling uses grinding balls/beads to crush while agitation exploits impeller blades to shear the raw pigments[160,161]. High-speed mixing uses meshed screens and high-speed rotating blades to break up the raw pigments[160,161]. This technique is suitable for medium viscosity systems (*e.g.* gravure and flexographic inks). Three-roll milling is suitable for highly viscous systems (*e.g.* screen inks). It employs a set of cylindrical rolls with precisely controlled gaps to shear the passed through raw pigments[160,161].

4.1.4 Ink spreading and drying

Once an ink is produced and printed, the subsequent ink spreading and drying define the morphologies of the printed patterns. The spreading of ink over a solid surface is defined by wetting, which can be explained by Young's equation[177]:

$$\gamma_s = \gamma_{s-ink} + \gamma_{ink} \cos\theta \qquad (1)$$

where γ_s is the surface energy of the solid surface, γ_{ink} is the surface tension of the ink, γ_{s-ink} is the interfacial energy between the solid and ink, and θ is the formed contact angle, as depicted in Fig. 6(A). A small contact angle ($\ll 90°$) suggests a good wetting, while a large contact angle ($\gg 90°$) indicates a poor wetting. For instance, $0°$ is perfect wetting and spreading, while $180°$ is perfect non-wetting. A good wetting means that the ink is capable of spreading over and maintaining contact with the solid surface for
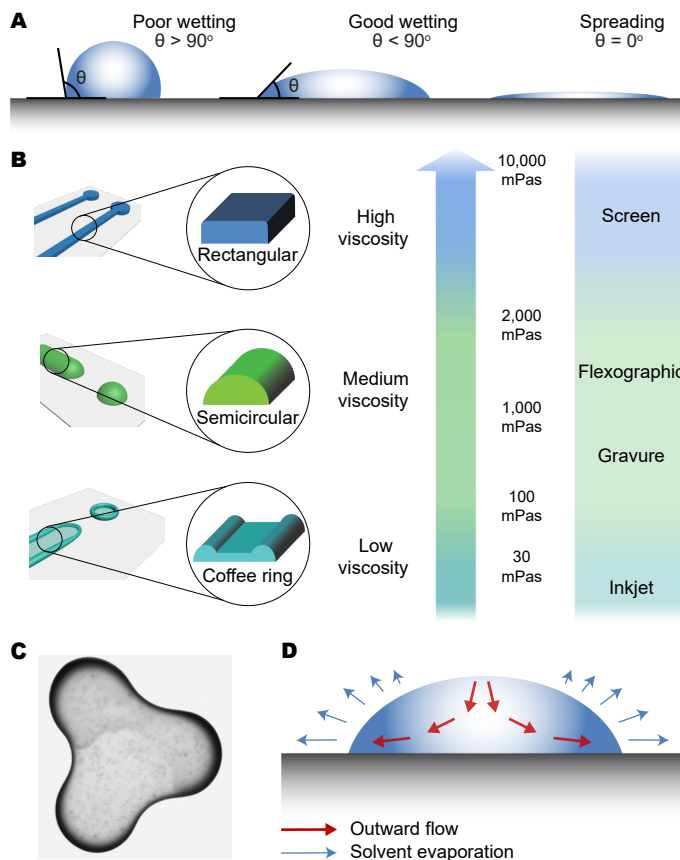

Fig. 6 Ink wetting and drying: (A) Different wetting behaviour of a droplet on substrates. (B) Typical cross section profiles of printed lines, showing low viscosity inks tend to form coffee ring. (C) Photograph of a dried coffee drop. Reproduced with permission[179]. Copyright 1997, Nature Publishing Group. (D) Schematic of a typical evaporation profile in a drying droplet for coffee ring formation. Due to higher evaporation rates at the droplet edge, an outward flow from the droplet centre is initiated. This carries the suspended particles to the droplet edges.

a continuous feature, in which case $\gamma_{ink} < \gamma_s$. Therefore, metals with high surface energies such as copper are easy to wet, while plastics such as polytetrafluoroethylene (PTFE) with a low surface energy are difficult to wet. A poor wetting means that the ink cannot remain in contact with the surface and as such the ink tends to retract and *bead up*, leading to a discontinuous material deposition.

Within the print industry, it is generally considered that if the surface tension of the ink is 7-10 mNm^{-1} lower than the surface energy of the substrate, appropriate wetting can be achieved[178]. For functional printing, a good wetting is of critical importance as a continuous deposition of the functional materials is required for reliable device fabrication, especially with regard to conductive or dielectric formulations. Table 3 lists the surface tensions and surface energies of some solvents and substrates, respectively. As presented, to perform functional printing on substrates commonly used in electronics and optoelectronics, *e.g.* Si/SiO$_2$, glass and plastics such as polyethylene terephthalate (PET), the ink surface tension should be sufficiently low (*e.g.* <30 mNm^{-1})[12,22,25].

Assuming reliable ink spreading, the morphology of the printed

Table 3 Surface tensions (at 20°C) and energies of common solvents and substrates. Data collected from Ref. 180–182.

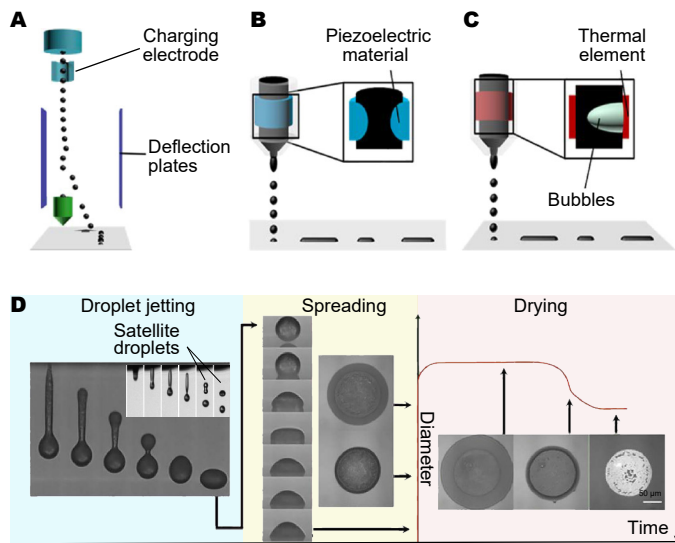| Solvent	γ_{ink} (mNm^{-1})	Substrate	γ_s (mNm^{-1})
Water	72	Copper	1,000
Glycerol	64	Aluminium	500
Ethylene glycol	48	Kapton (DuPont)	50
Epoxy resin	43	PET	48
NMP	40	Polyamide	46
CHO	34	Polycarbonate	46
Chlorobenzene	34	Polyurethane	40
Terpineol	33	Polyimide	40
Ethyl acetate	24	Si/SiO$_2$	36
2-butanol	23	Glass	36
IPA	23	Polystyrene	34
Ethanol	22	Silicone	21
Hexane	18	PTFE	18

Fig. 7 Inkjet printing principles: Schematics of (A) CIJ, and DoD inkjet printing with (B) piezoelectric and (C) thermal head. (D) The complete inkjet printing process, showing the droplet jetting, spreading and drying stages. Reproduced with permission [185]. Copyright 2014, Elsevier B.V. Inset: jetting with unwanted satellite droplets. Reproduced with permission [186]. Copyright 2009, American Chemical Society.

pattern is further defined by the ink viscosity. Figure 6(B) schematically presents typical cross-sectional profiles for printed lines with inks of high, medium or low viscosities [125]. High viscosity inks that contain high levels of pigments and binders, for instance screen inks and in some cases viscous gravure and flexographic inks, tend to form a rectangular shape. This represents a uniform deposition of ink, and hence a uniform distribution of material properties required for device fabrication. For medium viscosity gravure and flexographic inks and low viscosity inkjet inks, an ideal cross-sectional printed profile is usually a semi-circular arc due to lower binder and pigment content. However, a common profile for inkjet inks may be represented by an unwanted 'coffee ring' shape, where the deposited material dries to be concentrated on the periphery of the print, leaving a concave central area. Figure 6(C) shows a typical example of 'coffee ring'.

The coffee ring effect is a common and unwanted phenomenon related to ink drying [179]. A widely accepted explanation, reported by Deegan *et al.*, attributes this effect to a non-uniform solvent evaporation across the droplet during the ink drying process [179]. As presented in Fig. 6(D), when a droplet is deposited onto a substrate, the evaporation rate is typically highest at the edge of the droplet-substrate interface (also known as the contact line) due to the highest surface area to volume ratio. During drying, the contact lines may pin the droplet, such that an outward convection flow would have to be induced from the droplet centre to the edges to replenish the evaporated solvents [179]. This outward convection flow thereby deposits the dispersed material at the droplet edges, leaving little to no material at the droplet centre. This process is heavily dependent on the drying conditions and surrounding environment [183] and has not been extensively studied for functional ink formulation.

4.2 Inkjet printing of 2d materials
4.2.1 Inkjet printing principles

Inkjet printing is a digital, non-contact printing technique where the ink droplets are jetted and deposited in a rapid succession onto the substrate to generate an image [170]. The word 'digital'

means that the printing pattern is designed electronically, and the deposition of the ink droplets is controlled by a computer. When 2d materials are adapted to inkjet printing, flexible and rapid device design and fabrication is possible, especially during the prototyping stage. This is because a physical mask is not required [184].

Figure 7 (A-C) schematically presents the two prevalent droplet jetting mechanisms for inkjet: continuous inkjet (CIJ) and drop-on-demand inkjet (DoD). As shown, CIJ is a process where a stream of ink droplets is continuously generated and jetted; Fig. 7 (A). The droplets charged by the electrode are subjected to an electrostatic field and selectively deflected to deposit onto the substrate. On the other hand, DoD is a process where the ink droplets are only generated when demanded through a piezoelectric or a thermal inkjet process. In a piezoelectric inkjet process (Fig. 7 (B)), a voltage pulse is applied to the piezoelectric material to induce a change in the shape of the reservoir, and hence a pressure pulse on the ink that forces it out of the ink reservoir as ink droplets. In a thermal inkjet process (Fig. 7 (C)), the ink is rapidly heated up to generate bubbles, which propel the ink out of the ink reservoir as ink droplets. Among these mechanisms, CIJ allows a higher jetting speed, and hence a higher printing efficiency. However, the complexities in controlling of the jetting, deflecting and recycling of the inks have limited the widespread application of CIJ. Due to its simpler operation, DoD has therefore emerged as the main inkjet printing technology.

In the DoD process, a key requirement is a stable jetting of single droplets under each electrical impulse without the formation of satellite droplets (*i.e.* secondary droplets). The satellite droplets can lead to ink deposition on untargeted areas and even deviation from the droplet jetting trajectory [170]. This droplet jetting behaviour is determined by the ink fluidic properties, char-

This journal is © The Royal Society of Chemistry [year]

Chem. Soc. Rev., [year], [**vol.**], 1–35 | 11

Table 4 2d material inks and their printable applications demonstrated to date.

2d materials	Solvents	Binders & additives	Substrates	Applications	Ref.
Inkjet inks					
Graphene	NMP	–	Si/SiO$_2$, glass	FETs	7
Graphene, MoS$_2$	NMP	–	PET with coating	Photodetectors	8
Graphene, TMDs, h-BN	NMP	–	Si/SiO$_2$	FETs, photodetectors	9
Graphene, TMDs, h-BN	NMP	–	PET with coating	FETs	10
Graphene	IPA	–	PET, Polyurethane	FETs	24
Graphene	Water/ethanol	–	PET	Conductive inks	187
Graphene	Water/ethanol	–	Si/SiO$_2$	–	13
MoS$_2$	Water/IPA	–	Si/SiO$_2$	–	97
MoS$_2$	Water/IPA/glycerol	–	Si/SiO$_2$	Gas sensors	188
BP	IPA/2-butanol	–	Si/SiO$_2$, glass, PET	Photodetectors, SAs	12
BP	Acetonitrile	–	Glass	Humidity sensors	189
Graphene	Water	SDBS, PANI	Carbon	Supercapacitors	190
Graphene	Water	PEDOT:PSS	Carbon	Gas sensors	191
Graphene, TMDs	Water	PS1	Si/SiO$_2$	Photodetectors, memory	11
Graphene, MoS$_2$	IPA, NMP, Terpineol/CHO	Ethyl cellulose	PET	Photodetectors	192
Graphene	IPA	PVP	Si$_3$N$_4$	Humidity sensors	22
Graphene	IPA	PVP	FTO glass	Solar cells	25
Graphene	IPA	PVP	Kapton, glass	Thermoelectrics	92
Graphene	IPA/n-butanol	Plasdone S-630	Paper	Conductive inks	193
Graphene	Terpineol/ethanol	Ethyl cellulose	Si/SiO$_2$, glass	FETs	89
Graphene	Terpineol/CHO	Ethyl cellulose	Si/SiO$_2$, Kapton	Conductive inks	14
Graphene	Terpineol/CHO	Ethyl cellulose	Glass, PET, PEN, PI	Conductive inks	88
Graphene	Ethyl lactate/octyl acetate/ethylene glycol diacetate	Nitrocellulose	Glass, Kapton	Conductive inks	23
Graphene	Diethylene glycol/ethanol	PEDOT:PSS	Polyurethane	Temperature sensors	194
MoS$_2$	Terpineol/ethanol	Ethyl cellulose	Si/SiO$_2$	FETs	99
h-BN	Water	Na-CMC	PET, Polyurethane	Dielectric inks	24
Flexographic inks					
Graphene	Water/IPA	Na-CMC	ITO PET	Solar cells	19
Graphene/carbon ink	–	–	Glass, PET, paper	Conductive inks	20
Gravure inks					
Graphene	Terpineol/ethanol	Ethyl cellulose	Kapton	Conductive inks	21
Screen inks					
Graphene	Ethanol	PTFE, PANI	PET	Supercapacitors	15
Graphene	Terpineol/ethanol	Ethyl cellulose	Si/SiO$_2$, Kapton	Conductive inks	16
Graphene	Dipropylene glycol	PVP/PVA	PET	Conductive inks	17
Graphene	Water	Na-CMC	Glass, paper	Conductive inks	18
MoS$_2$/carbon-graphite ink	–	–	Paper	Oxygen reduction	195
h-BN	DMF	Polycarbonate	PET, copper foil	Dielectric inks	113

acterised by Z, a dimensionless inverse Ohnesorge (Oh) number[196,197]:

$$Z = \frac{1}{Oh} = \frac{\sqrt{\gamma \rho a}}{\eta} \qquad (2)$$

where η, γ and ρ are the viscosity (mPas), surface tension (mNm^{-1}) and density (gcm^{-3}) of the ink, respectively, and a is the diameter (μm) of the jetting nozzle. As a rule of thumb, a value of 1-14 for Z suggests stable ink jetting. A value of >14 indicates the formation of satellite droplets while <1 suggests elongated ligaments that may also break up into satellite droplets, or even prevent droplet formation from occurring at all[7,186,196].

The 'droplet jetting' stage in Fig. 7(D) is a demonstration of stable droplet jetting with $Z = 3.5$[185], while the inset shows generation of satellite droplets with $Z = 17.3$[186].

As presented in Fig. 7(D), immediately after jetting, the droplet impacts, spreads and dries on the substrate towards a designed printed image[185]. Upon impact, the droplet undergoes a spreading stage where the inertial force dominates[196]. This stage leads to a maximum droplet spreading until a capillary force driven spreading stage takes over[196]. The capillary driven stage is further divided into two situations depending on wetting. For inks with sufficient wettability, the droplet continues a capillary

spreading. For inks with insufficient wettability, the droplet retracts and *beads up* towards a discontinuous material deposition. Therefore, to ensure a continuous deposition, the ink surface tension has to be sufficiently low. Provided that the ink can wet the substrate, however, the drying of low viscosity inkjet inks may lead to coffee ring formation if they are not optimised, as illustrated in Fig. 7(D).

4.2.2 2d material inkjet inks

The as-produced LPE dispersions are the first generation and the most widely used 2d material inks for inkjet printing thus far. LPE dispersions have been demonstrated in a wide range of printable applications, including complex heterostructure devices (Table 4)[7–11]. Generally, LPE dispersions are characterised with a viscosity of <2 mPas, allowing the dispersions to be readily deposited with low viscosity printing and coating technologies like inkjet printing[7,23]. The lateral dimension of the dispersed flakes is typically <200 nm, fitting a general guideline of inkjet printing where the average particle size should be $<1/50^{th}$ of the nozzle diameter (*e.g.* 21 μm) to avoid nozzle clogging[7]. The LPE dispersions are therefore usually printed directly without further ink formulation, for instance the NMP based dispersions of graphene, WS$_2$ and *h*-BN as shown in Fig. 8(A)[9]. However, these dispersions usually deliver inefficient, time consuming printing due to low concentration of 2d materials (<1 gL^{-1}) and the high boiling point of commonly used solvents such as NMP[11,82,94]. Evolving from the NMP based dispersions, printing of LPE dispersions in low boiling point solvents (*e.g.* water and alcohols) emerged. For example, Fig. 8(B) shows an inkjet-printed image from water based graphene dispersion on paper (stabilised with 1-pyrenesulfonic acid sodium salt (PS1))[11].

However, LPE dispersions usually present challenges in achieving controlled patterning of 2d materials, as a result of unstable droplet jetting, poor wetting and the coffee ring effect. The reported Z values are usually >14, suggesting the possibility of satellite droplet formation, especially during long printing sessions[7,8,11,198]. In addition, the LPE dispersions with higher surface tension (*e.g.* NMP and water based) present poor wetting of common substrates (Table 3), as shown in Fig. 8(C). These low viscosity dispersions may also be subjected to a strong coffee ring effect[7,11]. Substrate surface treatment may help towards addressing the above challenges. Torrisi *et al.* showed that self-assembling of bis(trimethylsilyl)amine (HMDS) could lead to a more uniform distribution of graphene flakes; Fig. 8(C)[7]. The authors also showed that that O$_2$-plasma treatment resulted in a poorer flake distribution. This was due to ink overspreading as a result of the increased substrate surface energy. Using absorbent substrates (*e.g.* paper and solid surfaces with porous coating) is an alternative approach[8,10], whereby the 2d material flakes are retained on the surface as the solvents 'wick' into the substrates, leading to an even material deposition.

To address these challenges, evolving from the LPE dispersions, ink formulations using polymeric binders have been developed[14,89,198]. This is usually achieved by extracting the exfoliated 2d materials flakes from the dispersions *via* filtration, sedimentation, solvent exchange or solvent evaporation, and
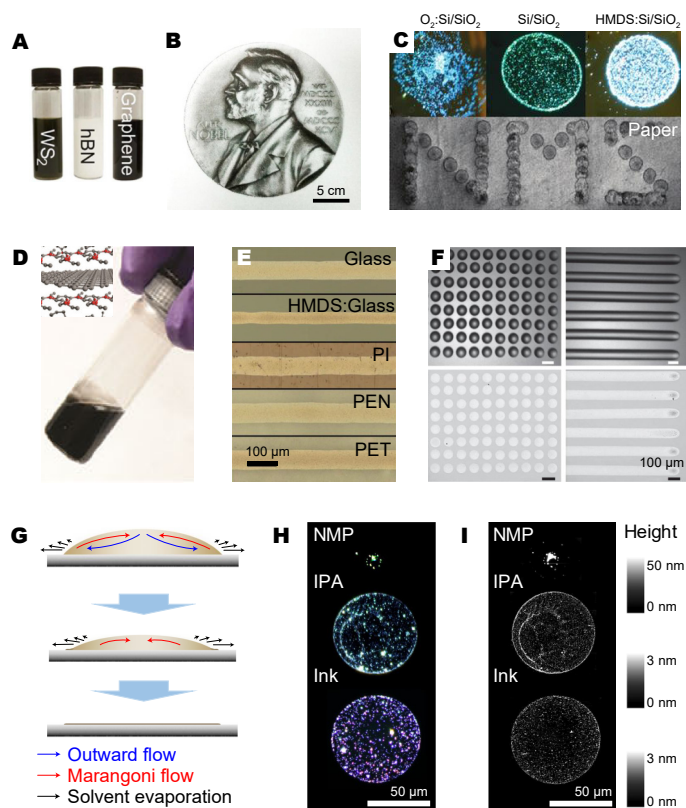
Fig. 8 Inkjet printing of 2d materials: (A) Photograph of representative NMP based 2d material inks. Reproduced with permission[9]. Copyright 2014, American Chemical Society. (B) Inkjet-printed graphene pattern on paper using water based inks. Reproduced with permission[11]. Copyright 2017, Nature Publishing Group. (C) Micrograph of inkjet-printed NMP based inks on Si/SiO$_2$ substrates and paper. Reproduced with permission[7]. Copyright 2012, American Chemical Society. (D) Photograph of ethyl cellulose stabilised graphene ink, and (E) corresponding optical micrographs of inkjet-printed graphene lines onto different substrates, showing uniform pattern definition. Reproduced with permission[88]. Copyright 2015, Wiley-VCH Verlag GmbH & Co. KGaA, Weinheim. (F) Optical micrographs of inkjet-printed MoS$_2$ on Si/SiO$_2$. Reproduced with permission[99]. Copyright 2014, Wiley-VCH Verlag GmbH & Co. KGaA, Weinheim. (G) Schematic of droplet drying process of a binary alcohol-based BP ink, showing induced Marangoni suppresses coffee ring effect, and the corresponding (H) optical micrographs and (I) AFM images of the dried droplets. (G-I) Reproduced with permission[12]. Copyright 2017, Nature Publishing Group.

then redispersing the extracted flakes in selected solvents with polymers for highly concentrated ink formulation. Figure 8(D) is a demonstration of such inks, where graphene produced in ethanol/ethyl cellulose was sedimentated and redispersed in terpineol/cyclohexanone (CHO) with ethyl cellulose[14,88,199]. As shown, this ink formulation supported highly controlled patterning of graphene flakes with spatially uniform flake distribution on a wide range of substrates; Fig. 8(E). This binder ink strategy has also been extended to ink formulation of other 2d materials, for example MoS$_2$; Fig. 8(F). For these inks, it may be necessary to remove the polymeric binders after printing since unlike solvents, the polymers form an integral part of the printed thin films. In the case of applications such as conductive inks, transis-

This journal is © The Royal Society of Chemistry [year]

Chem. Soc. Rev., [year], [**vol.**], 1–35 | 13

tors and photodetectors, polymers in inks can significantly compromise the functionalities (*e.g.* electrical conductivity) of the 2d materials, and hence the intended device performance. The removal of the polymers may be achieved by high temperature annealing or intense pulsed light [14,88]. These post-print treatments, although very effective, may prove too expensive or cumbersome and thereby risk limiting the development of printable flexible applications using polymeric substrates.

Alternatively, to avoid residual binders in printed thin films, a mixed solvent ink formulation approach can be considered. Hu *et al.* demonstrated a binder-free, stable BP ink formulation using a mixture of IPA/2-butanol solvents [12]. The authors proposed that the alcohol mixture induced a recirculating Marangoni flow during ink drying, arising from a surface tension gradient from the generated composition/temperature gradients, as depicted in Fig. 8(G). This Marangoni flow suppressed the coffee ring effect, while the low surface tension ensured wetting of a variety of untreated substrates, enabling spatially uniform, low temperature printing of BP; Fig. 8(H, I).

The morphologies of the printed patterns are further defined by printing parameters such as the spacing between neighbouring droplets. An ideal situation is that the merging of the neighbouring droplets does not cause neither over- nor insufficient-spreading [12,200]. A suboptimal print morphology results in a non-uniformity in the material properties across the patterns. Typically, when the spacing is small, an excessive merging of a track of droplets may lead to overspreading, forming lines with the so-called 'stacked coins' or 'bulging' morphologies. On the other hand, when the spacing is large, the merging is insufficient, forming 'scalloped' lines or even 'isolated droplets'. Using geometric considerations, Hu *et al.* showed that for the mixed solvent ink a droplet spacing of ∼0.5-0.8 to the dried droplet size ensured optimal droplet merging [200], forming lines with 'uniform edges' to represent optimal printing [12]. Similar printing parameters have also been defined previously for other types of ink formulations [200,201].

4.3 Screen printing of 2d materials

4.3.1 Screen printing principles

Screen printing is a stencil process whereby ink is transferred on to the substrate through a stencil screen made of a fine, porous mesh of fabric, silk, synthetic fibres or metal threads. The pores of the mesh are closed in the non-printing areas by a photo-polymerised resin, while the remaining pores in the printing areas are left open to allow ink to flow through [160,202].

Figure 9(A) shows a schematic of a typical flat-bed screen printing process. During printing, the ink is first spread over the screen mesh. A squeegee is then drawn across it, forcing the ink through the open pores. At the same time, the substrate is held in contact with the screen to receive the ink. Many flat-bed screen printing systems still consist of a simple hand-operated unit, which can be particularly useful when printing on very thick or thin substrates that cannot be automatically fed, or where a test run of a new image is required. Flat-bed screen printing systems offer an additional advantage of being able to register precise prints directly
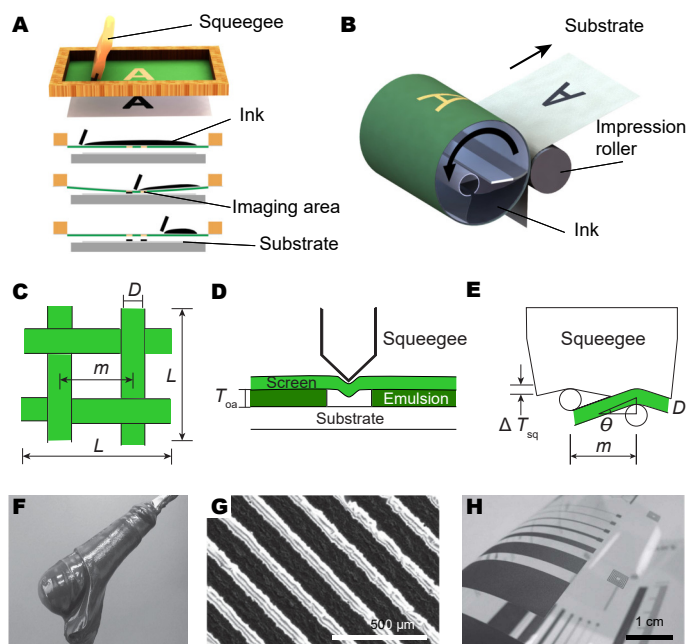

Fig. 9 Screen printing: Schematic figures showing (A) flat-bed and (B) R2R screen printing. (C-E) Schematics illustration of for screen printing principles. (F) Photograph of a graphene ink for screen printing. (G) SEM micrograph of an array of screen-printed graphene lines. (H) Screen-printed graphene pattern on PET. (F-H) Reproduced with permission [17]. Copyright 2016, Wiley-VCH Verlag GmbH & Co. KGaA, Weinheim.

on top of each other [203]. This is important during functional printing where precisely registered contacts and overlapping layers of functional materials are required [204]. Semiautomatic machines have the substrates fed and taken off by hand but utilise a mechanised squeegee blade. Fully automatic flat-bed presses are also available where the substrate is fed in and taken off by automatic feed and delivery systems [171].

Highly efficient cylinder presses can be employed for high-speed R2R printing. As shown in Fig. 9(B), in this setup, the presses and the squeegee remain stationary, while the screen, the cylinder and the substrate move in unison. This permits faster operation, since the substrate does not have to be brought to a halt and fed into a vacuum base as with flat-bed presses. Speeds of up to 80 m^2s^{-1} can be achieved with this process.

In screen printing, the volume of the ink deposited is governed by several factors: (1) the thread count of the screen (*i.e.* the number of threads per unit distance and thread diameter), which in turn defines the open area percentage of the screen; (2) the thread diameter which defines the thickness of the screen (D), and hence the depth of the ink column at each open hole in the mesh (Fig. 9(C)); (3) the pressure, the angle that in turn defines the area of the squeegee in contact with the screen, and the speed of the blade in respect to the screen during ink deposition [160,202,204,205].

According to a model derived in 1990 by Owczarek and Howland [206], the thickness of the ink under the squeegee, T_{ink}, can be

expressed by the following equation with reference to Fig. 9(C-E):

$$T_{ink} = D\left[2 - \frac{\pi}{2}DM\sqrt{1 + (DM)^2}\right]$$

$$= \Delta T_{sq} + T_{oa}$$

(3)

where ΔT_{sq} is the change in height of the squeegee as it is drawn across the screen, T_{oa} is the equivalent open area, M is the mesh count per inch given by $M = 1/m$, and m is the distance between the centre lines of two parallel wires on the mesh. Note that T_{ink} represents the wet ink thickness. The dry ink thickness typically depends on the solid content (*e.g.* pigment, binder) in the ink formulation. Because of their simplicity, screens can be produced cheaply, making screen printing a very attractive process for short-run work.

4.3.2   2d material screen inks

Unlike inkjet ink formulation, 2d material screen ink formulations started with polymeric binders due to the requirement in high ink viscosities. Prior to ink formulation of solution-processed, chemically pristine 2d materials, Zhang *et al.* first demonstrated a rGO ink by dispersing rGO in terpineol with ethyl cellulose as the ink binder[207]. The authors used this ink to develop counter-electrodes for dye-sensitised solar cells (DSSCs)[207]. However, this rGO screen ink required a 400°C treatment to effectively burn off the binder, adversely affecting the adhesion of rGO to the substrate.

Screen ink formulation of solution-processed pristine 2d materials are now beginning to emerge. Graphene has typically been the most investigated subject, although there also have been attempts to incorporate MoS$_2$[195] and *h*-BN[113]. In addition to ethyl cellulose, other polymers have also been experimented with as screen ink binder systems. These include PVP/polyvinyl alcohol (PVA)[17] and polyaniline (PANI)[208]. Figure 9(F) is a photograph of a graphene/PVP/PVA ink, followed by the screen printed patterns using the ink (Fig. 9(G, H))[17]. This graphene screen ink exhibited high electrical conductivity (30 Ω/sq at 25 μm thickness) after drying at 100°C, avoiding the need for high temperature annealing, doping or any other treatments. A graphene/PANI ink, on the other hand, was exploited for printing of supercapacitor electrodes, which could withstand ∼200 bending cycles[208]. Ink formulation by blending graphene with existing carbon/graphite conductive ink formulations, already rheologically optimised for screen printing, has also been demonstrated[209].

Ethyl cellulose has proved popular for 2d material screen ink formulation[207,210,211]. Inherent issues with alternative polymers such as the graphene/PVP/PVA ink, which required highly controlled heating processes to achieve *pseudoplasticity*[17]. The demonstrated *pseudoplasticity*, although eventually shear thinning, proved not ideal for screen printing due to the lack of flow (*i.e.* too high viscosity) when not under shear which therefore was prone to damaging the screens. Though surviving multiple (∼200) bend cycles, the graphene PANI ink required lamination between two plastic sheets in order to be mechanically robust[208]. Ethyl cellulose ink formulations have shown appropriate rheological properties for screen printing and exhibited superior electro-

chemical responses when compared to other binders evaluated to date[195].

4.4   Gravure and flexographic printing of 2d materials

Gravure and flexographic printing are two widely used high-speed R2R processes used in a number of packaging applications, such as labels, plastic and foil packaging. Both gravure and flexographic printing rely on large metal rolls (called the gravure roller and anilox roller, respectively) to meter and control the ink deposited on the surface. Gravure printing is a form of 'direct' printing upon which ink is carried directly from the ink trough to the substrate *via* the gravure roller which not only meters the wet ink application weight but also acts as the print image carrier. Flexographic printing, however, is a form of 'indirect' printing, which involves control of the wet ink application weight by the anilox roller, transferring the metered ink from the anilox to an image plate before the ink is deposited on to the substrate.

As a method of printing 2d materials, however, little work has been done thus far using these printing technologies. This is largely due to the high set up and prototyping cost of producing gravure rollers and printing plates and importantly, the large quantities of ink (>1 L) required to be able to achieve stable trial print runs. However, both these printing processes remain strong viable candidates for high-speed, low-cost manufacturing of 2d material printable applications due to their high throughput.

4.4.1   Gravure printing principles

Figure 10(A, B) show typical schematics of gravure printing process[160,161,171–173]. The printing unit of a gravure press consists of an ink trough in which a metal gravure roller rotates in a fluid ink, and a metal doctor blade which spans the width of the roller and scrapes excess ink from the roller surface[160,171–173,212]. The desired pattern is directly engraved into the metal gravure roller in the form of cells which are designed to get filled with ink as the roller rotates in the ink[160,172,205,213]. Ink transfer is achieved by passing the substrate between the gravure roller and an impression roller.

The ink used for gravure printing usually has a medium viscosity (100-1,000 mPas). Due to the inherent R2R feeding system, gravure printing can deliver a printing speed of up to 1,000 m per minute. Hence, low boiling point solvents are usually required to allow rapid ink drying. As gravure printing use deep-etched engraved cells, it is capable of delivering dense layers, with a wet thickness of ∼7 μm. The printing resolution is typically 100 μm.

Nguyen *et al.* developed a model for the ink-transfer mechanism of gravure printing that would allow an effective control of the printing process for fine line prints[173,212]. In this model, the gravure printing process can be divided into four distinct phases: (1) the inking phase at the ink trough; (2) the doctoring phase where the ink is metered by the doctor blade; (3) the printing phase where the substrate meets the gravure roller; and (4) the setting phase when ink is successfully released from the cylinder cell to complete the print.

A successful print during these four phases would mean that the gravure cells are filled with inks at the inking phase and become completely empty as the gravure roller meets the substrate.

This journal is © The Royal Society of Chemistry [year]

Chem. Soc. Rev., [year], [**vol.**], 1–35 | 15

This is governed by the forces acting on the ink, given as:

$$F_{afs} > F_{afc} > F_{cf} \quad (4)$$

where F represent three distinct forces acting on the ink: the cohesive force (F_{cf}), the adhesive forces on the cell surface (F_{afc}) and the adhesive force on the substrate (F_{afs}); Fig. 10(C). If $F_{afc} > F_{afs}$ and $F_{cf} > F_{afs}$ occur over the entire interface, no ink will transfer. If $F_{cf} < F_{afs}$ and $F_{cf} < F_{afc}$, the ink will ideally be transferred. When $F_{afs} > F_{afc}$, most of the ink is transferred to the substrate without leaving pinholes or voids in the printed pattern.

The difference between F_{afs} and F_{afc} is termed as the ΔF, a dimensionless adhesion-force difference which acts as a unit of measure for the success of a gravure printing process. With reference to Fig. 10(D), it is hence derived by Nguyen *et al.* that:

$$\Delta F = F_{afs} - F_{afc}$$

$$= W_{cell}\left[\gamma_{ink}(1+\cos\theta_s) - \frac{\gamma_{ink}(1+\cos\theta_c)}{\cos\left(tan^{-1}[2d_{cell}/W_{cell}]\right)}\right] > 0 \quad (5)$$

where γ_{ink} is the surface tension of the ink, θ_c is the contact angle of the ink on the cell surface, and θ_s is the contact angle of the ink on the substrate. Hence, the success of a gravure printing process is dependent largely on the surface tension of the ink γ_{ink} and the viscosity of the ink which determines F_{cf}.
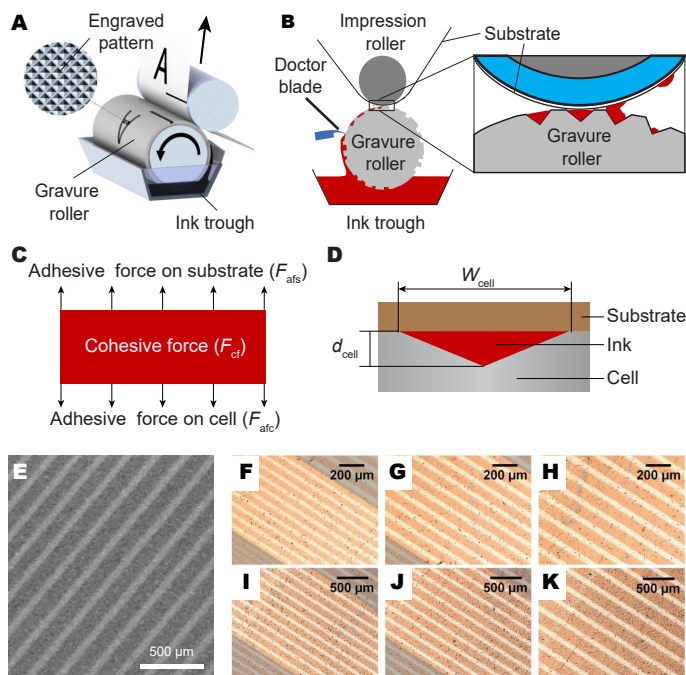

Fig. 10 Gravure printing: (A, B) Schematics of gravure printing highlighting the different components. (C, D) Schematics for illustration of gravure printing principles. (E) Large-area SEM micrograph of gravure-printed graphene lines on Kapton substrate. (F-K) Optical microscope images of printed graphene lines using cell sizes of 15, 20, 25, 30, 35 and 50 μm, respectively. Lines printed without the specified cell size are shaded in grey. (E-K) Reproduced with permission[21]. Copyright 2014, Wiley-VCH Verlag GmbH & Co. KGaA, Weinheim.
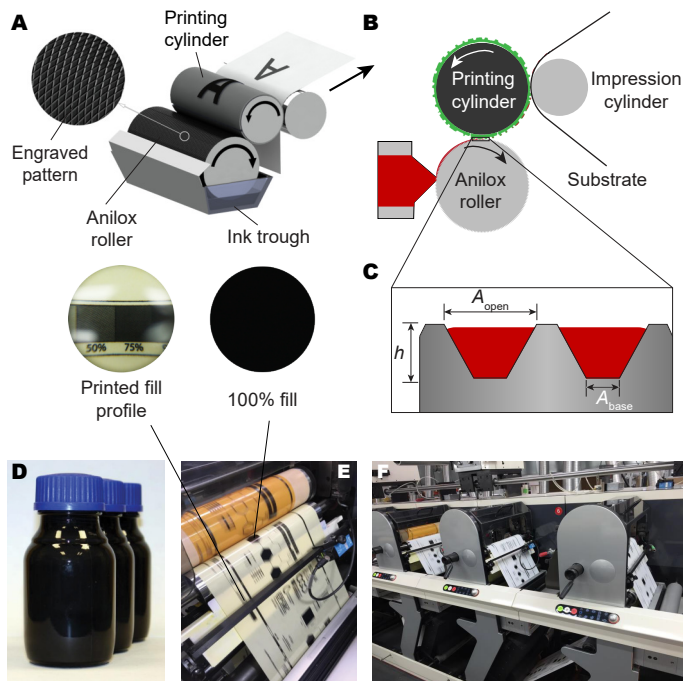

Fig. 11 Flexographic printing: (A, B, C) Schematic figures showing flexographic printing principles. (D) Photograph of graphene/carbon flexographic ink. Printing trials of the ink shown in (D) on (E) PET and (F) paper substrates using a commercial graphics printing press. Inset: zoomed-in photographs of the printed fill profiles.

4.4.2 Flexographic printing principles

Figure 11(A, B) show typical schematics of the flexographic printing process[160,161,171]. Flexographic printing can be considered as a relief printing process in which the impression stands out of the printing cylinder in a relief as opposed to being 'flat' on a plate like in screen printing or recessed like in gravure printing[160,171,205,214,215].

When compared to gravure printing, flexographic printing uses a slightly more convoluted ink transfer process. As shown in the schematic figures, to form an image, soft and flexible relief printing plates are mounted and registered on a plate cylinder. Ink is first applied to the surface of a screened anilox roller, which is rolled through an ink trough to fill the cells with ink. The anilox roller is a hard cylinder with engraved cells.

Any excess ink is then screened off *via* a doctor blade, ensuring an even regulation of the ink on the anilox roller surface. The ink is then transferred to the relief printing plate mounted on a second cylinder before the ink is deposited onto the final substrate.

The ink used in the flexographic printing process is also usually of a medium viscosity (1,000-2,000 mPas). Due to the R2R feeding system, flexographic printing delivers a printing speed of up to 500 m per minute, and hence low boiling point solvents are required in ink formulation to allow for rapid ink drying. As flexographic printing utilises a direct-contact relief process, it is incapable of depositing as dense a layer as gravure or screen printing. It typically deposits a wet film thickness of up to $\sim$3 μm. The normal printing resolution is between 100-200 μm.

Similar to gravure printing, the flexographic printing process

begins with inking and doctoring of the anilox roller. However, unlike gravure printing, these cells are not the main image-forming region and are responsible purely for metering the amount of ink to ensure continuous patterns. The amount of ink that a single cell (V_{cell}) can hold is given as

$$V_{cell} = h \bigg/ \frac{3(A_{open} + A_{base})}{\sqrt{A_{open}A_{base}}} \qquad (6)$$

where h is the height of the cell, A_{open} is the area of the opening of the cell and A_{base} is the area of the base of the cell; Fig. 11(C). The volume obtained, then, can be multiplied by the total number of cells on the roller to give the total volume of ink the roller can hold.

Besides the cell illustrated, there are also a variety of other cell structures which may be used [176,205]. For instance, tri-helical cells, which are shaped as long, unbroken valley etched at a 45° angle, are useful for printing of high viscosity inks. Quadrangular cells, shaped like inverted pyramids with the point cut off, can also be specified. This shape tends to release ink better and also has less variability in the ink volume during printing cycles.

4.4.3 2d material gravure and flexographic inks

Gravure printing of 2d materials was first reported by Secor *et al.* in 2014 [21]. The authors exchanged LPE graphene from ethyl cellulose/ethanol into ethyl cellulose/terpineol/ethanol for ink formulation, where the loading of graphene and ethyl cellulose was controlled to suit gravure printing [21]. The small flake size of the LPE graphene flakes ($\sim$50 nm $\times$ 50 nm with typical thickness of $\sim$2 nm) was critical for a high-resolution gravure printing process [21,172]. As shown in Fig. 10(E-K), the authors demonstrated that the ink allowed high-resolution (printed line width down to $\sim$30 μm) patterning of graphene on Kapton [21]. This ink was used to demonstrate continuous, electrically conductive printed stripes.

Flexographic printing of 2d materials was first reported by Baker *et al.* in 2014 [19]. The authors developed a graphene/sodium carboxymethylcellulose (Na-CMC) ink in water/IPA solutions, where the graphene/binder (*i.e.* Na-CMC) ratio was controlled to suit flexographic printing. The ink could be printed onto ITO substrates to fabricate counter-electrodes for photovoltaics [19].

In 2015, a research group at the University of Cambridge developed a conductive carbon-graphene ink (Fig. 11(D)) and demonstrated a full-scale flexographic press (Nilpeter FA-4) run on both paper and PET in collaboration with *Novalia*, as shown in Fig. 11(E, F) [20]. The press run achieved a printing speed of $\sim$100 m per minute, allowing the printing of hundreds of electronic circuits for capacitive touchpads. The measured R_s was $\sim$16.5 kΩ/sq and $\sim$11.5 kΩ/sq for paper and PET, respectively, demonstrating a significant improvement from conventional carbon inks of which R_s is $\sim$40 kΩ/sq.

5 Printable 2d material applications

Although there have been numerous demonstrations and device prototypes based on solution processed 2d materials over the last 10 years, applications based on printed 2d material inks, with op-

timised rheological properties specific to target applications, are only beginning to emerge. The key application areas include conductive inks, (opto)electronics and photonics, sensors and energy storage. We note that many of the 'solution processed' 2d material applications not included in this section may also potentially benefit from functional ink formulation when scalable device development is envisaged. Table 4 lists the demonstrated key applications to date.

5.1 Conductive inks

Printable electronics hold a huge potential in the fields of logic circuits, sensors, photodetectors, flexible displays, RFID and portable energy storage [5,6,155]. This requires conductive inks for the fabrication of electrodes and interconnects for circuits. Currently available commercial conductive inks for printing are predominantly carbon or metal (such as copper or silver) based. Although carbon inks are significantly cheaper, they offer insufficient electrical conductivity for a wide variety of applications. On the other hand, metal based inks are usually expensive and usually require demanding curing or sintering conditions [199]. Due to cost-performance benefits, graphene inks are particularly promising for printed electronics [199], with its electrical conductivity lying between the traditional carbon and metal based inks. For example, Hyun *et al.* reported the use of screen-printed graphene as the source and drain contacts for flexible transistor fabrication on a Kapton substrate (channel material: poly(3-hexylthiophene)) [16].

Figure 12 presents the evolution of graphene conductive inks. Investigation for this application started with the LPE dispersions [7]. However, Torrisi *et al.* showed that the inkjet-printed graphene from NMP dispersions demonstrated a measured electrical conductivity of up to $\sim$100 Sm^{-1} [7], far below typical metal ($>1 \times 10^5$ Sm^{-1}) and even carbon based inks ($\sim$1,000 Sm^{-1} [219]). This low electrical conductivity was probably due to the poor inter-flake percolation of the graphene flakes, arising from the spatially non-uniform deposition as a result of the coffee ring effect.

Recent advances suggest that a practical strategy would be to develop high loading graphene/binder inks devoid of the coffee ring effect, as demonstrated in Ref. 14, 16, 21, where the respective graphene loading in the graphene/ethyl cellulose inks
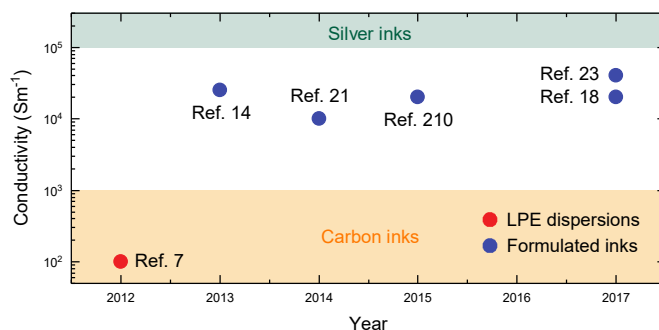

Fig. 12 Electrical conductivity of selected graphene inks demonstrated to date.

This journal is ©The Royal Society of Chemistry [year]

Chem. Soc. Rev., [year], [**vol.**], 1–35 | 17

Table 5 State of the art performances of printed 2d materials in selected applications

Printable applications		Demonstrated performances	Features
Conductive inks	Inkjet inks	*e.g.* Ref. 23: electrical conductivity up to 40,000 Sm^{-1}.	Mechanically and environmentally durable: withstanding rigorous bending cycles, adhesion testing and sonication.
	Screen inks	*e.g.* Ref. 18: electrical conductivity up to 20,000 Sm^{-1}.	Allowing multiple printing repetitions; Printing scale over 29×29 cm^2; Line resolution $\sim$100 μm.
	Gravure inks	*e.g.* Ref. 21: electrical conductivity up to 10,000 Sm^{-1}.	Line resolution $\sim$30 μm; Withstanding over 500 bending cycles of a strain of 3.1%.
	Flexographic inks	*e.g.* Ref. 20: electrical conductivity up to 500 Sm^{-1}.	Requiring no overprint of silver for printed electrodes in capacitive touchpads; Printing speed over 100 meters per minute.
(Opto)electronics	Transistors	*e.g.* Ref. 24: graphene channel based transistors with mobility of up to 204 $cm^2V^{-1}s^{-1}$ and I_{ON}/I_{OFF} limited to 2.5.	All-inkjet-printed; Mechanically durable, and withstanding bending testing and washing.
		e.g. Ref. 10: TMDs channel based transistors with I_{ON}/I_{OFF} of up to $\sim$600 and mobility limited to 0.22 $cm^2V^{-1}s^{-1}$.	All-inkjet-printed; Flexible.
	Photodetectors	*e.g.* Ref. 11: TMDs heterostructure devices with photosensitivity of up to 1 mAW^{-1} under 514 nm excitation.	All-inkjet-printed; Flexible.
		e.g. Ref. 12: BP integrated Schottky diodes with photosensitivity of up to 164 mAW^{-1} under 450 nm excitation, and 1.8 mAW^{-1} at 1550 nm under excitation.	High performance; Long-term ($>$7 days) stability and device operation; Near infrared light detection.
Photonics	Ultrafast lasers	*e.g.* Ref. 12: Inkjet-printed BP SAs which allowed generation of femtosecond ultrashort pulses under 32.7 $MWcm^{-2}$ irradiation.	Long-term ($>$30 days) stability and laser operation.
Sensors	Humidity	*e.g.* Ref. 22: CMOS devices integration of graphene with sensitivity of up to 0.3%/*%RH*.	Device-to-device consistent performances; Long-term ($>$4 weeks) device operation stability; CMOS platform.
	Gas	*e.g.* Ref. 216: gravure-printed rGO chemiresistive sensors with sensitivity of up to 45% and fast response (12 s) and recovery (20 s) times; high selectively to different chemicals.	High sensitivity and selectivity; All-printed; Flexible.
Energy	Batteries	*e.g.* Ref. 217: 3D printed Li-ion batteries with discharge specific capacities of up to 40 mAh g^{-1}.	High speed, highly efficient 3D printing; Printing with commercial graphene/polymer composite filaments.
	Supercapacitors	*e.g.* Ref. 218: inkjet-printed graphene micro-supercapacitors with an average specific capacitance of $\sim$221 $\pm$ 16 μF cm^{-2} at cyclic voltammetry scan rate of 100 mVs^{-1}.	Large-scale all-inkjet-printed devices; Device-to-device consistent performances; Mechanically durable, withstanding over 1,000 bending cycles.
	Thermoelectrics	*e.g.* Ref. 92: inkjet-printed graphene thermoelectrics with a thermoelectric power factor of 18.7 $\mu Wm^{-1}K^{-2}$ at room temperature.	All-inkjet-printed; Flexible; Large-scale.

was ∼0.34 wt.%, ∼3 wt.% and ∼8 wt.% for inkjet, gravure and screen printing. These inks were shown to be capable of producing spatially uniform printed structures, ensuring a better inter-flake percolation, and hence a higher electrical conductivity. Indeed, the measured respective electrical conductivity after binder decomposition was ∼2.5 × 10^4 Sm^{-1}, ∼1 × 10^4 Sm^{-1}, and ∼2 × 10^4 Sm^{-1}. Recently, Secor et al. reported that by using nitrocellulose as the binder, an electrical conductivity of up to ∼4 × 10^4 Sm^{-1} could be achieved after binder decomposition[23]. Compared to the graphene/ethyl cellulose systems, this increase might arise from the improved inter-flake percolation, as the printed structures exhibited superior mechanical durability and withstood rigorous bending cycles, adhesion testing and sonication[23]. However, for such inks, the binder decomposition process required high temperature annealing (> 200°C)[14,16,21]. The conductive inks are therefore mostly suitable for substrates that can withstand high temperature, such as Si/SiO$_2$, glass and Kapton. Following this annealing strategy, the success of graphene/binder conductive inks lies in finding the 'sweet spot' temperature which will allow decomposition of binders to improve percolation, yet not cause damages to the substrates or the printed graphene.

To address the challenges caused by high temperature annealing, Secor et al. developed a rapid photonic annealing process, where a high intensity xenon lamp was employed to decompose the polymeric binders after printing[88,220]. The authors showed that this strategy could effectively decompose ethyl cellulose without damaging polymeric substrates or the printed graphene, and retain a high electrical conductivity (∼2.5 × 10^4 Sm^{-1})[88]. This method produced robust printed structures, with little change in the electrical conductivity even after 1,000 bending cycles.

The good electrical properties and cost-performance advantages have garnered a general expectation by the research community that printed graphene has a huge potential in printed electronics. Nevertheless, the electrical conductivity of graphene inks to date still fall well short of that of the metal inks and therefore, will require further improvement. This may potentially be achieved by stable graphene doping and functionalization to promote inter-flake percolation[6,155,199].

5.2 Printed (opto)electronics and photonics

Although 2d materials from mechanical exfoliation and CVD have been widely reported in the demonstration of high performance (opto)electronics and photonics[62,63,69], their scalable device development towards real applications has been primarily restricted due to low yield and high production cost[1,3]. In response, there have been efforts to develop printable 2d material (opto)electronics and photonics[7,10–12].

The high carrier mobility of graphene has raised expectations within high-speed printed electronics applications. This was first demonstrated by Torrisi et al. in 2012[7]. As schematically illustrated in Fig. 13(A), the authors inkjet-printed graphene as the channel for transistor fabrication. To avoid residual impurities in the devices, the graphene ink used was NMP based LPE dispersions. The authors showed that the fabricated transistors ex-

hibited a carrier mobility of up to 95 cm^{2}V^{-1}s^{-1}[7], which is far greater than that of typical printed organic transistors (usually <1 cm^{2}V^{-1}s^{-1})[221]. The I$_{ON}$/I$_{OFF}$ from the printed transistors, however, was limited to only 10 (compared to >10^5 for organic transistors) due to the lack of a bandgap in graphene[7]. To address this low I$_{ON}$/I$_{OFF}$, the authors then deposited poly[5,50-bis(3-dodecyl-2-thienyl)-2,20-bithiophene] (PQT-12) on top of graphene, as presented in Fig. 13(A). This strategy was demonstrated viable and indeed, increased the I$_{ON}$/I$_{OFF}$ to 4 × 10^5. The mobility, however, was decreased to 0.1 cm^{2}V^{-1}s^{-1}.

There were few reports on printed graphene transistors after this demonstration until recently when Carey et al. reported inkjet-printed graphene based heterostructure transistors[24]. Figure 13(B) are the photographs of the devices on textile, where the inkjet-printed graphene was exploited as the channel and contacts, while inkjet-printed h-BN was used as the dielectric layer[24]. The authors showed that the devices exhibited a significantly increased carrier mobility of up to 204 cm^{2}V^{-1}s^{-1} (average mobility: ∼150 cm^{2}V^{-1}s^{-1} on PET and ∼91 cm^{2}V^{-1}s^{-1} on polyurethane textile)[24]. The authors also showed that the textile devices possessed a high mechanical durability, withstanding up to ∼4% strain and even more than 20 washing cycles[24]. However, as shown in Fig. 13(C), the typical output characteristics of the textile devices exhibited an I$_{ON}$/I$_{OFF}$ of only ∼1.2[24].

In contrast to graphene, semiconducting TMDs show great promise for the development of electronics with high I$_{ON}$/I$_{OFF}$[38,69]. Kelly et al. reported inkjet-printed heterostructure transistors employing WSe$_2$ instead of graphene as the channel, as shown in Fig. 13(D)[10]. The transistors exhibited an I$_{ON}$/I$_{OFF}$ of up to ∼600, significantly higher than these aforementioned graphene transistors. However, the carrier mobility was limited to 0.22 cm^{2}V^{-1}s^{-1}. An effective way to increase the I$_{ON}$/I$_{OFF}$ while retaining a high mobility, critical to any real-world applications, remains elusive so far.

Besides transistors, printed electronic circuits are also beginning to emerge. Figure 13(E) shows a schematic of a printed read-only memory (ROM) based on 2d material junctions[11] while Fig. 13(F) shows the printed ROM with the corresponding circuit design[11]. As shown, in this ROM, the graphene/WS$_2$/graphene junction with higher electrical resistance was interpreted as logic '0', while the graphene/graphene junction was interpreted as logic '1'[11]. This printed ROM output experimental results in a good agreement with simulation results; Fig. 13(G)[11]. For practical interest, the ROM could be used as RFID tags to store identification information or integrated with additional electronics for more complex circuits and functions[11].

2d materials such as semiconducting TMDs and BP offer potential for optoelectronic applications, such as photodetectors[33,69]. A printed 2d material photodetector was first reported by Finn et al. in 2014[8]. In this work, the device was consisted of inkjet-printed interdigitated graphene electrodes with an inkjet-printed MoS$_2$ active photodetection channel. The calculated photoresponsivity, however, is <1 μAW^{-1} (at 532 nm). Different from this planar structure, the aforementioned heterostructure graphene/WS$_2$/graphene junction was also utilised for photodetection[11]. This heterostructure device exhibited a photorespon-

This journal is © The Royal Society of Chemistry [year]

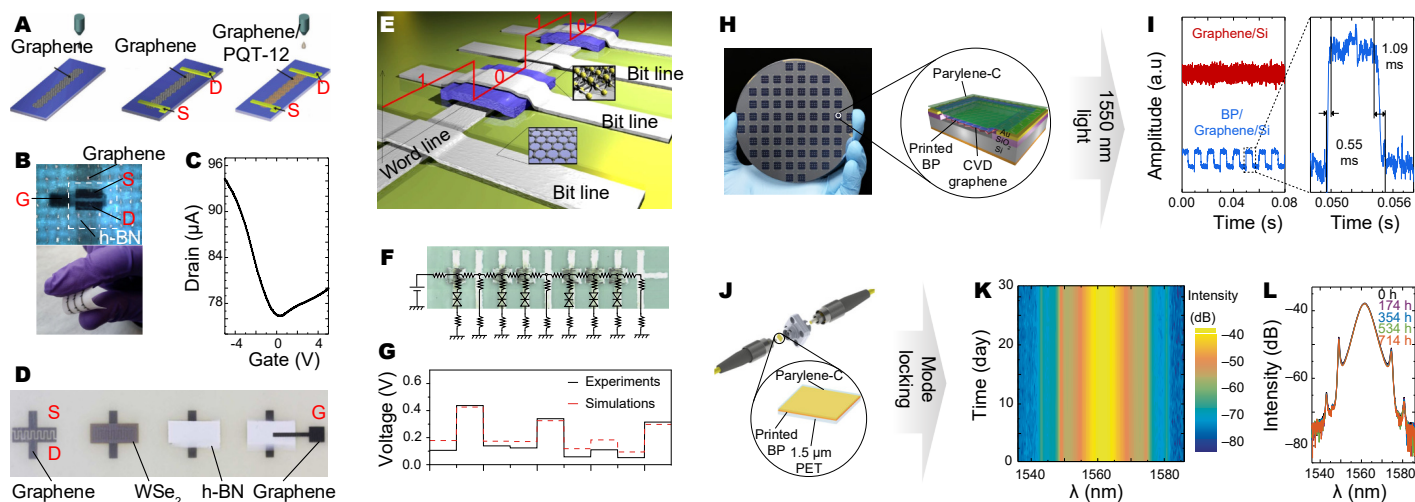Chem. Soc. Rev., [year], [vol.], 1–35 | 19

Fig. 13 Printed (opto)electronics and photonics: (A) Schematic of the first demonstration of inkjet-printed graphene transistors. Reproduced with permission[7]. Copyright 2012, American Chemical Society. (B) Photographs of all inkjet-printed 2d material transistors on textile, and (C) associated transfer characteristics. Reproduced with permission[24]. Copyright 2017, Nature Publishing Group. (D) All inkjet-printed 2d material transistors. Reproduced with permission[10]. Copyright 2017, American Association for the Advancement of Science. (E) Schematic all inkjet-printed read-only memory, (F) the corresponding circuit designs and (G) the electrical response. Reproduced with permission[11]. Copyright 2017, Nature Publishing Group. (H) Graphene/Si Schottky junction/inkjet-printed BP photodetector arrays across a silicon wafer, and (I) the corresponding measured response at 1550 nm light. (J) Schematic showing integration of inkjet-printed BP-SAs into a laser cavity to generate ultrafast lasers, and (K) the corresponding output laser spectrum across 30 days and (L) overlay of the spectrum acquired after 0, 174, 354, 534 and 714 h of operation, highlighting the stability of printed and encapsulated BP. Reproduced with permission[12]. Copyright 2017, Nature Publishing Group.

sivity of >1 mAW^{-1} (at 514 nm). To further improve the photoresponsivity, Hu *et al.* proposed a hybrid photodetector structure where inkjet-printed BP was integrated with graphene/Si Schottky junction[12]. Figure 13(H) shows a photograph of printed devices across a silicon wafer, while the inset schematically shows the structure of this hybrid device[12]. Since BP tends to degrade due to oxidation under ambient conditions, the hybrid device was encapsulated with parylene-C[12]. The device exhibited a photoresponsivity of up to 164 mAW^{-1} at 450 nm[12], significantly higher than those of the aforementioned photodetectors. More importantly, as presented in Fig. 13(I), due to the layer-dependent bandgap of BP (0.3-2.0 eV), the device responded to 1,550 nm light with a photoresponsivity of 1.8 mAW^{-1}, beyond the bandgap of Si (1.1 eV)[12].

Beyond (opto)electronics, the nonlinear optical absorption and ultrafast carrier dynamics of 2d materials (*e.g.* graphene, MoS$_2$ and BP) make them attractive for nanomaterial based saturable absorber (SA) development[12,70,71]. SAs may be used for ultrafast optical pulse generation and are an underpinning technology in a wide range of applications, ranging from materials processing, time-resolved spectroscopy, industrial micromachining to biomedical imaging[70,222]. One dominant, well-developed technology for 2d material based SA fabrication is through developing their polymer composites from solution-processed dispersions[71,100–102,223]. However, it can be challenging to precisely control the optical parameters of the fabricated SA devices. The composite preparation can also be time consuming due to slow solvent evaporation, especially when high boiling point solvents (*e.g.* NMP) are used. To address these challenges, Hu *at al.* first employed inkjet-printed BP as SA devices to mode-lock ultrafast lasers; Fig. 13(J)[12]. The issue of BP degradation and

operation stability was again addressed by encapsulation with parylene-C[12]. Figure 13(K, L) show stable ultrafast pulse generation from the printed BP-SAs for over 30 days, far exceeding the performance of prior demonstrations using BP. Functional inks and inkjet printing therefore could therefore be a very attractive approach for both discrete as well as hybrid and integrated photonic and optoelectronic device applications enabled by 2d materials.

5.3 Printed sensors

Sensors are widely used in electronics, manufacturing, medicine, robotics, automobiles, as well as in aerospace applications. A major application potential of 2d materials lies in the field of sensors due to their unique (opto)electronic, photonic, optical, mechanical properties as well the large specific surface area[1,3,224]. When exposed to ambient conditions (*e.g.* gas, moisture, stress or other environmental elements) through contact/non-contact chemical/physical reactions, 2d material-based sensing layers may respond to and convert the information into a signal that can be read out and interpreted. Indeed, high performance, proof-of-concept sensors based on 2d materials from mechanical exfoliation and CVD have been widely reported, for example sensors for individual gas molecules[225], *in-vitro* bacterial sensors[226], and even environmental sensors for internet of things (IoT) applications[227].

As with printed (opto)electronics and photonics, printed 2d material sensors are now beginning to emerge as a promising route to meet the increasing demands for sensors in real-life applications. Resistive sensors, in particular, appear to be viable for printable 2d material sensor development due to their simple, flexible device design and easy read-out with basic electronic cir-
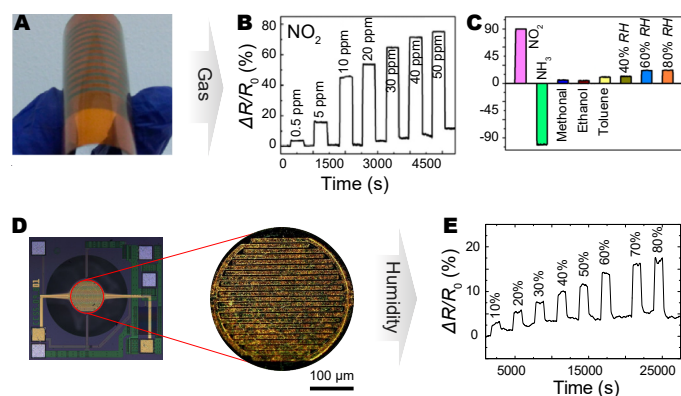
Fig. 14 Printed chemical sensors: (A) Photograph of inkjet-printed rGO/Ag gas sensors, and (B) the corresponding response with respect to NO_2 concentration and (C) selective response to various gases and humidity levels. Reproduced with permission[216]. Copyright 2014, American Chemical Society. (D) CMOS integration of inkjet-printed graphene/PVP polymer composites for humidity sensing, and (E) sensor response at different humidity (*RH*) levels. Inset: the microhotplate area with printed graphene/PVP polymer. Reproduced with permission[22]. Copyright 2015, Nature Publishing Group.

Fig. 15 Printed temperature and biosensors: (A) Photograph of graphene/PEDOT:SS temperature sensors attached on to the skin, and (B) the corresponding response to temperature change. Reproduced with permission[194]. Copyright 2016, Nature Publishing Group. (C) Schematic of biosensors with SEM micrograph of the molecularly imprinted film (MIF) morphology on rGO-NH_2 modified electrode, and (D) the corresponding device response. Reproduced with permission[230]. Copyright 2013, The Royal Society of Chemistry.

cuitry. Generally, fabrication of resistive sensors involves printing of 2d materials-based sensing materials over parallel, interdigitated or fractal electrodes.

5.3.1 Chemical sensors

Chemical sensors find widespread use in healthcare, environmental monitoring, industrial process, agriculture and smart buildings. 2d materials represent an attractive platform for this. For example, Yao *et al.* demonstrated inkjet-printed MoS_2 sensors for NH_3 detection[188]. The sensors were fabricated by printing LPE MoS_2 over microelectrodes. The sensors exhibited resistance changes when exposed to NH_3, with a detection capability of down to 5 ppm[188]. However, as noted by the authors, the sensors needed optimisation to reduce the recovery time. This might require better selection of the 2d materials, the underlying materials processing and engineering, and/or an optimised device design.

Besides semiconducting MoS_2, Cho *et al.* showed that other 2d materials such as graphene and BP produced from LPE exhibited resistance changes to chemicals such as NO_2, NH_3, ethanol and acetaldehyde[105]. When compared with MoS_2 and graphene, the authors demonstrated that the sensitivity from BP was up to 20 times higher, and that the response time was ~40 times faster. This suggested a strong potential of BP in sensing applications. However, the development of printable BP sensors for long term use could be significantly limited due to BP degradation in the ambient environment.

In spite of demonstrating good sensitivity, such sensors typically have poor selectivity (*i.e.* ability to uniquely respond to specific analytes). This has prompted the design of 2d material-based functionalised hybrid materials. Functionalisation of 2d materials *via* chemical doping or decoration with other functional materials (*e.g.* metal/metal oxide nanoparticles) has been demonstrated to be a viable strategy for enhancing sensing capabilities
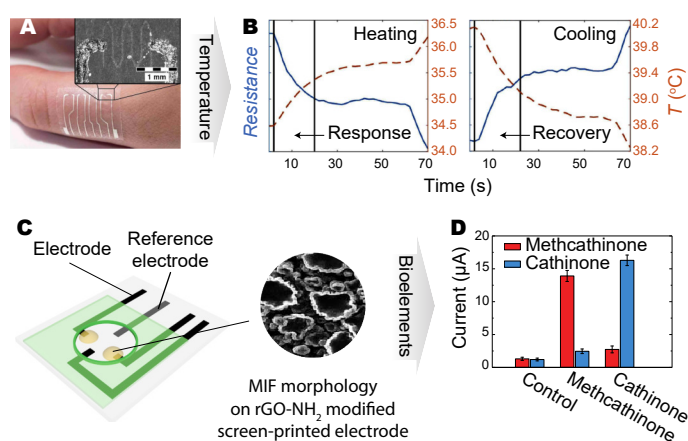
in sensitivity, response/recovery times and selectivity[228,229]. For instance, functionalisation of graphene with groups such as =O, -NH_2, -OH, -F, -CH_3 and -SO_3H can significantly expand its sensing capabilities to a wide range of chemicals, including NO, NO_2, Cl_2, SO_2, $CHCl_3$, CH_3OH and C_6H_{14} (hexane)[216,228,229]. Figure 14(A) shows a chemiresistive sensor employing rGO-SO_3H decorated with Ag nanoparticles[216]. The sensors were fabricated by gravure printing of the functional ink over interdigitated metal contacts. As presented in Fig. 14(B, C), the sensors exhibited a fast response over NO_2 and selectivity for NO_2 and NH_3 as well as linear response to humidity[216].

Figure 14(D) shows a micrograph of a CMOS integrated graphene humidity sensor[22]. The sensor was fabricated by inkjet printing a graphene-PVP sensing layer over the interdigitated electrode of the CMOS chip. The sensor exhibited resistance changes for relative humidity in 10-80%[22]. The authors proposed that the response (*i.e.* resistance change) arose from the change in the graphene inter-flake percolative network in the swelling hygroscopic PVP upon exposure to humidity[22]. This approach was the first to combine inkjet printing of 2d materials and the scalability of CMOS, foreseeing a prospect of seamless integration of printed 2d materials with existing silicon technologies for flexible and miniaturised 2d material based devices.

5.3.2 Temperature sensors

Temperature sensors are widely applied in research and industrial process monitoring, diagnostics, as well as in smart buildings, electrical or electronic products and thermal management[231,232]. Recent research is experiencing a rapid growth in wearable temperature sensors that are capable of monitoring on-skin temperature which can provide insights into general wellbeing and physical activities[232,233]. Composites of graphene and thermoelectrics, for instance, thermoelectric poly-

This journal is © The Royal Society of Chemistry [year]

Chem. Soc. Rev., [year], [**vol.**], 1–35 | 21

mers (*e.g.* poly(3,4-ethylenedioxythiophene) polystyrene sulfonate (PEDOT:PSS))[234,235] and 2d materials (*e.g.* Bi$_2$Te$_3$)[236], are a promising material platform for printable temperature sensors.

However, to date, only limited developments have been seen in this field exploiting 2d materials. Figure 15 (A) is photograph of an inkjet-printed epidermal temperature sensor[194]. The sensors were fabricated by inkjet printing graphene/PEDOT:PSS onto stretchable polyurethane substrate. As shown in Fig. 15(B), when in operation, the temperature sensors exhibited changes in resistance in the heating and cooling processes between 34-40°C; the 90 percentile response time was 18 seconds, and the 90 percentile recovery time was 20 seconds.

5.3.3 Biosensors

Biosensors can be described as integrated miniaturised devices employing biological recognition elements (*e.g* enzymes, antibodies, oligonucleotides, receptor proteins, microorganisms or cells) as active sensing components[237]. With an ever-increasing demand for miniaturised, smart healthcare systems, the field of biosensor technology demands advances in the underlying materials technology and engineering for high-level, novel biosensing performance[1,238]. 2d materials appear to be a promising carrier platform for the biological recognition elements, as pioneered by Ref. 226 where CVD graphene carried antimicrobial peptides for *in-vitro* bioselective detection of bacteria. The reports on printed 2d material biosensors, however, are very limited, with the majority of them are being based on rGO. This is due to the fact that rGO can be readily decorated with a wide variety of biological recognition elements.

Figure 15(C) schematically shows a molecularly imprinted film (MIF) based biosensor for psychotropic compound detection, where MIF was synthesised by electro-polymerisation on rGO decorated electrodes[230]. MIF is a widely applied process in biosensor fabrication where functional and cross-linking monomers are polymerised in the presence of a target imprint molecule that acts as a molecular template[239]. This template can be then used to detect similar biological compounds[239]. For sensor fabrication, rGO was functionalised with -NH$_2$, and was subsequently dropcasted onto screen printed graphite electrodes. It was shown that the rGO-NH$_2$ flakes were flat and that -NH$_2$ were exposed, such that MIF could be synthesised on top. The inset shows the morphology of the synthesised MIF. As shown Fig. 15(D), the fabricated sensors based on methcathinone and cathinone MIFs exhibited a highly selective sensitivity for methcathinone and cathinone, respectively[230]. Kong *et al.* later followed a similar strategy to demonstrate a blood glucose biosensor[240].

Instead of making the use of biological recognition elements, hybrids of 2d materials and other functional materials (*e.g.* metals, metal oxides and quantum dots) are also emerging promising material platform[211,237,241]. For instance, Zhang *et al.* demonstrated ultrasensitive non-enzymatic glucose sensors based on screen-printed rGO/copper oxide (CuO)[211]. The authors showed that the addition of rGO to CuO significantly improved the sensitivity to glucose.
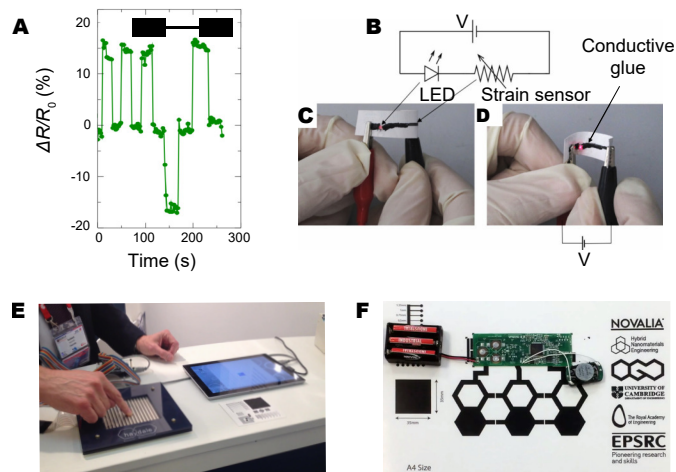
Fig. 16 Printed strain, pressure and touch sensors: (A) Response of inkjet-printed graphene strain sensor (inset) upon tensile and compressive strains. (B) Schematic circuit employing the graphene strain sensor as a variable resistor under to (C) tensile and (D) compressive strains[242]. (E) *Haydale* graphene pressure sensors demonstration, source - *ieee.org*[243]. (F) Flexographic-printed graphene-based capacitive touchpads.

5.3.4 Strain, pressure and touch sensors

Strain sensors, or strain gauges, are attractive for wide variety of applications, in particular, for stretchable, skin-mountable wearables[244,245]. The strain sensors typically consist of a conductive pattern that is capable of producing a change in the electrical read-out upon geometric deformation[244,246,247]. Although graphene has been widely reported in compact strain sensor fabrication as a standalone material[248–250] or in form of composites (*e.g.* polyvinylidene fluoride (PVDF)[251] and nanocellulose[252]), reports on printed 2d material strain sensors remain scarce.

Casiraghi *et al.* recently reported an inkjet printed graphene strain sensor on paper[242]. The schematic sensor configuration is in the inset of Fig. 16(A), showing that the sensors were composed of inkjet-printed conductive contacts and an active strain sensing line in between. As presented, the printed graphene strain sensors exhibited fast, prominent change in electrical resistance under tensile and compressive strains. The authors further employed the printed sensor in an electrical circuit as a variable resistance to tune the luminosity of an LED under tensile or compressive strains; Fig. 16(B-D).

Pressure and touch sensors can detect either physical pressure, physical contact or even proximity. They represent another interactive technology widely applied in consumer portable devices such as smart phones or touch pads. Pressure sensors can be created *via* structures where an active sensing layer is 'sandwiched' between contacts, or where the active sensing spots are connected to contacts, or a combination of both. Published reports on printed 2d material pressure and touch sensors are scarce. However, there have been a number of demonstrations of such devices by commercial entities. Figure 16(E) shows a printed graphene thin film pressure sensing panel demonstrated by *Haydale*. In this panel design, printed graphene/binder composite was 'sand-

22 | *Chem. Soc. Rev.*, [year], [**vol.**], 1–35

This journal is ©The Royal Society of Chemistry [year]

wiched' between a printed electrode matrix, such that the matrix could detect resistance changes of the graphene/binder composite upon pressure and indicate the location of touch.

The flexographic-printed graphene based circuits as presented in Fig. 11(E, F) were designed for the demonstration of large scale production of capacitive touch surfaces for interactive devices. In the example shown in Fig. 16(F), the touch surface was attached to a PCB board programmed to process the received capacitive changes from the touch panel upon touch, and hence to trigger a sound output through a speaker. This technology works through by detecting capacitive changes, and therefore the active surface area (printed graphene) may also be laminated behind thin paper or plastic substrates, enabling the development of a wide variety of interactive surface applications ranging from wireless keyboards, pianos and educational posters.

5.4 Printed energy storage

The applications for energy storage technology range from portable electronic devices, industrial manufacturing, to next generation wearable electronics and vehicles[253,254]. Batteries and supercapacitors are the most common forms of energy storage devices for such applications. A battery relies on electrochemical reactions at the electrodes to deliver energy[253,255]. A supercapacitor (*i.e.* electric double-layer capacitor), however, utilises a double-layer effect on the electrodes to store electrical energy[77,256]. Achieving highly efficient and dense energy storage therefore requires optimal underlying electrode materials technology and engineering[77,255–258].

2d materials with high specific surface area are emerging as a promising material platform for novel, high performance electrode materials[3,33,52,77,259]. It has been proposed that graphene electrodes can lead to a decrease in electrode thickness while an increase in electrode-to-electrolyte contact, which when combined with good electrical conductivity, offers better performance than current electrode material technologies[77,260]. Indeed, there are already many successful demonstrations with solution-processed graphene[78,261,262] and other 2d materials such as MoS_2[263,264] and in particular, MXenes[118,265–268]. Although the current progress is mostly focused on printed supercapacitors, such solution based electrode fabrication for energy storage technologies can potentially be adapted to printing for high-speed, low-cost device manufacturing of both batteries and supercapacitors.

Inkjet printing has been used as a high-precision deposition method for the fabrication of such electrodes. For example, Le *et al.* reported graphene supercapacitors using inkjet-printed and subsequently thermally reduced GO electrodes[269]. More recently, Hyun *et al.* demonstrated all-printed micro-supercapacitors that employed inkjet-printed graphene electrodes[218]. As schematically shown in Fig. 17(A), the micro-supercapacitors were fabricated in three steps: an imprinted ink receiver was firstly prepared; a graphene/ethyl cellulose ink was then inkjet-printed to pattern the electrodes, followed by binder decomposition through photonic annealing; electrolyte was then deposited by inkjet printing. Figure 17(B) shows a photograph of an array of the
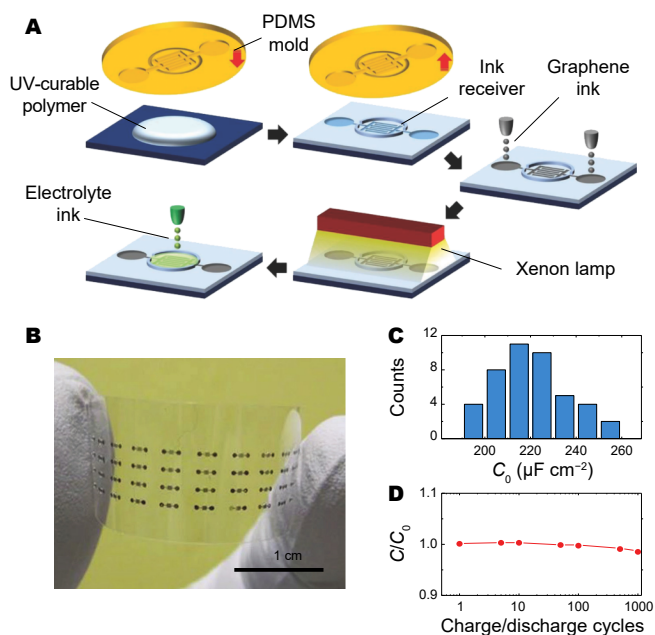
Fig. 17 Printed energy storage using 2d materials: (A) Schematic of the fabrication process for inkjet-printed graphene supercapacitors. (B) Photograph of an array of graphene supercapacitors on PET, and the corresponding (C) histogram of the specific capacitance and (D) typical relative specific capacitance over 1,000 charge/discharge cycles at a scan rate of 1,000 mV s^{-1}. Reproduced with permission[218]. Copyright 2017, WILEY-VCH Verlag GmbH & Co. KGaA, Weinheim.

inkjet-printed micro-supercapacitors. As presented in Fig. 17(C), the average specific capacitance of this micro-supercapacitor array was ~221 ± 16 μF cm^{-2} at a cyclic voltammetry scan rate of 100 mVs^{-1}, demonstrating a device performance variation of <10%. In addition, this micro-supercapacitor array exhibited good mechanical durability, withstanding over 1,000 bending cycles; Fig. 17(D). Although the amount of active materials that can be deposited using inkjet printing technology is limited due to ink formulation requirements, it is still a viable technology platform for the manufacturing of flexible, miniaturised, on-chip energy storage, in particular, for fully integrated and wearable devices.

Besides inkjet printing, there are also demonstrations of energy storage using other printing processes. For example, Hyun *et al.* reported supercapacitors based on screen-printed graphene/PANI electrodes[16]. Yeates *et al.* demonstrated screen-printed graphene supercapacitors on textiles for wearable electronics applications[273].

Beyond these conventional printing processes, recent advances on printable 2d material energy storage show 3D printing is a promising approach. Figure 18(A) schematically illustrates a 3D printing process, whereby the 'inks' (typically in the form of plastic filaments such as polycarbonate (PC), acrylonitrile butadiene styrene (ABS) and polyactic acid (PLA)) are extruded and deposited layer-by-layer onto the build platform.

For 3D printing of 2d materials, however, this 'direct-ink' writing typically requires in-situ formulation, gelation and curing of the inks, negating the relative throughput advantages that 3D printing brings. For example, García-Tuñon *at al.* developed

This journal is © The Royal Society of Chemistry [year]

Chem. Soc. Rev., [year], [**vol.**], 1–35 | 23

Fig. 18 3D printing of 2d materials: (A) Simplified schematic of 3D printing using fused deposition modelling. (B) Top-view (one layer) and side-view (three layer) photographs of 3D-printed graphene patterns, and the SEM micrographs of the printed graphene and printed graphene/CNTs hybrid for supercapacitors. Reproduced with permission[270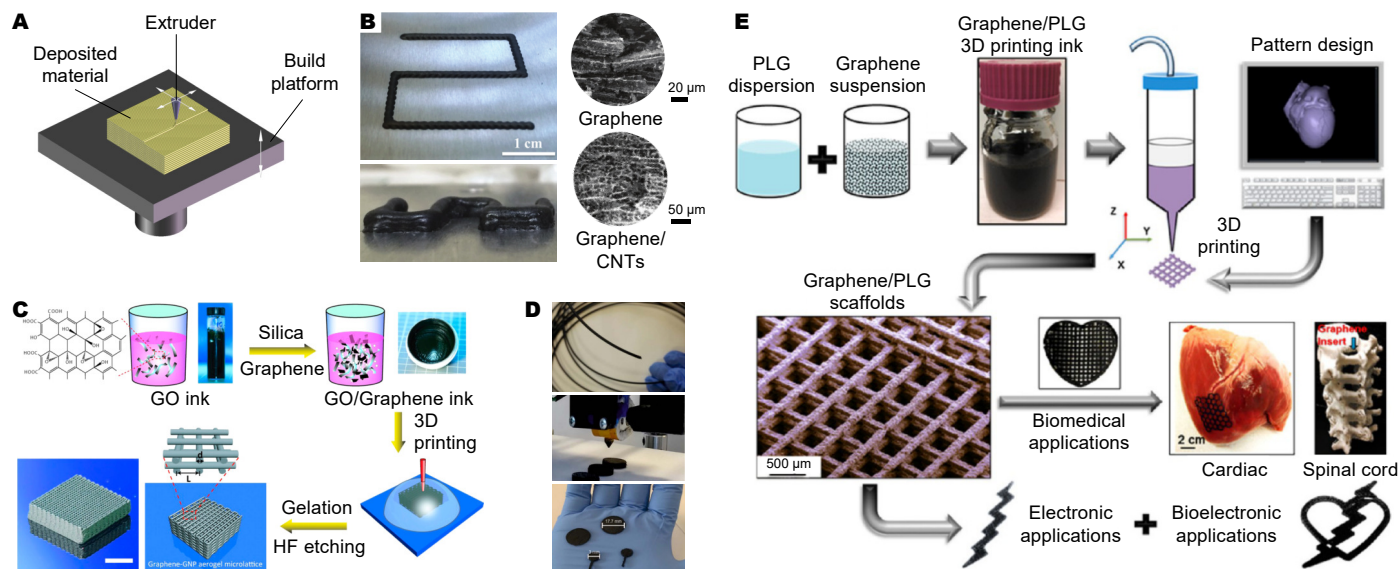]. Copyright 2016, WILEY-VCH Verlag GmbH & Co. KGaA, Weinheim. (C) Schematic of the fabrication process of 3D-printed GO/graphene supercapacitors. Reproduced with permission[271]. Copyright 2016, American Chemical Society. (D) Photographs of 3D-printed graphene based batteries and supercapacitors from printed filaments. Reproduced with permission[217]. Copyright 2017, Nature Publishing Group. (E) 3D-printed graphene scaffolds for electronic and biomedical applications. Reproduced with permission[272]. Copyright 2015, American Chemical Society.

an aqueous GO ink using a branched copolymer surfactant for 3D printing[274]. This approach allowed the ink to form self-supporting 3D structures after deposition. The printed 3D structures were then frozen in liquid nitrogen and subsequently freeze-dried for thermal reduction of GO. Alternatively, instead of using surfactants, Lin *et al.* developed a graphene aerogel through room temperature freeze gelation of graphene dispersions in phenol (C_6H_6O) or camphene ($C_{10}H_{16}$)[270]. This approach allowed self-solidified structures at room temperature after jetting, as shown in Fig. 18(B). The 3D printed structures could be removed from the solvents through sublimation at room temperature. The authors demonstrated that the 3D printed structures could be employed as electrodes for supercapacitors, delivering a specific capacitance of ~75 Fg^{-1} at a current density of 100 Ag^{-1}[270]. By using 3D printed graphene/CNTs, the authors showed that the specific capacitance could be improved to ~100 Fg^{-1}[270]. Zhu *et al.* also demonstrated 3D printing of a GO/graphene aerogel for the development of supercapacitor electrodes[271]; Fig. 18(C).

Besides supercapacitors, Sun *et al.* demonstrated 3D printed Li-ion batteries using lithium-based inks $Li_4Ti_5O_{12}$ (LTO) and $LiFePO_4$ (LFP) The authors jetted the ink from a syringe-like nozzle and subsequently cured it *via* annealing[275]. Similarly, Fu *et al.* demonstrated 3D printed cathode and anode for batteries from GO/LTO and GO/LFP inks which were later converted to rGO by annealing[276].

It was only recently in 2017 that Foster *et al.* first demonstrated 3D printed energy storage devices using commercial graphene/PLA filament[217]. As shown in Fig. 18(D), the authors printed graphene/PLA discs from the filament, and demonstrated that the discs could be employed as the anode of Li-ion batter-

ies and could sandwich solid electrolyte for solid-state supercapacitor fabrication[217]. The authors also demonstrated that the 3D printed graphene/PLA could find uses in hydrogen evolution reaction and fuel cells. This 3D printing process of filaments required no additional treatment and as such, provided an effective proof-of-concept for a true 3D-printed, 2d material based energy application.

We note that in addition to energy storage, 3D printing of graphene is also of special interest for other application areas. For example, Jakus *et al.* demonstrated a graphene/polylactide-co-glycolide (PLG) ink that could be printed to develop robust, flexible graphene scaffolds[272]; Fig. 18(E). Through *in vitro* experiments, the authors demonstrated that the graphene scaffolds could support human mesenchymal stem cell adhesion, viability, proliferation, and neurogenic differentiation with significant upregulation of glial and neuronal genes[272]. 3D printing of graphene and other 2d materials therefore promises an attractive pathway towards miniaturised and customised device prototyping for energy, sensing and biomedical applications[272].

Beyond the aforementioned conventional energy applications in supercapacitors and batteries, 2d materials are also promising for thermoelectric energy conversion. Recently, Juntunen *et al.* reported inkjet-printed large-scale graphene thermoelectric devices[92]. The devices were intrinsically inkjet-printed disordered nanoporous all-graphene structures. The authors demonstrated a room-temperature thermoelectric power factor of 18.7 $\mu Wm^{-1}K^{-2}$, a three-fold improvement to previous solution-processed all-graphene structures. This potentially foresees future flexible, scalable and low-cost thermoelectric applications, such as harvesting energy from body heat in wearable applica-

24 | *Chem. Soc. Rev.*, [year], [**vol**.], 1–35

This journal is © The Royal Society of Chemistry [year]

tions[92].

6 Conclusion and perspectives

6.1 Conclusion

This review summarises the current position of 2d material inks and printing. Since the first demonstration of printed graphene electronics, this field has witnessed four major advances: the functional material set has evolved from graphene alone to a wider range of available 2d materials; 2d material inks have advanced from simple solution-processed dispersions into formulated inks adapted for specific print processes; the exploitable printing technologies have expanded from inkjet printing to a broader printing platform (including screen, gravure and flexographic, as well as 3D printing) offering faster production speeds and more complex device structures; the investigated applications have extended to several major technology areas, including optoelectronics, photonics, sensors and energy storage. Taken together, these represent significant advances for the scope of 2d material inks, and associated printing, as a promising platform for a next generation of disruptive technologies.

Despite these advances, there are huge opportunities to improve the reliability and performance of the applications discussed above. It is necessary to scale-up from laboratory demonstrations to device manufacturing ready for real-world applications. Realising this requires significant improvements towards the development of application-specific 'ideal inks' through the underlying materials processing and engineering, and ink formulations. Though notable progress has been made in the past decade, there is still much to be done on solution processing to improve the exfoliation efficiency, to raise the production yield and reduce the production cost, and to better sort the exfoliated flakes[3]. Indeed, it is important to achieve high production yield of mono-layers with mono-dispersed, precisely controlled flake size and thickness, to ensure the formulated ink delivers access to full-potential, mono-dispersed material properties of the 2d materials. On this basis, optimising the ink formulations to achieve ideal fluidic properties, drying dynamics and ink-substrate interactions, and fundamental research into binders, solvent and additive compatibility are of critical importance. In general, an ideal ink relies on an optimal selection of solvents, binders and additives, where the ink compositions (*i.e.* the 2d materials, the solvents, the binders and the additives) are formulated in a 'sweet spot' such that the ink renders optimal ink physical properties for the specific desired printing technology, that the ink can appropriately wet the targeted substrates, that the deposited 2d materials can adhere onto the substrates with high mechanical durability, and that the use of binders and the additives leads to minimal compromisation of the functionalities of the 2d materials for the applications. However, in some cases such as in (opto)electronics and heterostructure devices applications at the current development stages where such optimal ink composition selection and 'sweet spot' of the functional ink compositions have not been established, an ideal ink should be free from any impurities including the binders as the impurities can significantly degrade the device performance. Even with this ideal ink, to harness the full po-

tential of 2d materials in applications, optimal device designs are also essential for high-level device performance, and expansion of the currently demonstrated applications. It will also be of a great interest to combine 2d material ink formulations with other functional materials, such as biomolecules, 0d and 2d perovskites and 1d nanowires/nanotubes such as CNTs, for more flexible material selection and device design.

6.2 Research landscape

6.2.1 Inkjet inks

In this review, we have shown that digital inkjet printing process has thus far been the most prevalently used method in printable 2d material applications. However, the demonstrated 2d material inkjet inks commonly face mechanical failures. Flexibility in general is not a problem as the inks take the form of the substrates they are deposited on. Instead, adhesion to the substrates can pose a significant challenge, for instance when fabricating (opto)electronics and heterostructure devices. This is due to the inability to use polymeric binders in ink formulation as they limit the overall functionalities of the 2d materials. Therefore, a strong barrier to the widespread use of 2d material inks is the development of compatible binder systems for such applications, *i.e.* binders that do not significantly compromise the device performance. Despite this, the current binder-free inks can still find interesting applications in laboratory-scale device demonstrations.

It is also crucial to scale-up the printing, *i.e.* developing inks in a way that enables efficient, large-scale printing with excellent device-to-device uniformity. Though insights from printed organic transistors could be useful, the nature of 'nanoparticle based' 2d material inks may require a fundamentally different approach when such large-scale printability is envisaged. At present, this is perhaps the most important challenge in this field. A large part of this challenge is dependent on the ability to maintain stable jetting, deposition and drying phases of the inkjet inks throughout the entire process in an industrial printing environment. As discussed, strategies such as inducing controlled Marangoni flow, ensuring good wetting of the substrates and retaining a good viscosity control will need to be adopted in a comprehensive manner to enable this degree of process control.

Conductive inks offer a major opportunity for 2d material inkjet inks in the near future. However, such inks utilising graphene as the main functional material have not been able to achieve the electrical conductivity levels of the current incumbent, metal inks. This limits the full potential of graphene conductive inks. As already discussed, a key solution to overcome this is to improve the inter-flake percolation. Some work has been done in this regard, for instance by employing a photonic annealing process for binder decomposition[88], or by optimising binder selection in ink formulation[23]. Nevertheless, the ultimate goal of graphene conductive inks is to be capable of replacing expensive metal inks fully in printed circuits. Metallic MXenes could be another potential alternative for the formulation of highly conductive inks.

For other applications such as optoelectronics, photonics, sensors and energy storage, as with conductive inks, large-scale printability, device-to-device repeatability, the inter-flake perco-

lation and connectivity remain critical as these can result in poor or inconsistent device performance. Fabrication of inkjet-printed 2d material based miniaturised on-chip photonic devices on bulk semiconductors such as high speed modulators and photonic integrated circuits represents a potentially scalable and attractive functional device platform. However, for high-speed and I_{ON}/I_{OFF} devices, such as those required for electronics and optoelectronics, it is unlikely that the current 2d material inkjet inks will be used in isolation for industrial scale manufacturing in the near future. It is more likely that the inks for these applications will be exploited with other functional materials (*e.g.* semiconducting polymers[194], perovskites, metal oxides and biomolecules[230] for sensing applications), in hybrid/heterostructure devices (*e.g.* graphene-silicon Schottky devices[12]), or on bulk semiconductor based technology platform (*e.g.* for photonic integrated circuits or CMOS sensors [22,277]). Among other materials, in addition to conductive inks, MXenes can potentially be used for many of these applications, including in energy storage, optoelectronics and sensing.

6.2.2 Screen, gravure and flexographic inks

Compared to inkjet printing, screen, gravure and flexographic printing processes are not yet highly developed and widely reported. This is largely due to the high loading of 2d materials and the typical ink volume required during prototyping when compared with inkjet printing where minimal solution-processed dispersions can be used directly. As such, only graphene has been widely demonstrated in screen, gravure and flexographic inks; Table 4.

The primary goal for screen inks is to develop conductive inks that will be of lower cost than metal inks and yet offer higher electrical conductivity than carbon conductive inks. At present, graphene conductive screen inks have already surpassed the carbon inks by a great deal (up to ∼96% reduction in electrical resistance). However, as with inkjet, these inks are also behind the metal inks, limiting their full potential. This is especially true for applications requiring high electrical conductivity, for example, electrodes and interconnects in printed electronics where the electrical conductivity of printed graphene is orders of magnitude below acceptable values. There have been a few approaches adopted to enhance the electrical conductivity, for example by passing the printed substrates between two high pressure rollers to force better percolation and higher packing density within the printed structures. Conventional sintering *via* high temperature annealing in polymeric binder decomposition, as proposed in inkjet printing, is unlikely to be an option due to the higher requirement for adhesion to the substrates. Alternatively, the electrical conductivity could be potentially further improved by using chemical dopants that can co-exist with the binder and other compositions in the screen printable ink system and can remain stable over prolonged period. However, such strategies are yet to be fully developed.

Though there are very limited 2d material inks demonstrated for gravure and flexographic printing processes due to the high prototyping costs, these methods offer significantly lower costs at volume production. At present, only graphene inks have been demonstrated on these systems with the highest reported conductivities at ∼10,000 Sm^{-1} and with printed resolutions as fine as ∼20 μm[21]. However, we note that while this printed resolution has been demonstrated at the lab scale, such fine resolution is unlikely to be adopted in a commercial setting where the smallest consistent line widths printed over thousands and even millions of prints are ∼100 μm. Much work is therefore required for 2d material gravure and flexographic inks, in terms of ink formulation, electrical performance and the control of print parameters.

Compared to graphene, printing of other 2d materials such as *h*-BN, mica and MXenes is relatively nascent. Research in *h*-BN for screen printing[113] is at a very early stage. It is unlikely to achieve a high dielectric value because of the inherently low dielectric constant of *h*-BN itself. However, *h*-BN can be combined with the current generation of polymeric binders to significantly increase their dielectric properties in devices that require capacitive structures (*e.g.* RFID applications). Such strategies could also improve thermal conductivity of the polymeric binders in the printed structures. Other 2d materials such as mica can be used to make printable dielectric inks, following a strategy similar to the *h*-BN inks[113].

6.2.3 Future research directions

In the short and near term, the advantages offered by printing technologies, such as controlled additive patterning, thin-form factors and mechanical flexibility, may enable improved device performance and even new technologies and applications. Seamless integration of printed 2d materials with the existing CMOS electronics, optoelectronics and sensing technologies and even integrated circuits may also be possible. Early, rudimentary examples have been demonstrated. Such technologies may also involve incorporation of other functional materials such that multiple concurrent functions are realised, leading to the development of 'multifunctional' inks.

In the longer term, this fusion of technologies, materials platform and functionality would lead to manufacturing flexibility, high-level integration and miniaturisation for 2d material based printable electronics, sensing and interactive devices. This will require precisely controlled, additive patterning of multiple 2d materials and other functional materials over large areas and/or for thousands of devices with tight manufacturing tolerance, and could potentially lead to the development of all-printed, complex device structures (*e.g.* heterostructures) for unprecedented new applications in light detection and imaging, energy storage, interactive touch surfaces, wearable sensors, RFID tags and even artificial skins.

6.3 Economic landscape
6.3.1 Functional printing industry

The printing industry is a market estimated to be worth USD $124 billion by 2020[278]. Although still in the early stages of adoption when compared to the wider print industry, there is a growing interest in incorporating functional materials including the 2d materials as active pigments for functional ink formulation and printing. Demand for such functional printing has been driven by

the increased miniaturisation, technological advancements and portability needs of electronic products in different sectors such as telecommunications, packaging, automotive and medicine[5,279].

Examples of devices produced using printing include inkjet-printed smart packaging systems[280], gravure-printed wireless power transmitters[281] and flexographic-printed paper-based chipless RFID tags[282]. The prospective growth of cost efficient functional printing is hallmarked by the evolution of printing technologies from rigid to flexible substrates, printing from cm^2 to m^2 structures and gradually moving from sheet or batch printing to R2R production[283]. These advances point to a growth in the functional printing market that is estimated to be worth USD $13.79 billion worldwide by 2020[284].

Beyond printing, 2d material dispersions and the formulated inks can also be used for functional coating[285]. For instance, Karim *et al.* reported graphene coated textiles, 'E-textiles', for wearable electronics[245]; Zhang *et al.* demonstrated stamping of water-based MXene dispersions on paper for flexible, coplanar micro-supercapacitors[115]. Functional coating represents a subset of coating that renders specific properties for applications[286,287]. These properties may be diverse, with typical examples that are self-cleaning[288], easy to clean (anti-graffiti)[289], anti-fouling[290], soft feel[291], antibacterial[292], or smart (*e.g.* responding to external stimuli). At present, functional coating is prevalent in home furniture, cars, laptops, mobile phones and solar panels, and in more advanced applications such as medical devices and orthopedic implants, invisible paints and even radars and satellites[293]. More recently, there is a strong emphasis on the development of smart coating for corrosion protection in different technological applications, especially in infrastructure[293].

6.3.2 2d material printing industry

Current research and market on 2d material functional inks have been firmly focussed on graphene. In 2015, the *Global Market for Graphene* report by *Technavio* conservatively estimated the market size for all graphene-related industries (including manufacturing and applications) to be worth USD $24.5 million. By 2020 the market is expected to be worth USD $126 million, with a compound annual growth rate (CAGR) of 66.4%[294]. Note that these estimations may vary widely between market reports, depending on the market research methods employed by analysts. These projections point towards a highly bullish graphene market with a great expectation for growth, largely due to increasingly competitive research and development efforts from leading universities and large corporations as patents mature into end-user applications.

Of the many applications for graphene and its precursors for graphene inks, analysis from the *Beige Group* predicts that printing and coating are likely to offer the most significant growth; Fig. 19(A)[295]. These include applications in electronics and semiconductors, energy storage, healthcare, photovoltaics and filtration. This understandably has led to the projected trend seen in Fig. 19(B). The value of graphene in printing and coating applications has been estimated to be USD $4.2 million in 2015. By 2021, predictions point towards an increase to USD $34.6 million, growing at a CAGR of 47.1%. The growth of the graphene
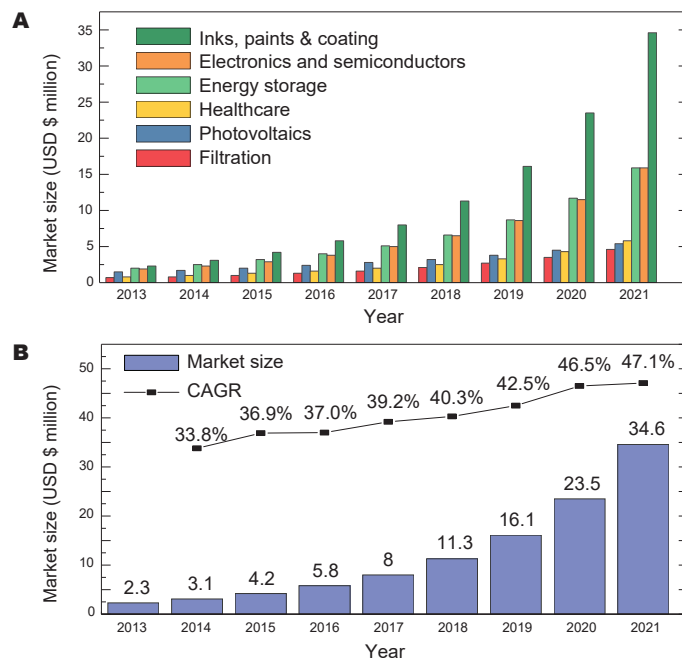
Fig. 19 (A) Projected growth of graphene inks, printing and coating in relation to other graphene applications through 2021. (B) Projected growth in graphene inks, printing and coating market through 2021. Data collected from Ref. 295.

inks and printing industry is largely due to the discovery of new uses for graphene and related 2d materials as functional additives, such as the incorporation of graphene oxide into inks and coatings to add anti-corrosive and anti-scuff properties and in membranes for water filtration and desalination[294].

Globally, the Asia-Pacific region is the largest and the fastest growing graphene market, and also the single-largest supplier of graphene nanoplatelets[294]. The growth of the graphene industry in Europe at present is driven largely by research and development activities and funding for research. For instance, the European Union is funding Euro €1 billion over a span of 10 years since 2011 in the *Graphene Flagship program*, to understand and promote graphene and related 2d materials. Market analysis values show that the graphene market in North America was USD $8.75 million in 2016 with an ambitious prediction of USD $38.5 million by 2020, growing at a CAGR of 38.75%. *Technavio* also predicts that the market in North America will be mainly driven by the electrical and electronics industries. The market is led by research and development in graphene-related fields in the universities, spin-off companies from university and large national laboratories in the United States. It is likely that the other 2d materials will fuel this growth in the near future as the technologies and applications enabled by them are further developed and matured.

6.3.3 Development stages

To conclude this review, we present the various applications of 2d material inks according to their individual stages and, if successful, our conservatively estimated timeline for full-scale commercialisation; Fig. 20. The key applications range from

This journal is © The Royal Society of Chemistry [year]

Chem. Soc. Rev., [year], [**vol.**], 1–35 | 27

Fig. 20 Current stage of development of inks, solution processed coating and composites of 2d materials , and their estimated timeline for commercialisation.

functional coating (*e.g.* paints, barriers and filtration) to printable applications (*e.g.* (opto)electronics and photonics, sensors, and energy storage). The present extent of commercialisation varies widely across the stages with most of these technologies sitting at the proof-of-concept prototyping or early-stage commercial sale/semi-commercial trial stages. Promising applications that are likely to achieve early market penetration first are the fields of smart packaging, interconnects, sensors, RFID tags, composites, coating, and electromagnetic interference shielding. There is a growing increase in the global demand for electronic smart packaging devices (*e*-packaging). In early 2012, *MeadWestvaco* launched printable security tags by flexographic printing of graphene ink developed by *Vorbeck*. Companies such as *Bemis Company*, *Thin Film Electronics ASA*, as well as start-up company *Mevia* are developing printable packaging interconnects, RFID tags, sensors or a combination of these for various application fields. *FADEL* and *Momodesign*, through collaboration with research institutes and organisations, are also incorporating graphene based composites and coating into shoes and helmets.

The *European Graphene Flagship* postulated that the current and near future market for 2d materials will be largely driven by production strategies for these materials[1]. One of the main goals for the 2d material industry is therefore to achieve scalable, cost-effective material production. Indeed, products for research and development of 2d materials currently form the largest portion of the market in the industry. Companies such as *Haydale*, *Perpetuus Advanced Materials*, *Graphitene*, *Graphenea*, *Cambridge Nanosytems*, *Talga Resources* and *Thomas Swan & Co.* are typical examples that specialise in source material production of 2d materials (typically in the form of nanoplatelets and powders) and target towards academia and industrial R&D. Current progress is

now approaching a point where the production cost is reasonably low and consistent. Commercialisation efforts have recently begun the shift to scaled-up production towards real-world applications. In particular, producers are waking up to the fact that one of the best ways to maximise their market share is to demonstrate and develop applications for their products, rather than relying on the market pull of graphene alone. Recent years have therefore seen increasing numbers of partnerships between producers and end users to deliver more practical applications for the materials. Printing remains a promising strategy for large-scale, low-cost manufacturing of application driven devices. Based on the level of interest in printable 2d material applications, the adaptation of 2d material printing technology to end-user applications will likely be pursued and refined over at least the next decade. Overall, the commercial prospects for this approach are extremely bright, representing one of the main ways, if not the key way to achieve mass-market, scalable and practical applications.

Acknowledgments

Author contributions statement

GH, JK, LWTN and XZ prepared the figures. All authors wrote and commented on the manuscript.

Potential conflicts of interest

The technology developed jointly by University of Cambridge and Novalia in Ref. 20 is currently being commercialised by Cam-

28 | *Chem. Soc. Rev.*, [year], [**vol**.], 1–35

This journal is © The Royal Society of Chemistry [year]

bridge Enterprise. Authors GH, LN, RCTH, CJ and TH declare commercial interest in this technology. One of the authors (CJ) is employed by Novalia and is affiliated with the Hybrid Nanomaterials Engineering Group at the Cambridge Graphene Centre. All other authors report no conflicts of interest relevant to this article.

References

1 A. C. Ferrari, F. Bonaccorso, V. Fal'ko, K. S. Novoselov, S. Roche, P. Bøggild, S. Borini, F. H. L. Koppens, V. Palermo, N. Pugno, J. A. Garrido, R. Sordan, A. Bianco, L. Ballerini, M. Prato, E. Lidorikis, J. Kivioja, C. Marinelli, T. Ryhänen, A. Morpurgo, J. N. Coleman, V. Nicolosi, L. Colombo, A. Fert, M. Garcia-Hernandez, A. Bachtold, G. F. Schneider, F. Guinea, C. Dekker, M. Barbone, Z. Sun, C. Galiotis, A. N. Grigorenko, G. Konstantatos, A. Kis, M. Katsnelson, L. Vandersypen, A. Loiseau, V. Morandi, D. Neumaier, E. Treossi, V. Pellegrini, M. Polini, A. Tredicucci, G. M. Williams, B. H. Hong, J.-H. Ahn, J. M. Kim, H. Zirath, B. J. van Wees, H. van der Zant, L. Occhipinti, A. Di Matteo, I. A. Kinloch, T. Seyller, E. Quesnel, X. Feng, K. Teo, N. Rupesinghe, P. Hakonen, S. R. T. Neil, Q. Tannock, T. Löfwander and J. Kinaret, *Nanoscale*, 2015, **7**, 4598–4810.

2 L. W. T. Ng, G. Hu, R. C. T. Howe, X. Zhu, Z. Yang, C. Jones and T. Hasan, *Functional inks and printing of graphene and related 2D materials: Technology, formulation and applications*, Springer, New York, US, in press, 2018.

3 V. Nicolosi, M. Chhowalla, M. G. Kanatzidis, M. S. Strano and J. N. Coleman, *Science*, 2013, **340**, 1226419.

4 J. Kang, V. K. Sangwan, J. D. Wood and M. C. Hersam, *Acc. Chem. Res.*, 2017, **50**, 943–951.

5 Z. Cui, *Printed electronics: Materials, technologies and applications*, John Wiley & Sons Singapore Pte. Ltd, Singapore, 1st edn., 2016, p. 360.

6 R. C. T. Howe, G. Hu, Z. Yang and T. Hasan, *SPIE Nanosci. + Eng.*, 2015, 95530R.

7 F. Torrisi, T. Hasan, W. Wu, Z. Sun, A. Lombardo, T. S. Kulmala, G.-W. Hsieh, S. Jung, F. Bonaccorso, P. J. Paul, D. Chu and A. C. Ferrari, *ACS Nano*, 2012, **6**, 2992–3006.

8 D. J. Finn, M. Lotya, G. Cunningham, R. J. Smith, D. McCloskey, J. F. Donegan and J. N. Coleman, *J. Mater. Chem. C*, 2014, **2**, 925–932.

9 F. Withers, H. Yang, L. Britnell, A. P. Rooney, E. Lewis, A. Felten, C. R. Woods, V. Sanchez Romaguera, T. Georgiou, A. Eckmann, Y. J. Kim, S. G. Yeates, S. J. Haigh, a. K. Geim, K. S. Novoselov and C. Casiraghi, *Nano Lett.*, 2014, **14**, 3987–3992.

10 A. G. Kelly, T. Hallam, C. Backes, A. Harvey, A. S. Esmaeily, I. Godwin, J. Coelho, V. Nicolosi, J. Lauth, A. Kulkarni, S. Kinge, L. D. A. Siebbeles, G. S. Duesberg and J. N. Coleman, *Science*, 2017, **356**, 69–73.

11 D. McManus, S. Vranic, F. Withers, V. Sanchez-Romaguera, M. Macucci, H. Yang, R. Sorrentino, K. Parvez, S.-K. Son, G. Iannaccone, K. Kostarelos, G. Fiori and C. Casiraghi, *Nat. Nanotechnol.*, 2017, **12**, 343–350.

12 G. Hu, T. Albrow-Owen, X. Jin, A. Ali, Y. Hu, R. C. T. Howe, K. Shehzad, Z. Yang, X. Zhu, R. I. Woodward, T.-C. Wu, H. Jussila, J.-B. Wu, P. Peng, P.-H. Tan, Z. Sun, E. J. R. Kelleher, M. Zhang, Y. Xu and T. Hasan, *Nat. Commun.*, 2017, **8**, 278.

13 V. Bianchi, T. Carey, L. Viti, L. Li, E. H. Linfield, A. G. Davies, A. Tredicucci, D. Yoon, P. G. Karagiannidis, L. Lombardi, F. Tomarchio, A. C. Ferrari, F. Torrisi and M. S. Vitiello, *Nat. Commun.*, 2017, **8**, 15763.

14 E. B. Secor, P. L. Prabhumirashi, K. Puntambekar, M. L. Geier and M. C. Hersam, *J. Phys. Chem. Lett.*, 2013, **4**, 1347–1351.

15 Y. Xu, M. G. Schwab, A. J. Strudwick, I. Hennig, X. Feng, Z. Wu and K. Müllen, *Adv. Energy Mater.*, 2013, **3**, 1035–1040.

16 W. J. Hyun, E. B. Secor, M. C. Hersam, C. D. Frisbie and L. F. Francis, *Adv. Mater.*, 2015, **27**, 109–115.

17 K. Arapov, E. Rubingh, R. Abbel, J. Laven, G. de With and H. Friedrich, *Adv. Funct. Mater.*, 2016, **26**, 586–593.

18 P. G. Karagiannidis, S. A. Hodge, L. Lombardi, F. Tomarchio, N. Decorde, S. Milana, I. Goykhman, Y. Su, S. V. Mesite, D. N. Johnstone, R. K. Leary, P. A. Midgley, N. M. Pugno, F. Torrisi and A. C. Ferrari, *ACS Nano*, 2017, **11**, 2742–2755.

19 J. Baker, D. Deganello, D. T. Gethin and T. M. Watson, *Mater. Res. Innov.*, 2014, **18**, 86–90.

20 *New graphene based inks for high-speed manufacturing of printed electronics | University of Cambridge. Available at: http://www.cam.ac.uk/research/news/new-graphene-based-inks-for-high-speed-manufacturing-of-printed-electronics (Accessed: 19/10/2015).*

21 E. B. Secor, S. Lim, H. Zhang, C. D. Frisbie, L. F. Francis and M. C. Hersam, *Adv. Mater.*, 2014, **26**, 4533–4538.

22 S. Santra, G. Hu, R. C. T. Howe, A. De Luca, S. Z. Ali, F. Udrea, J. W. Gardner, S. K. Ray, P. K. Guha and T. Hasan, *Sci. Rep.*, 2015, **5**, 17374.

23 E. B. Secor, T. Z. Gao, A. E. Islam, R. Rao, S. G. Wallace, J. Zhu, K. W. Putz, B. Maruyama and M. C. Hersam, *Chem. Mater.*, 2017, **29**, 2332–2340.

24 T. Carey, S. Cacovich, G. Divitini, J. Ren, A. Mansouri, J. M. Kim, C. Wang, C. Ducati, R. Sordan and F. Torrisi, *Nat. Commun.*, 2017, **8**, 1202.

25 D. Dodoo-Arhin, R. C. T. Howe, G. Hu, Y. Zhang, P. Hiralal, A. Bello, G. Amaratunga and T. Hasan, *Carbon*, 2016, **105**, 33–41.

26 K. S. Novoselov, A. K. Geim, S. V. Morozov, D. Jiang, Y. Zhang, S. V. Dubonos, I. V. Grigorieva and A. A. Firsov, *Science*, 2004, **306**, 666–669.

27 M. Garašanin, in *Cambridge Anc. Hist.*, ed. J. Boardman, I. E. S. Edwards, N. G. L. Hammond and E. Sollberger, Cambridge University Press, Cambridge, 1982, pp. 136–162.

28 R. Mas-Ballesté, C. Gómez-Navarro, J. Gómez-Herrero and F. Zamora, *Nanoscale*, 2011, **3**, 20–30.

29 P. R. Wallace, *Phys. Rev.*, 1947, **71**, 622–634.

30 J. W. McClure, *Phys. Rev.*, 1956, **104**, 666–671.

31 J. C. Slonczewski and P. R. Weiss, *Phys. Rev.*, 1958, **109**, 272–279.

This journal is © The Royal Society of Chemistry [year]

Chem. Soc. Rev., [year], [**vol.**], 1–35 | 29

32 A. K. Bodenmann and A. H. MacDonald, *Phys. Today*, 2007, **60**, 35–41.

33 M. Xu, T. Liang, M. Shi and H. Chen, *Chem. Rev.*, 2013, **113**, 3766–3798.

34 A. Lipp, K. Schwetz and K. Hunold, *J. Eur. Ceram. Soc.*, 1989, **5**, 3–9.

35 L. Li, Y. Yu, G. J. Ye, Q. Ge, X. Ou, H. Wu, D. Feng, X. H. Chen and Y. Zhang, *Nat. Nanotechnol.*, 2014, **9**, 372–377.

36 R. F. Frindt and A. D. Yoffe, *Proc. R. Soc. A Math. Phys. Eng. Sci.*, 1963, **273**, 69–83.

37 P. Joensen, R. Frindt and S. Morrison, *Mater. Res. Bull.*, 1986, **21**, 457–461.

38 B. Radisavljevic, A. Radenovic, J. Brivio, V. Giacometti and A. Kis, *Nat. Nanotechnol.*, 2011, **6**, 147–150.

39 P. W. Bridgman, *J. Am. Chem. Soc.*, 1914, **36**, 1344–1363.

40 J. Kang, S. A. Wells, J. D. Wood, J.-H. Lee, X. Liu, C. R. Ryder, J. Zhu, J. R. Guest, C. A. Husko and M. C. Hersam, *Proc. Natl. Acad. Sci. U.S.A.*, 2016, **13**, 11688–11693.

41 J. D. Wood, S. A. Wells, D. Jariwala, K.-S. Chen, E. Cho, V. K. Sangwan, X. Liu, L. J. Lauhon, T. J. Marks and M. C. Hersam, *Nano Lett.*, 2014, **14**, 6964–6970.

42 V. Artel, Q. Guo, H. Cohen, R. Gasper, A. Ramasubramaniam, F. Xia and D. Naveh, *npj 2D Mater. Appl.*, 2017, **1**, 6.

43 J. Kang, J. Wood, S. Wells, J.-H. Lee, X. Liu, K.-S. Chen and M. Hersam, *ACS Nano*, 2015, **9**, 3596–3604.

44 X.-F. Jiang, Q. Weng, X.-B. Wang, X. Li, J. Zhang, D. Golberg and Y. Bando, *J. Mater. Sci. Technol.*, 2015, **31**, 589–598.

45 L. Liu, Y. P. Feng and Z. X. Shen, *Phys. Rev. B*, 2003, **68**, 104102.

46 I. Jo, M. T. Pettes, J. Kim, K. Watanabe, T. Taniguchi, Z. Yao and L. Shi, *Nano Lett.*, 2013, **13**, 550–554.

47 H. Liem and H. Choy, *Solid State Commun.*, 2013, **163**, 41–45.

48 C. R. Dean, A. F. Young, I. Meric, C. Lee, L. Wang, S. Sorgenfrei, K. Watanabe, T. Taniguchi, P. Kim, K. L. Shepard and J. Hone, *Nat. Nanotechnol.*, 2010, **5**, 722–726.

49 M. Naguib, M. Kurtoglu, V. Presser, J. Lu, J. Niu, M. Heon, L. Hultman, Y. Gogotsi and M. W. Barsoum, *Adv. Mater.*, 2011, **23**, 4248–4253.

50 B. Anasori, Y. Xie, M. Beidaghi, J. Lu, B. C. Hosler, L. Hultman, P. R. C. Kent, Y. Gogotsi and M. W. Barsoum, *ACS Nano*, 2015, **9**, 9507–9516.

51 M. Naguib, V. N. Mochalin, M. W. Barsoum and Y. Gogotsi, *Adv. Mater.*, 2014, **26**, 992–1005.

52 B. Anasori, M. R. Lukatskaya and Y. Gogotsi, *Nat. Rev. Mater.*, 2017, **2**, 16098.

53 E. Carroll, D. Buckley, N. V. V. Mogili, D. McNulty, M. S. Moreno, C. Glynn, G. Collins, J. D. Holmes, K. M. Razeeb and C. O'Dwyer, *Chem. Mater.*, 2017, **29**, 7390–7400.

54 W. Zheng, T. Xie, Y. Zhou, Y. L. Chen, W. Jiang, S. Zhao, J. Wu, Y. Jing, Y. Wu, G. Chen, Y. Guo, J. Yin, S. Huang, H. Q. Xu, Z. Liu and H. Peng, *Nat. Commun.*, 2015, **6**, 6972.

55 V. D. Das and N. Soundararajan, *J. Appl. Phys.*, 1989, **65**, 2332–2341.

56 S. K. Mishra, S. Satpathy and O. Jepsen, *J. Phys. Condens. Matter*, 1997, **9**, 461–470.

57 R. B. Jacobs-Gedrim, M. Shanmugam, N. Jain, C. A. Durcan, M. T. Murphy, T. M. Murray, R. J. Matyi, R. L. Moore and B. Yu, *ACS Nano*, 2014, **8**, 514–521.

58 D. A. Bandurin, A. V. Tyurnina, G. L. Yu, A. Mishchenko, V. Zólyomi, S. V. Morozov, R. K. Kumar, R. V. Gorbachev, Z. R. Kudrynskyi, S. Pezzini, Z. D. Kovalyuk, U. Zeitler, K. S. Novoselov, A. Patanè, L. Eaves, I. V. Grigorieva, V. I. Fal'ko, A. K. Geim and Y. Cao, *Nat. Nanotechnol.*, 2017, **12**, 223–227.

59 S. Ghosh, P. D. Patil, M. Wasala, S. Lei, A. Nolander, P. Sivakumar, R. Vajtai, P. Ajayan and S. Talapatra, *2D Mater.*, 2017, **5**, 015001.

60 J. O. Island, S. I. Blanter, M. Buscema, H. S. J. van der Zant and A. Castellanos-Gomez, *Nano Lett.*, 2015, **15**, 7853–7858.

61 R. R. Nair, P. Blake, A. N. Grigorenko, K. S. Novoselov, T. J. Booth, T. Stauber, N. M. R. Peres and A. K. Geim, *Science*, 2008, **320**, 1308–1308.

62 F. Bonaccorso, Z. Sun, T. Hasan and A. C. Ferrari, *Nat. Photonics*, 2010, **4**, 611–622.

63 A. K. Geim and K. S. Novoselov, *Nat. Mater.*, 2007, **6**, 183–191.

64 A. H. Castro Neto, F. Guinea, N. M. R. Peres, K. S. Novoselov and A. K. Geim, *Rev. Mod. Phys.*, 2009, **81**, 109–162.

65 F. Schwierz, *Nat. Nanotechnol.*, 2010, **5**, 487–496.

66 A. Splendiani, L. Sun, Y. Zhang, T. Li, J. Kim, C.-Y. Chim, G. Galli and F. Wang, *Nano Lett.*, 2010, **10**, 1271–1275.

67 R. S. Sundaram, M. Engel, A. Lombardo, R. Krupke, A. C. Ferrari, P. Avouris and M. Steiner, *Nano Lett.*, 2013, **13**, 1416–1421.

68 N. Youngblood, C. Chen, S. J. Koester and M. Li, *Nat. Photonics*, 2015, **9**, 247.

69 F. Xia, H. Wang, D. Xiao, M. Dubey and A. Ramasubramaniam, *Nat. Photonics*, 2014, **8**, 899–907.

70 Z. Sun, T. Hasan, F. Torrisi, D. Popa, G. Privitera, F. Wang, F. Bonaccorso, D. M. Basko and A. C. Ferrari, *ACS Nano*, 2010, **4**, 803–810.

71 R. C. T. Howe, R. I. Woodward, G. Hu, Z. Yang, E. J. R. Kelleher and T. Hasan, *Phys. Status Solidi B*, 2016, **253**, 911–917.

72 F. Hui, C. Pan, Y. Shi, Y. Ji, E. Grustan-Gutierrez and M. Lanza, *Microelectron. Eng.*, 2016, **163**, 119–133.

73 L. H. Li, E. J. G. Santos, T. Xing, E. Cappelluti, R. Roldán, Y. Chen, K. Watanabe and T. Taniguchi, *Nano Lett.*, 2015, **15**, 218–223.

74 T. Ramanathan, A. A. Abdala, S. Stankovich, D. A. Dikin, M. Herrera-Alonso, R. D. Piner, D. H. Adamson, H. C. Schniepp, X. Chen, R. S. Ruoff, S. T. Nguyen, I. A. Aksay, R. K. Prud'Homme and L. C. Brinson, *Nat. Nanotechnol.*, 2008, **3**, 327–331.

75 Q. Li, L. Chen, M. R. Gadinski, S. Zhang, G. Zhang, H. Li, A. Haque, L.-Q. Chen, T. Jackson and Q. Wang, *Nature*,

30 | *Chem. Soc. Rev.*, [year], [**vol**.], 1–35

This journal is © The Royal Society of Chemistry [year]

2015, **523**, 576–579.

76 A. Peigney, C. Laurent, E. Flahaut, R. Bacsa and A. Rousset, *Carbon*, 2001, **39**, 507–514.

77 Y. Shao, M. F. El-Kady, L. J. Wang, Q. Zhang, Y. Li, H. Wang, M. F. Mousavi and R. B. Kaner, *Chem. Soc. Rev.*, 2015, **44**, 3639–3665.

78 T. Liu, M. Leskes, W. Yu, A. J. Moore, L. Zhou, P. M. Bayley, G. Kim and C. P. Grey, *Science*, 2015, **350**, 530–533.

79 K. S. Novoselov, D. Jiang, F. Schedin, T. J. Booth, V. V. Khotkevich, S. V. Morozov and A. K. Geim, *Proc. Natl. Acad. Sci. U.S.A.*, 2005, **102**, 10451–10453.

80 F. Bonaccorso, A. Lombardo, T. Hasan, Z. Sun, L. Colombo and A. C. Ferrari, *Mater. Today*, 2012, **15**, 564–589.

81 K. S. Novoselov, V. I. Fal'ko, L. Colombo, P. R. Gellert, M. G. Schwab and K. Kim, *Nature*, 2012, **490**, 192–200.

82 Y. Hernandez, V. Nicolosi, M. Lotya, F. M. Blighe, Z. Sun, S. De, I. T. McGovern, B. Holland, M. Byrne, Y. K. Gun'Ko, J. J. Boland, P. Niraj, G. Duesberg, S. Krishnamurthy, R. Goodhue, J. Hutchison, V. Scardaci, A. C. Ferrari and J. N. Coleman, *Nat. Nanotechnol.*, 2008, **3**, 563–568.

83 W. Zhao, M. Fang, F. Wu, H. Wu, L. Wang and G. Chen, *J. Mater. Chem.*, 2010, **20**, 5817.

84 K. R. Paton, E. Varrla, C. Backes, R. J. Smith, U. Khan, A. O'Neill, C. Boland, M. Lotya, O. M. Istrate, P. King, T. Higgins, S. Barwich, P. May, P. Puczkarski, I. Ahmed, M. Moebius, H. Pettersson, E. Long, J. Coelho, S. E. O'Brien, E. K. McGuire, B. M. Sanchez, G. S. Duesberg, N. McEvoy, T. J. Pennycook, C. Downing, A. Crossley, V. Nicolosi and J. N. Coleman, *Nat. Mater.*, 2014, **13**, 624–630.

85 X. Li, G. Zhang, X. Bai, X. Sun, X. Wang, E. Wang and H. Dai, *Nat. Nanotechnol.*, 2008, **3**, 538–542.

86 C. Valles, C. Drummond, H. Saadaoui, C. A. Furtado, M. He, O. Roubeau, L. Ortolani, M. Monthioux and A. Penicaud, *J. Am. Chem. Soc.*, 2008, **130**, 15802–15804.

87 S. Stankovich, D. A. Dikin, R. D. Piner, K. A. Kohlhaas, A. Kleinhammes, Y. Jia, Y. Wu, S. T. Nguyen and R. S. Ruoff, *Carbon*, 2007, **45**, 1558–1565.

88 E. B. Secor, B. Y. Ahn, T. Z. Gao, J. A. Lewis and M. C. Hersam, *Adv. Mater.*, 2015, **27**, 6683–6688.

89 J. Li, F. Ye, S. Vaziri, M. Muhammed, M. C. Lemme and M. Östling, *Adv. Mater.*, 2013, **25**, 3985–3992.

90 T. Hasan, F. Torrisi, Z. Sun, D. Popa, V. Nicolosi, G. Privitera, F. Bonaccorso and A. C. Ferrari, *Phys. Status Solidi B*, 2010, **247**, 2953–2957.

91 M. F. El-Kady, V. Strong, S. Dubin and R. B. Kaner, *Science*, 2012, **335**, 1326–1330.

92 T. Juntunen, H. Jussila, M. Ruoho, S. Liu, G. Hu, T. Albrow-Owen, L. W. T. Ng, R. C. T. Howe, T. Hasan, Z. Sun and I. Tittonen, *Adv. Funct. Mater.*, accepted for publication, 2018.

93 S. Santra, S. Z. Ali, P. K. Guha, G. Zhong, J. Robertson, J. a. Covington, W. I. Milne, J. W. Gardner and F. Udrea, *Nanotechnology*, 2010, **21**, 485301.

94 J. N. Coleman, M. Lotya, A. O'Neill, S. D. Bergin, P. J. King, U. Khan, K. Young, A. Gaucher, S. De, R. J. Smith, I. V.

Shvets, S. K. Arora, G. Stanton, H.-Y. Kim, K. Lee, G. T. Kim, G. S. Duesberg, T. Hallam, J. J. Boland, J. J. Wang, J. F. Donegan, J. C. Grunlan, G. Moriarty, A. Shmeliov, R. J. Nicholls, J. M. Perkins, E. M. Grieveson, K. Theuwissen, D. W. McComb, P. D. Nellist and V. Nicolosi, *Science*, 2011, **331**, 568–571.

95 Y. Yao, Z. Lin, Z. Li, X. Song, K.-S. Moon and C.-P. Wong, *J. Mater. Chem.*, 2012, **22**, 13494.

96 E. Varrla, C. Backes, K. R. Paton, A. Harvey, Z. Gholamvand, J. McCauley and J. N. Coleman, *Chem. Mater.*, 2015, **27**, 1129–1139.

97 J. Zheng, H. Zhang, S. Dong, Y. Liu, C. T. Nai, H. S. Shin, H. Y. Jeong, B. Liu and K. P. Loh, *Nat. Commun.*, 2014, **5**, 3905–3911.

98 G. Eda, H. Yamaguchi, D. Voiry, T. Fujita, M. Chen and M. Chhowalla, *Nano Lett.*, 2011, **11**, 5111–5116.

99 J. Li, M. M. Naiini, S. Vaziri, M. C. Lemme and M. Ostling, *Adv. Funct. Mater.*, 2014, **24**, 6524–6531.

100 R. I. Woodward, E. J. R. Kelleher, R. C. T. Howe, G. Hu, F. Torrisi, T. Hasan, S. V. Popov and J. R. Taylor, *Opt. Express*, 2014, **22**, 31113.

101 M. Zhang, R. C. T. Howe, R. I. Woodward, E. J. R. Kelleher, F. Torrisi, G. Hu, S. V. Popov, J. R. Taylor and T. Hasan, *Nano Res.*, 2015, **8**, 1522–1534.

102 R. I. Woodward, R. C. T. Howe, T. H. Runcorn, G. Hu, F. Torrisi, E. J. R. Kelleher and T. Hasan, *Opt. Express*, 2015, **23**, 20051.

103 C. George, A. J. Morris, M. H. Modarres and M. De Volder, *Chem. Mater.*, 2016, **28**, 7304–7310.

104 M. Acerce, D. Voiry and M. Chhowalla, *Nat. Nanotechnol.*, 2015, **10**, 313–318.

105 S.-Y. Cho, Y. Lee, H.-J. Koh, H. Jung, J.-S. Kim, H.-W. Yoo, J. Kim and H.-T. Jung, *Adv. Mater.*, 2016, **28**, 7020–7028.

106 X. Wang, W. Xing, X. Feng, B. Yu, L. Song, G. H. Yeoh and Y. Hu, *Compos. Sci. Technol.*, 2016, **127**, 142–148.

107 D. Hanlon, C. Backes, E. Doherty, C. Cucinotta, N. Berner, C. Boland, K. Lee, A. Harvey, P. Lynch, Z. Gholamvand, S. Zhang, K. Wang, G. Moynihan, A. Pokle, Q. Ramasse, N. McEvoy, W. Blau, J. Wang, G. Abellan, F. Hauke, A. Hirsch, S. Sanvito, D. O'Regan, G. S. Duesberg, V. Nicolosi and J. Coleman, *Nat. Commun.*, 2015, **6**, 8563.

108 P. Yasaei, B. Kumar, T. Foroozan, C. Wang, M. Asadi, D. Tuschel, J. E. Indacochea, R. F. Klie and A. Salehi-Khojin, *Adv. Mater.*, 2015, **27**, 1887–1892.

109 J. Sotor, G. Sobon, M. Kowalczyk, W. Macherzynski, P. Paletko and K. M. Abramski, *Opt. Lett.*, 2015, **40**, 3885.

110 C. Hao, B. Yang, F. Wen, J. Xiang, L. Li, W. Wang, Z. Zeng, B. Xu, Z. Zhao, Z. Liu and Y. Tian, *Adv. Mater.*, 2016, **28**, 3194–3201.

111 A. E. Del Rio Castillo, V. Pellegrini, H. Sun, J. Buha, D. A. Dinh, E. Lago, A. Ansaldo, A. Capasso, L. Manna and F. Bonaccorso, *Chem. Mater.*, 2018, **30**, 506–516.

112 L. H. Li, Y. Chen, G. Behan, H. Zhang, M. Petravic and A. M. Glushenkov, *J. Mater. Chem.*, 2011, **21**, 11862.

113 A. M. Joseph, B. Nagendra, E. B. Gowd and K. P. Surendran, *ACS Omega*, 2016, **1**, 1220–1228.

114 M. Ghidiu, M. R. Lukatskaya, M.-Q. Zhao, Y. Gogotsi and M. W. Barsoum, *Nature*, 2014, **516**, 78–81.

115 C. J. Zhang, M. P. Kremer, A. Seral-Ascaso, S.-H. Park, N. McEvoy, B. Anasori, Y. Gogotsi and V. Nicolosi, *Adv. Funct. Mater.*, 2018, **28**, 1705506.

116 J. Chen, K. Chen, D. Tong, Y. Huang, J. Zhang, J. Xue, Q. Huang and T. Chen, *Chem. Commun.*, 2015, **51**, 314–317.

117 X. Li, Y. Dai, Y. Ma, Q. Liu and B. Huang, *Nanotechnology*, 2015, **26**, 135703.

118 Z. Ling, C. E. Ren, M.-Q. Zhao, J. Yang, J. M. Giammarco, J. Qiu, M. W. Barsoum and Y. Gogotsi, *Proc. Natl. Acad. Sci. U.S.A.*, 2014, **111**, 16676–16681.

119 A. Harvey, J. B. Boland, I. Godwin, A. G. Kelly, B. M. Szydłowska, G. Murtaza, A. Thomas, D. J. Lewis, P. O'Brien and J. N. Coleman, *2D Mater.*, 2017, **4**, 025054.

120 T. J. Pinnavaia, *Science*, 1983, **220**, 365–371.

121 T. P. Dolley, *2008 minerals yearbook: Mica*, National Minerals Information Center, 2008, p. 13.

122 F. Annabi-Bergaya, *Microporous Mesoporous Mater.*, 2008, **107**, 141–148.

123 B. Chen, J. R. G. Evans, H. C. Greenwell, P. Boulet, P. V. Coveney, A. A. Bowden and A. Whiting, *Chem. Soc. Rev.*, 2008, **37**, 568–594.

124 A. Arora, V. Choudhary and D. K. Sharma, *J. Polym. Res.*, 2011, **18**, 843–857.

125 K. Suganuma, *Introduction to printed electronics*, Springer New York, New York, US, 1st edn., 2014, vol. 74, p. 132.

126 M. Dresselhaus and G. Dresselhaus, *Adv. Phys.*, 1981, **30**, 139–326.

127 Z. Zeng, T. Sun, J. Zhu, X. Huang, Z. Yin, G. Lu, Z. Fan, Q. Yan, H. H. Hng and H. Zhang, *Angew. Chemie Int. Ed.*, 2012, **51**, 9052–9056.

128 R. Ma and T. Sasaki, *Adv. Mater.*, 2010, **22**, 5082–5104.

129 T. Hasan, Z. Sun, F. Wang, F. Bonaccorso, P. H. Tan, A. G. Rozhin and A. C. Ferrari, *Adv. Mater.*, 2009, **21**, 3874–3899.

130 K. D. Ausman, R. Piner, O. Lourie, R. S. Ruoff and M. Korobov, *J. Phys. Chem. B*, 2000, **104**, 8911–8915.

131 S. M. Bachilo, *Science*, 2002, **298**, 2361–2366.

132 S. Giordani, S. D. Bergin, V. Nicolosi, S. Lebedkin, M. M. Kappes, W. J. Blau and J. N. Coleman, *J. Phys. Chem. B*, 2006, **110**, 15708–15718.

133 M. A. Ibrahem, T.-W. Lan, J. K. Huang, Y.-Y. Chen, K.-H. Wei, L.-J. Li and C. W. Chu, *RSC Adv.*, 2013, **3**, 13193.

134 J. N. Coleman, *Acc. Chem. Res.*, 2013, **46**, 14–22.

135 L. Guardia, M. Fernandez-Merino, J. Paredes, P. Solis-Fernandez, S. Villar-Rodil, A. Martinez-Alonso and J. Tascon, *Carbon*, 2011, **49**, 1653–1662.

136 A. Ciesielski and P. Samor, *Chem. Soc. Rev.*, 2014, **43**, 381–398.

137 G. Cunningham, M. Lotya, C. S. Cucinotta, S. Sanvito, S. D. Bergin, R. Menzel, M. S. P. Shaffer and J. N. Coleman, *ACS Nano*, 2012, **6**, 3468–3480.

138 Y. Hernandez, M. Lotya, D. Rickard, S. D. Bergin and J. N. Coleman, *Langmuir*, 2010, **26**, 3208–3213.

139 M. Lotya, Y. Hernandez, P. J. King, R. J. Smith, V. Nicolosi, L. S. Karlsson, F. M. Blighe, S. De, Z. Wang, I. T. McGovern, G. S. Duesberg and J. N. Coleman, *J. Am. Chem. Soc.*, 2009, **131**, 3611–3620.

140 K.-G. Zhou, N.-N. Mao, H.-X. Wang, Y. Peng and H.-L. Zhang, *Angew. Chemie Int. Ed.*, 2011, **50**, 10839–10842.

141 M. Yi, Z. Shen, S. Ma and X. Zhang, *J. Nanoparticle Res.*, 2012, **14**, 1003.

142 A. A. Green and M. C. Hersam, *Nano Lett.*, 2009, **9**, 4031–4036.

143 J. N. Coleman, *Adv. Funct. Mater.*, 2009, **19**, 3680–3695.

144 P. May, U. Khan, J. M. Hughes and J. N. Coleman, *J. Phys. Chem. C*, 2012, **116**, 11393–11400.

145 T. Hasan, V. Scardaci, P. Tan, A. Rozhin, W. Milne and A. Ferrari, *J. Phys. Chem. C*, 2007, **111**, 12594–12602.

146 A. Ciesielski, S. Haar, M. El Gemayel, H. Yang, J. Clough, G. Melinte, M. Gobbi, E. Orgiu, M. V. Nardi, G. Ligorio, V. Palermo, N. Koch, O. Ersen, C. Casiraghi and P. Samorì, *Angew. Chemie Int. Ed.*, 2014, **53**, 10355–10361.

147 Y. T. Liang and M. C. Hersam, *J. Am. Chem. Soc.*, 2010, **132**, 17661–17663.

148 Y. Zhu, S. Murali, W. Cai, X. Li, J. W. Suk, J. R. Potts and R. S. Ruoff, *Adv. Mater.*, 2010, **22**, 3906–3924.

149 D. A. Dikin, S. Stankovich, E. J. Zimney, R. D. Piner, G. H. B. Dommett, G. Evmenenko, S. T. Nguyen and R. S. Ruoff, *Nature*, 2007, **448**, 457–460.

150 S. Park, J. An, I. Jung, R. D. Piner, S. J. An, X. Li, A. Velamakanni and R. S. Ruoff, *Nano Lett.*, 2009, **9**, 1593–1597.

151 D. Voiry, J. Yang, J. Kupferberg, R. Fullon, C. Lee, H. Y. Jeong, H. S. Shin and M. Chhowalla, *Science*, 2016, **353**, 1413–1416.

152 U. Khan, A. O'Neill, H. Porwal, P. May, K. Nawaz and J. N. Coleman, *Carbon*, 2012, **50**, 470–475.

153 J. M. J. M. Graham, *Biological centrifugation*, CRC Press, Boca Raton, US, 1st edn., 2001, p. 224.

154 C. Backes, R. J. Smith, N. McEvoy, N. C. Berner, D. McCloskey, H. C. Nerl, A. O'Neill, P. J. King, T. Higgins, D. Hanlon, N. Scheuschner, J. Maultzsch, L. Houben, G. S. Duesberg, J. F. Donegan, V. Nicolosi and J. N. Coleman, *Nat. Commun.*, 2014, **5**, 4576.

155 F. Bonaccorso, A. Bartolotta, J. N. Coleman and C. Backes, *Adv. Mater.*, 2016, **28**, 6136–6166.

156 J. Zhu, J. Kang, J. Kang, D. Jariwala, J. D. Wood, J.-W. T. Seo, K.-S. Chen, T. J. Marks and M. C. Hersam, *Nano Lett.*, 2015, **15**, 7029–7036.

157 J. Kang, J.-W. T. Seo, D. Alducin, A. Ponce, M. J. Yacaman and M. C. Hersam, *Nat. Commun.*, 2014, **5**, 5478.

158 J. Kang, V. K. Sangwan, J. D. Wood, X. Liu, I. Balla, D. Lam and M. C. Hersam, *Nano Lett.*, 2016, **16**, 7216–7223.

159 D. N. Carvalho, *Forty centuries of ink*, BiblioLife, Charleston, US, 2008, p. 308.

160 *The printing ink manual*, ed. R. H. Leach, R. J. Pierce, E. P.

32 | *Chem. Soc. Rev.*, [year], [**vol**.], 1–35

This journal is © The Royal Society of Chemistry [year]

Hickman, M. J. Mackenzie and H. G. Smith, Springer Netherlands, Dordrecht, the Netherlands, 5th edn., 1993.

161 A. Goldschmidt, H.-J. Streitberger and A. Goldschmidt, *BASF handbook on basics of coating technology*, Vincentz Network, Hannover, Germany, 2nd edn., 2007, p. 792.

162 E. W. Flick, *Printing ink and overprint varnish formulations*, William Andrew, Norwich, US, 2nd edn., 1999, p. 127.

163 H.-H. Lee, K.-S. Chou and K.-C. Huang, *Nanotechnology*, 2005, **16**, 2436–2441.

164 B.-J. de Gans, P. C. Duineveld and U. S. Schubert, *Adv. Mater.*, 2004, **16**, 203–213.

165 P. Beecher, P. Servati, A. Rozhin, A. Colli, V. Scardaci, S. Pisana, T. Hasan, A. J. Flewitt, J. Robertson, G. W. Hsieh, F. M. Li, A. Nathan, A. C. Ferrari and W. I. Milne, *J. Appl. Phys.*, 2007, **102**, 043710.

166 G. Pangalos, J. M. Dealy and M. B. Lyne, *J. Rheol.*, 1985, **29**, 471–491.

167 D. Doraiswamy, *Rheol. Bull.*, 2002, **71**, 1–9.

168 H. A. Barnes, J. F. J. F. Hutton and K. Walters, *An introduction to rheology*, Elsevier, Amsterdam, The Netherlands, 1st edn., 1989, p. 199.

169 A. A. Tracton, *Coatings technology handbook*, CRC Press, Boca Raton, US, 3rd edn., 2005, p. 936.

170 *Inkjet technology for digital fabrication*, ed. I. M. Hutchings and G. D. Martin, John Wiley & Sons, Ltd, Chichester, UK, 2012, p. 390.

171 H. Lievens, *Surf. Coatings Technol.*, 1995, **76-77**, 744–753.

172 M. Lahti, S. Leppävuori and V. Lantto, *Appl. Surf. Sci.*, 1999, **142**, 367–370.

173 H. A. D. Nguyen, C. Lee, K.-H. Shin and D. Lee, *IEEE Trans. Components, Packag. Manuf. Technol.*, 2015, **5**, 1516–1524.

174 T. Smith, *Pigment Resin Technol.*, 1986, **15**, 11–12.

175 F. C. Krebs, *Sol. Energy Mater. Sol. Cells*, 2009, **93**, 394–412.

176 *Handbook of print media : Technologies and production methods*, ed. H. Kipphan, Springer-Verlag Berlin Heidelberg, Heidelberg, Germany, 1st edn., 2001, p. 1207.

177 *Contact angle, wettability, and adhesion*, ed. F. M. Fowkes, American Chemical Society, Washington, D.C., US, 1st edn., 1964, p. 389.

178 G. L. Robertson, *Food packaging: Principles and practice*, CRC Press, Boca Raton, US, 3rd edn., 2012, p. 733.

179 R. D. Deegan, O. Bakajin, T. F. Dupont, G. Huber, S. R. Nagel and T. A. Witten, *Nature*, 1997, **389**, 827–829.

180 E. W. Flick, *Industrial solvents handbook*, William Andrew, Norwich, US, 5th edn., 1998, p. 994.

181 D. Papakonstantinou, E. Amanatides, D. Mataras, V. Ioannidis and P. Nikolopoulos, *Plasma Process. Polym.*, 2007, **4**, S1057–S1062.

182 S. Luo, T. Harris and C. Wong, Proc. Int. Symp. Adv. Packag. Mater. Process. Prop. Interfaces (IEEE Cat. No. 01TH8562), 2001.

183 R. G. Larson, *AIChE J.*, 2014, **60**, 1538–1571.

184 M. Singh, H. M. Haverinen, P. Dhagat and G. E. Jabbour, *Adv. Mater.*, 2010, **22**, 673–685.

185 H. Yoo and C. Kim, *Colloids Surfaces A Physicochem. Eng. Asp.*, 2015, **468**, 234–245.

186 D. Jang, D. Kim and J. Moon, *Langmuir*, 2009, **25**, 2629–2635.

187 A. Capasso, A. Del Rio Castillo, H. Sun, A. Ansaldo, V. Pellegrini and F. Bonaccorso, *Solid State Commun.*, 2015, **224**, 53–63.

188 Y. Yao, L. Tolentino, Z. Yang, X. Song, W. Zhang, Y. Chen and C.-P. Wong, *Adv. Funct. Mater.*, 2013, **23**, 3577–3583.

189 P. He, J. R. Brent, H. Ding, J. Yang, D. J. Lewis, P. O'Brien and B. Derby, *Nanoscale*, 2018.

190 Y. Xu, I. Hennig, D. Freyberg, A. J. Strudwick, M. G. Schwab, T. Weitz and K. C.-P. Cha, *J. Power Sources*, 2014, **248**, 483–488.

191 C. Sriprachuabwong, C. Karuwan, A. Wisitsorrat, D. Phokharatkul, T. Lomas, P. Sritongkham and A. Tuantranont, *J. Mater. Chem.*, 2012, **22**, 5478.

192 R. F. Hossain, I. G. Deaguero, T. Boland and A. B. Kaul, *npj 2D Mater. Appl.*, 2017, **1**, 28.

193 K. Arapov, R. Abbel, G. de With and H. Friedrich, *Faraday Discuss.*, 2014, **173**, 323–336.

194 T. Vuorinen, J. Niittynen, T. Kankkunen, T. M. Kraft and M. Mäntysalo, *Sci. Rep.*, 2016, **6**, 35289.

195 S. J. Rowley-Neale, G. C. Smith and C. E. Banks, *ACS Applied Materials & Interfaces*, 2017, **9**, 22539–22548.

196 B. Derby, *Annu. Rev. Mater. Res.*, 2010, **40**, 395–414.

197 J. E. Fromm, *IBM J. Res. Dev.*, 1984, **28**, 322–333.

198 M. Michel, J. A. Desai, C. Biswas and A. B. Kaul, *Nanotechnology*, 2016, **27**, 485602.

199 E. B. Secor and M. C. Hersam, *Graphene inks for printed electronics. Available at: http://www.sigmaaldrich.com/technical-documents/articles/technology-spotlights/graphene-inks-for-printed-electronics.html (Accessed: 24/05/2015)*.

200 D. Soltman and V. Subramanian, *Langmuir*, 2008, **24**, 2224–2231.

201 Y. J. Moon, H. Kang, S. H. Lee, K. Kang, Y. J. Cho, J. Y. Hwang and S. J. Moon, *J. Mech. Sci. Technol.*, 2014, **28**, 1441–1448.

202 S. Scherp and S. J. D. Ericsson, *US4267773 - Silkscreen Printing Machine*, 1981.

203 S. J. D. Ericsson, *US4226181 - Method and apparatus for adjusting the position of a stencil relative to a printing table*, 1980.

204 B. Kang, W. H. Lee and K. Cho, *ACS Appl. Mater. Interfaces*, 2013, **5**, 2302–2315.

205 A. Goldschmidt and H.-J. Streitburger, *BASF Handbook on Basics of Coating Technology*, William Andrew, Hannover, Germany, 2003.

206 J. A. Owczarek and F. L. Howland, *IEEE Trans. Compon. Packag. Manuf. Technol.*, 1990, **13**, 358–367.

207 D. Zhang, X. Li, H. Li, S. Chen, Z. Sun, X. Yin and S. Huang, *Carbon*, 2011, **49**, 5382–5388.

208 C. Xu, B. Xu, Y. Gu, Z. Xiong, J. Sun and X. S. Zhao, *Energy*

This journal is © The Royal Society of Chemistry [year]

Chem. Soc. Rev., [year], [**vol.**], 1–35 | 33

Environ. Sci., 2013, **6**, 1388.

209 C. Karuwan, A. Wisitsoraat, P. Chaisuwan, D. Nacapricha, A. Tuantranont, W. C. Hooper, V. Vaccarino, R. W. Alexander, D. G. Harrison and A. A. Quyyumi, *Anal. Methods*, 2017, **9**, 3689–3695.

210 W. J. Hyun, E. B. Secor, G. A. Rojas, M. C. Hersam, L. F. Francis and C. D. Frisbie, *Adv. Mater.*, 2015, **27**, 7058–7064.

211 Z. Zhang, P. Pan, X. Liu, Z. Yang, J. Wei and Z. Wei, *Mater. Chem. Phys.*, 2017, **187**, 28–38.

212 H. A. D. Nguyen, J. Lee, C. H. Kim, K.-H. Shin and D. Lee, *J. Micromech. Microeng.*, 2013, **23**, 095010.

213 K. I. Bardin, *US4003311 - Gravure printing method*, 1977.

214 J. A. Martens, *EP0468745 A2 - Flexographic printing plate process*, 1992.

215 R. N. Fan, *US5719009 - Laser ablatable photosensitive elements utilized to make flexographic printing plates*, 1990.

216 L. Huang, Z. Wang, J. Zhang, J. Pu, Y. Lin, S. Xu, L. Shen, Q. Chen and W. Shi, *ACS Appl. Mater. Interfaces*, 2014, **6**, 7426–7433.

217 C. W. Foster, M. P. Down, Y. Zhang, X. Ji, S. J. Rowley-Neale, G. C. Smith, P. J. Kelly and C. E. Banks, *Sci. Rep.*, 2017, **7**, 1–11.

218 W. J. Hyun, E. B. Secor, C.-H. Kim, M. C. Hersam, L. F. Francis and C. D. Frisbie, *Adv. Energy Mater.*, 2017, **7**, 1700285.

219 C. Phillips, A. Al-Ahmadi, S.-J. Potts, T. Claypole and D. Deganello, *J. Mater. Sci.*, 2017, **52**, 9520–9530.

220 E. B. Secor, T. Z. Gao, M. H. dos Santos, S. G. Wallace, K. W. Putz and M. C. Hersam, *ACS Appl. Mater. Interfaces*, 2017, **9**, 29418–29423.

221 H. Sirringhaus, *Adv. Mater.*, 2014, **26**, 1319–1335.

222 U. Keller, *Nature*, 2003, **424**, 831–838.

223 M. Zhang, G. Hu, G. Hu, R. C. T. Howe, L. Chen, Z. Zheng and T. Hasan, *Sci. Rep.*, 2015, **5**, 17482.

224 F. Yavari and N. Koratkar, *J. Phys. Chem. Lett.*, 2012, **3**, 1746–1753.

225 F. Schedin, A. K. Geim, S. V. Morozov, E. W. Hill, P. Blake, M. I. Katsnelson and K. S. Novoselov, *Nat. Mater.*, 2007, **6**, 652–655.

226 M. S. Mannoor, H. Tao, J. D. Clayton, A. Sengupta, D. L. Kaplan, R. R. Naik, N. Verma, F. G. Omenetto and M. C. McAlpine, *Nat. Commun.*, 2012, **3**, 763.

227 K. Shehzad, T. Shi, A. Qadir, X. Wan, H. Guo, A. Ali, W. Xuan, H. Xu, Z. Gu, X. Peng, J. Xie, L. Sun, Q. He, Z. Xu, C. Gao, Y.-S. Rim, Y. Dan, T. Hasan, P. Tan, E. Li, W. Yin, Z. Cheng, B. Yu, Y. Xu, J. Luo and X. Duan, *Adv. Mater. Technol.*, 2017, **2**, 1600262.

228 V. Dua, S. P. Surwade, S. Ammu, S. R. Agnihotra, S. Jain, K. E. Roberts, S. Park, R. S. Ruoff and S. K. Manohar, *Angew. Chemie Int. Ed.*, 2010, **49**, 2154–2157.

229 M. G. Chung, D. H. Kim, H. M. Lee, T. Kim, J. H. Choi, D. K. Seo, J.-B. Yoo, S.-H. Hong, T. J. Kang and Y. H. Kim, *Sensors Actuators B Chem.*, 2012, **166-167**, 172–176.

230 D. Zang, M. Yan, S. Ge, L. Ge and J. Yu, *Analyst*, 2013, **138**, 2704.

231 B. W. Kennedy, *Rev. Sci. Instrum.*, 1969, **40**, 1169–1172.

232 W.-H. Yeo, Y.-S. Kim, J. Lee, A. Ameen, L. Shi, M. Li, S. Wang, R. Ma, S. H. Jin, Z. Kang, Y. Huang and J. A. Rogers, *Adv. Mater.*, 2013, **25**, 2773–2778.

233 D. Son, J. Lee, S. Qiao, R. Ghaffari, J. Kim, J. E. Lee, C. Song, S. J. Kim, D. J. Lee, S. W. Jun, S. Yang, M. Park, J. Shin, K. Do, M. Lee, K. Kang, C. S. Hwang, N. Lu, T. Hyeon and D.-H. Kim, *Nat. Nanotechnol.*, 2014, **9**, 397–404.

234 C. Bali, A. Brandlmaier, A. Ganster, O. Raab, J. Zapf and A. Hübler, *Mater. Today Proc.*, 2016, **3**, 739–745.

235 S. Y. Hong, Y. H. Lee, H. Park, S. W. Jin, Y. R. Jeong, J. Yun, I. You, G. Zi and J. S. Ha, *Adv. Mater.*, 2016, **28**, 930–935.

236 K. Agarwal, V. Kaushik, D. Varandani, A. Dhar and B. Mehta, *J. Alloys Compd.*, 2016, **681**, 394–401.

237 K. Shavanova, Y. Bakakina, I. Burkova, I. Shtepliuk, R. Viter, A. Ubelis, V. Beni, N. Starodub, R. Yakimova and V. Khranovskyy, *Sensors (Switzerland)*, 2016, **16**, 1–23.

238 J. Li, F. Rossignol and J. Macdonald, *Lab Chip*, 2015, **15**, 2538–2558.

239 K. Haupt Mosbach, K., *Chem. Rev.*, 2000, **100**, 2495–2504.

240 F.-Y. Kong, S.-X. Gu, W.-W. Li, T.-T. Chen, Q. Xu and W. Wang, *Biosens. Bioelectron.*, 2014, **56**, 77–82.

241 A. Ambrosi, C. K. Chua, A. Bonanni and M. Pumera, *Chemical Reviews*, 2014, **114**, 7150–7188.

242 C. Casiraghi, M. Macucci, K. Parvez, R. Worsley, Y. Shin, F. Bronte, C. Borri, M. Paggi and G. Fiori, *Carbon*, 2018, **129**, 462–467.

243 *Piezoelectric graphene ink enables thin-film pressure sensors of any size. Available at: https://spectrum.ieee.org/nanoclast/semiconductors/materials/piezoelectric-graphene-ink-enables-thin-film-pressure-sensors-of-any-size.*

244 M. Amjadi, K. U. Kyung, I. Park and M. Sitti, *Adv. Funct. Mater.*, 2016, **26**, 1678–1698.

245 N. Karim, S. Afroj, S. Tan, P. He, A. Fernando, C. Carr and K. S. Novoselov, *ACS Nano*, 2017, **11**, 12266–12275.

246 E. E. Simmons, *US2393714 A - Strain gauge*, 1946.

247 S. Beeby, G. Ensel, M. Kraft and N. White, *MEMS mechanical sensors*, Artech House, London, UK, 2004, p. 269.

248 S.-H. Bae, Y. Lee, B. K. Sharma, H.-J. Lee, J.-H. Kim and J.-H. Ahn, *Carbon*, 2013, **51**, 236–242.

249 Y. Wang, L. Wang, T. Yang, X. Li, X. Zang, M. Zhu, K. Wang, D. Wu and H. Zhu, *Adv. Funct. Mater.*, 2014, **24**, 4666–4670.

250 M. Hempel, D. Nezich, J. Kong and M. Hofmann, *Nano Lett.*, 2012, **12**, 5714–5718.

251 V. Eswaraiah, K. Balasubramaniam and S. Ramaprabhu, *J. Mater. Chem.*, 2011, **21**, 12626.

252 C. Yan, J. Wang, W. Kang, M. Cui, X. Wang, C. Y. Foo, K. J. Chee and P. S. Lee, *Adv. Mater.*, 2014, **26**, 2022–2027.

253 M. Yilmaz and P. T. Krein, *IEEE Trans. Power Electron.*, 2013, **28**, 2151–2169.

254 L. Lu, X. Han, J. Li, J. Hua and M. Ouyang, *J. Power Sources*, 2013, **226**, 272–288.

255 R. Marom, S. F. Amalraj, N. Leifer, D. Jacob and D. Aurbach,

J. Mater. Chem., 2011, **21**, 9938.

256 P. Simon and Y. Gogotsi, *Nat. Mater.*, 2008, **7**, 845–854.

257 A. Manthiram, A. V. Murugan, A. Sarkar and T. Muraliganth, *Energy Environ. Sci.*, 2008, **1**, 621.

258 A. S. Aricò, P. Bruce, B. Scrosati, J.-M. Tarascon and W. van Schalkwijk, *Nat. Mater.*, 2005, **4**, 366–377.

259 R. Raccichini, A. Varzi, S. Passerini and B. Scrosati, *Nat. Mater.*, 2014, **14**, 271–279.

260 R. A. Fisher, M. R. Watt, W. J. Ready, S. I. Cho, S. B. Lee, G. A. Snook, P. Kao, A. S. Best, G. Lota, K. Fic, E. Frackowiak, F. Béguin, M. D. Stoller, R. S. Ruoff, G. Arunabha, Y. Lee, O. Inganäs, S. Admassie, M. Vangari, T. Pryor, L. Jiang, J.-F. Lu, L. L. Wang, Q.-Y. Lai, H.-Y. Chu, Y. Zhao, G. Ćirić-Marjanovic, Y. Zhang, H. Feng, X. Wu, L. L. Wang, A. Zhang, T. Xia, H. Dong, X. Li, L. Zhang, T. H. Nguyen, A. Fraiwan, S. Choi, A. S. Aricò, P. Bruce, B. Scrosati, J.-m. Tarascon, W. V. A. N. Schalkwijk, U. D. Picardie, J. Verne, C. Umr, G. Yu, X. Xie, L. Pan, Z. Bao, Y. Cui, L. Dong, Z. Chen, D. Yang and H. Lu, *Energy Environ. Sci*, 2013, **3**, 4889–4899.

261 X. Yang, C. Cheng, Y. Wang, L. Qiu and D. Li, *Science*, 2013, **341**, 534–537.

262 M. F. El-Kady and R. B. Kaner, *Nat. Commun.*, 2013, **4**, 1475.

263 J. Xiao, D. Choi, L. Cosimbescu, P. Koech, J. Liu and J. P. Lemmon, *Chem. Mater.*, 2010, **22**, 4522–4524.

264 H. Hwang, H. Kim and J. Cho, *Nano Lett.*, 2011, **11**, 4826–4830.

265 Y. Dall'Agnese, P.-L. Taberna, Y. Gogotsi and P. Simon, *J. Phys. Chem. Lett.*, 2015, **6**, 2305–2309.

266 G. Zou, Z. Zhang, J. Guo, B. Liu, Q. Zhang, C. Fernandez and Q. Peng, *ACS Appl. Mater. Interfaces*, 2016, **8**, 22280–22286.

267 N. Kurra, B. Ahmed, Y. Gogotsi and H. N. Alshareef, *Adv. Energy Mater.*, 2016, **6**, 1601372.

268 G. Li, F. W. R. Rivarola, N. J. L. K. Davis, S. Bai, T. C. Jellicoe, F. de la Peña, S. Hou, C. Ducati, F. Gao, R. H. Friend, N. C. Greenham and Z.-K. Tan, *Adv. Mater.*, 2016, **28**, 3528–3534.

269 L. T. Le, M. H. Ervin, H. Qiu, B. E. Fuchs and W. Y. Lee, *Electrochem. commun.*, 2011, **13**, 355–358.

270 Y. Lin, F. Liu, G. Casano, R. Bhavsar, I. A. Kinloch and B. Derby, *Adv. Mater.*, 2016, **28**, 7993–8000.

271 C. Zhu, T. Liu, F. Qian, T. Y.-J. Han, E. B. Duoss, J. D. Kuntz, C. M. Spadaccini, M. A. Worsley and Y. Li, *Nano Lett.*, 2016, **16**, 3448–3456.

272 A. E. Jakus, E. B. Secor, A. L. Rutz, S. W. Jordan, M. C. Hersam and R. N. Shah, *ACS Nano*, 2015, **9**, 4636–4648.

273 A. M. A. Yeates, N. Karim, C. Vallés, S. Afroj, K. S. Novoselov and S. G, *2D Materials*, 2017, **4**, 35016.

274 E. García-Tuñon, S. Barg, J. Franco, R. Bell, S. Eslava, E. D'Elia, R. C. Maher, F. Guitian and E. Saiz, *Adv. Mater.*, 2015, **27**, 1688–1693.

275 K. Sun, T.-S. Wei, B. Y. Ahn, J. Y. Seo, S. J. Dillon and J. A. Lewis, *Adv. Mater.*, 2013, **25**, 4539–4543.

276 K. Fu, Y. Wang, C. Yan, Y. Yao, Y. Chen, J. Dai, S. Lacey, Y. Wang, J. Wan, T. Li, Z. Wang, Y. Xu and L. Hu, *Adv. Mater.*, 2016, **28**, 2587–2594.

277 S. M. Mortazavi Zanjani, M. Holt, M. M. Sadeghi, S. Rahimi and D. Akinwande, *npj 2D Mater. Appl.*, 2017, **1**, 36.

278 Technavio, *Global printing inks market 2016-2020*, Infiniti research limited technical report, 2017.

279 K. Fukuda and T. Someya, *Adv. Mater.*, 2017, **29**, 1602736.

280 J. Miettinen, V. Pekkanen, K. Kaija, P. Mansikkamäki, J. Mäntysalo, M. Mäntysalo, J. Niittynen, J. Pekkanen, T. Saviauk and R. Rönkkä, *Microelectronics J.*, 2008, **39**, 1740–1750.

281 H. Park, H. Kang, Y. Lee, Y. Park, J. Noh and G. Cho, *Nanotechnology*, 2012, **23**, 344006.

282 A. Vena, E. Perret, S. Tedjini, G. E. P. Tourtollet, A. Delattre, F. Garet and Y. Boutant, *IEEE Trans. Antennas Propag.*, 2013, **61**, 5868–5877.

283 K. Spree, *Introduction to Organic and Printed Electronics*, Holst centre technical report, 2012.

284 *Functional Printing Market by Materials (Substrate, Inks), Technology (Inkjet, Screen, Flexo, Gravure), Application (Sensors, Displays, Batteries, RFID, Lighting, PV, Medical), and Geography (North America, Europe, APAC, ROW) - Global Forecasts and Analysis*, Markets and markets technical report, 2013.

285 S. Nazarpour, in *Thin Film. coatings Biol.*, ed. S. Nazarpour, Springer Netherlands, Dordrecht, the Netherlands, 2014, pp. 1–9.

286 V. Stenzel and N. Rehfeld, *Functional coatings (European coatings tech files)*, Vincentz Network, 2011, p. 176.

287 U. Riaz, C. Nwaoha and S. M. Ashraf, *Progress in Organic Coatings*, 2014, **77**, 743–756.

288 I. P. Parkin and R. G. Palgrave, *J. Mater. Chem.*, 2005, **15**, 1689–1695.

289 M. Kuhr, S. Bauer, U. Rothhaar and D. Wolff, *Thin Solid Films*, 2003, **442**, 107–116.

290 L. D. Chambers, K. R. Stokes, F. C. Walsh and R. J. K. Wood, *Surf. Coat. Technol.*, 2006, **201**, 3642–3652.

291 A. Mathiazhagan and R. Joseph, *International Journal of Chemical Engineering and Applications*, 2011, **2**, 228–237.

292 J. C. Tiller, C. J. Liao, K. Lewis and A. M. Klibanov, *Proc. Natl. Acad. Sci. U.S.A.*, 2001, **98**, 5981–5985.

293 M. F. Montemor, *Surf. Coat. Technol.*, 2014, **258**, 17–37.

294 Technavio, *Global graphene market 2016-2020*, Infiniti research limited technical report, 2017.

295 B. M. Intelligence, *Strategic assessment of worldwide graphene, composites market-till 2021*, Beige group technical report, 2017.

This journal is © The Royal Society of Chemistry [year]

Chem. Soc. Rev., [year], [**vol.**], 1–35 | 35